

INTERFERENCE AVOIDANCE OF ROBOT MANIPULATORS  
USING ARTICULATION AND TIME SCHEDULING

By

MING-JER LIN

A DISSERTATION PRESENTED TO THE GRADUATE SCHOOL  
OF THE UNIVERSITY OF FLORIDA IN PARTIAL FULFILLMENT  
OF THE REQUIREMENTS FOR THE DEGREE OF  
DOCTOR OF PHILOSOPHY

UNIVERSITY OF FLORIDA

1991  
- - -

## ACKNOWLEDGEMENTS

The author wishes to express his gratitude and appreciation to the members of his supervisory committee, Dr. Joseph Duffy, Dr. Carl D. Crane, Dr. Ali Seireg, Dr. John Staudhammer, and Dr. Ralph G. Selfridge, for their assistance and guidance.

The author is especially grateful to his advisor, Dr. J. Duffy, for suggesting the research topic and for his encouragement and patience throughout the research. He would like to thank his fellow students in CIMAR (Center for Intelligent Machines and Robotics) for their friendship and sharing of knowledge. Thanks are also given to Professor Marc Jaeger M.D. of the Department of Physiology for his help with various aspects of this research.

Finally, but certainly not least, he thanks his parents, Mr. and Mrs. Jarng Lin, his wife, Feng-Yuan, and his son, Eric, for their endless love, understanding, and support during this work.

## TABLE OF CONTENTS

ACKNOWLEDGEMENTS .....	ii
ABSTRACT .....	v
CHAPTERS	
1 INTRODUCTION .....	1
2 INTERSECTIONS OF SOME GEOMETRIC OBJECTS .....	7
2.1 Intersection of Two Line Segments .....	7
2.2 Intersection of a Line Segment and a Circle .....	10
2.3 Intersection of a Line Segment and an Ellipse .....	13
2.4 Intersection of a Cone and a Sphere .....	15
2.5 Intersection of a Cone and a Cylinder .....	18
3 INTERFERENCE AVOIDANCE OF LINE-SEGMENT-MODELED ROBOT MANIPULATORS .....	29
3.1 Permissible Orientations of Robot Links .....	30
3.2 Allowable Orientations of Robot Links .....	35
3.3 Favorable Orientations .....	40
3.4 Coordination of Two Robot Manipulators .....	41
3.5 Computation of Joint Angles .....	48
4 INTERFERENCE AVOIDANCE OF ROBOT MANIPULATORS WITH SOLID LINKS .....	68
4.1 Expansion of Obstacles .....	68
4.2 Master-Slave Operations of Two Robot Manipulators .....	70
4.3 Parallel Operations of Two Robot Manipulators .....	81
5 TIME SCHEDULING OF TWO ROBOT MANIPULATORS .....	96
5.1 Potential Collision Regions .....	97
5.2 Modification of Trajectories .....	104

6	NUMERICAL EXAMPLES .....	121
6.1	Permissible Orientations .....	121
6.2	Spherical Obstacles .....	123
6.3	Polyhedral Obstacles .....	127
6.4	Coordination of Two Robot Manipulators .....	130
6.5	Time Scheduling of Two Robot Manipulators .....	134
7	CONCLUSIONS AND RECOMMENDATIONS .....	166
	REFERENCES .....	169
	BIOGRAPHICAL SKETCH .....	173

Abstract of Dissertation Presented to the Graduate School  
of the University of Florida in Partial Fulfillment of the  
Requirements for the Degree of Doctor of Philosophy

INTERFERENCE AVOIDANCE OF ROBOT  
MANIPULATORS USING ARTICULATION

By

Ming-Jer Lin

May 1991

Chairman : Dr. Joseph Duffy  
Major Department: Mechanical Engineering

This work addresses the kinematic and geometric questions associated with a robot manipulator moving in an environment having obstacles or adjacent manipulators. The kinematic and geometric properties of a robot manipulator are analyzed in terms of its articulation which is used to describe the capacity of the robot manipulator to continuously change its configuration while its end effector follows a prespecified path with free orientation.

In this research, the articulation of spatial robots with special geometries such as the PUMA and TRS robots is analyzed by determining the permissible, allowable and favorable orientations of robot links, which are used to describe motion capability of the robot links. The permissible orientations are determined by the flexure of the robot with its end effector pinned at some intermediate target position and can be obtained by analyzing the workspace and dexterity geometry. The

allowable orientations of a specific link of the manipulator direct the link avoiding interference with obstacles or the links of an adjacent robot manipulator. They are obtained by finding the intersection of some geometric figures such as line segments, circles, conics, cones, and cylinders. The favorable orientations of a link are contained in its allowable orientations and are consistent with all links avoiding interference. They are determined by the kinematic constraints of the robot links.

This analysis gives a range of favorable orientations which can be used to plan an interference-free motion of a robot manipulator to avoid spherical and polyhedral obstacles or an adjacent robot manipulator.

A time scheduling scheme of two robot manipulators moving in a coordinated manner is also presented. A potential collision region is obtained by detecting collisions along rectilinear trajectories of the manipulators using a sphere model for the end effector. An interference-free motion is then obtained by modifying the trajectory of one of the manipulators using time delay or speed reduction to avoid collision.

## CHAPTER 1 INTRODUCTION

In recent years a scientific basis for robotics has been evolving which will lead to superior motion planning capabilities. This scientific basis comprises of the knowledge and understanding of some principal aspects of robotics such as robot geometry and kinematics, workspace, dexterity, special configurations, obstacle avoidance and coordination of multi-robot systems.

A fundamental problem in motion planning is to determine whether a prespecified motion is possible or not. This problem can be couched in geometric terms and constitutes a proper basis for providing the robot with intelligence to improve and speed up its decision-making capability.

In the works of Krishnamurthy (1985) and Lipkin et al. (1985), the manipulator workspace geometry is used to develop time efficient algorithms which determine whether rectilinear motions by a planar 3R manipulator can be successfully executed. The end effector orientations are either prescribed or left unspecified along the path. Shieh and Duffy (1989a,b) extended the algorithm to plan a collision free rectilinear motion of the end effector of a planar 3R manipulator with a single circular obstacle inside the workspace.

This research is to apply a theory of articulation of robot manipulators to study collision detection and avoidance problems of a robot manipulator with obstacles inside the workspace and coordinated motions of two manipulators operating in parallel. The term "articulation" appeared first in the works of Young and Duffy (1987a, 1987b). Choi(1990) then applied the concept of articulation and a geometry of interference to develop a blue print algorithm for path planning of spatial robot manipulators.

Articulation is used to describe the capacity of a manipulator to continuously change its configuration such that it moves with a snake-like motion. The problems of interest here are the determination of possible execution of various types of tasks and the generation of a sequence of motions to achieve the tasks within an obstacles-strewn environment.

In this study, the links of a robot manipulator are modeled at first by line segments and then extended to solids such as parallelepipeds and cylinders. Since most objects can be properly approximated by polyhedrons or spheres or their combinations, obstacles are exemplified by polyhedrons or spheres. An interference avoidance strategy is to be developed which guarantees that a robot manipulator will arrive safely at its destination without interference by articulating its links while tracking specified trajectories or by rescheduling the trajectory of the robot manipulator. It is assumed that the positions and orientations of the robot manipulators at the beginning and end points are specified. In addition, the trajectory of the robot manipulator which connects the beginning and end points is also defined.



The end effector of the robot manipulator is considered to be moving on the specified trajectory for a specific task regardless of orientation which is considered to be a free parameter, and which together with the remaining link orientations is used to flex and hence articulate the arm to avoid interference. In other words, positional constraints of end effectors are imposed on the motion planning of robot manipulators. Geometric dexterity which describes a range of motion of a robot end effector about a point (Lovell 1983) can be applied to facilitate the analysis.

This analysis takes into consideration, firstly, the boundaries of the robot workspace which pose a primary constraint on the motion of the robot manipulator. This is followed by the consideration of intersections of various geometric objects which are used to model the links of robot manipulators and obstacles in the work environment. In this study, three sets of words, viz., permissible orientations, allowable orientations, and favorable orientations, are used to describe the robot link's orientations. The permissible orientations of a link are determined by the flexure with the end effector pinned at some intermediate target position on a trajectory. The allowable orientations of a particular link of a manipulator are determined by the relative locations of the links and the obstacles. It should be noted that the remaining links of the manipulator may well interfere with the obstacles. The favorable orientations of a link of a manipulator are contained in its allowable orientations and are consistent with all links avoiding interference.

As a result, a sequence of joint angles for the robot manipulators can be determined, and these joint angles satisfy the constraints imposed by the specified trajectory and the presence of obstacles. It should be noted that path refers to the

space curve traced by the end effector. However, trajectory also includes velocity and acceleration information.

Another interesting problem to be investigated here is the trajectory planning of robot manipulators for the purpose of coordinating movement of multi-robot operation. This problem is arisen from the possibility that one robot manipulator may not be able to arrive at the goal point without colliding with the other manipulator while tracking the specified trajectory. In this situation, modification of the trajectory is suggested. This investigation is also useful for the motion planning of robot manipulators when they work in an environment where obstacles are movable.

The design of a motion planning system to coordinate actions of multiple robot manipulators within a shared environment has attracted increasing research activity in recent years. The motions of multiple robots may be classified into two modes by means of their task descriptions: (1) A tightly coordinated mode refers to the motion such that the robot manipulators are collaborating to execute a common task function. (2) A loosely coordinated mode refers to the motion such that the robot manipulators are executing unrelated tasks independently (Chien et al. 1988).

In this research, the robot manipulators are considered to be executing in the loosely coordinated mode. Every manipulator in the system may consider another manipulator in the common workspace as a nonstationary obstacle.

In the work of Freund and Hoyer (1986), an approach was presented for the solution of the findpath problem in multi-robot systems. A hierarchical coordinator is designed for real-time collision avoidance. The coalition avoidance strategy is

based on an analytically described trajectory that serves for collision detection as well as avoidance. Each robot is assigned an order of precedence. The robot with highest precedence has the right of way and every robot must avoid a collision with robots with higher precedence.

Roach and Boaz (1987) proposed a time/space planning system to coordinate the actions of two robot manipulators for transfer movements. It is assumed that the path of motion for each manipulator has been determined without regard to spatial intersection. The planning system needs to check one manipulator's position against the other manipulator's position. The strategy for the collision avoidance is by temporally delaying or by altering the path of one arm.

Other research on collision-free motion planning for two moving robots in a common workspace can be found in the works of Lee and Lee (1987) and Basta et al. (1988). In their works the wrist of a manipulator is modeled as a sphere which includes the end effector and the workpiece grasped by the end effector. Collisions are restricted to between the wrists of the two robots, and the arm collisions are not taken into account. The strategy suggested is to use the time scheduling concept, namely, time delay or speed reduction of one of the robots to avoid potential collision.

In this research, the methods used by Lee and Lee (1987) and Basta et al. (1988) are modified and a faster trajectory is generated for one of the robots whose trajectory is changed to avoid potential collision.

The contents of this dissertation are briefly described as follows. Chapter 2 covers the detection and determination of intersection of some geometric objects

which will see applications in later chapters. Chapter 3 introduces the computation of permissible orientations of robot manipulators, followed by the computation of allowable orientations for the purpose of avoiding interference and concludes with the computation of favorable orientations. In this chapter, the robot links are modeled as line segments. Chapter 4 extends the line segment models to solid link models, accomplished by way of obstacles expansion and intersection of solid objects. Chapter 5 deals with the coordination of two robot manipulators, which is accomplished by way of scheduling the motions of two robots via time delay or speed reduction of one of the robots. Chapter 6 presents results of numerical examples of collision avoidance strategies described in the previous chapters. It should be noted that the paths considered here are by no means confined to rectilinear. In fact, the analysis in this work can be applied to any type of paths. However, due to the simplicity of rectilinear paths, they are used as examples. Finally, conclusions and recommendations for future work are given in Chapter 7.

## CHAPTER 2

### INTERSECTIONS OF SOME GEOMETRIC OBJECTS

The algorithm for planning interference-free motion of robot manipulators contains detection and determination of intersections of various geometric objects which model physical elements, e.g. links, of robot manipulators or perspective projections and planar sections of these physical elements. If these geometric objects do intersect, we must be able to mathematically describe the intersection. As the complexity of objects increases, the need for computational subtlety and complexity increases.

The purpose of this chapter is to provide mathematical representations of intersections of some geometric objects used to model physical objects in this work. In addition, some geometric transformations that may assist the determination of intersections are presented. The chapter begins with the simple problem of finding the points of intersection between a line segment and other geometric objects and concludes with the more subtle and complex problem of finding the intersection between a cone and a cylinder.

#### 2.1 Intersection of Two Line Segments

Let the endpoints of a pair of line segments  $\overline{AB}$  and  $\overline{GH}$  be represented by  $A(x_A, y_A)$ ,  $B(x_B, y_B)$  and  $G(x_G, y_G)$ ,  $H(x_H, y_H)$ , and the equations of these two line

segments in parametric forms can be expressed as follows

$$\overline{AB} : \begin{aligned} x &= x_A + s_1(x_A - x_B) \\ y &= y_A + s_1(y_A - y_B) \end{aligned} \quad 0 \leq s_1 \leq 1 \quad (2.1)$$

$$\overline{GH} : \begin{aligned} x &= x_G + s_2(x_G - x_H) \\ y &= y_G + s_2(y_G - y_H) \end{aligned} \quad 0 \leq s_2 \leq 1 \quad (2.2)$$

A direct method for determining the intersection of these two line segments is to compute the parameters of the point of intersection by solving Eqs. (2.1) and (2.2), which are given by

$$s_1 = (AG, DG) / (AB, HG) \quad (2.3)$$

$$s_2 = (AB, AG) / (AB, HG) \quad (2.4)$$

where

$$(IJ, MN) \equiv \begin{vmatrix} x_J - x_I & x_N - x_M \\ y_J - y_I & y_N - y_M \end{vmatrix} \quad (2.5)$$

If the values of these two parameters are both between 0 and 1, the two line segments intersect.

An affine transformation introduced in the work of Young and Duffy (1987a) can also be applied to check the intersection of a pair of line segments. Briefly, the relative position and orientation of a pair of line segments in a plane are transformed into a point in a 3-dimensional space. The 3-dimensional space is then converted into a 2-dimensional plane by a parallel perspective projection. In the 2-dimensional projection plane, a nonallowable manifold (NM) is determined which is used to check the interference of these two line segments.

The coordinates of the image point in the projection plane is computed by the following transformation matrix,

$$\begin{bmatrix} X \\ Y \end{bmatrix} = \begin{bmatrix} 1 & -\cot\Phi \\ 0 & -\csc\Phi \end{bmatrix} \begin{bmatrix} x \\ y \end{bmatrix} \quad (2.6)$$

where  $(x,y)$  is the relative position,  $\Phi$  is the relative orientation, and  $(X,Y)$  is the coordinates of the image point (see Fig. 2.1). The advantage of this transformation is that it transforms a sequence of relative locations of a pair of line segments into a planar curve. The condition for intersection is thus determined by the location of the curve.

It is interesting to note that when the relative position of a pair of line segments is fixed and their relative orientation varies from 0 to  $2\pi$ , the resulting image is a hyperbola. The equation of the hyperbola can be expressed as follows

$$Y^2 - (X - x)^2 = y^2 \quad (2.7)$$

where  $(x,y)$  is the fixed relative position. In this perspective, the image of all relative locations of two line segments in the projection plane is a set of hyperbolas. Analogously, when the relative orientation of two line segments is fixed and their relative position tracks a circle, the resulting image becomes an ellipse, a circle or two lines, the equation of which is given by

$$(X - x_c)^2 - 2\cos\Phi(X - x_c)(Y - y_c) + (Y - y_c)^2 = r_c^2 \quad (2.8)$$

where  $(x_c,y_c)$  and  $r_c$  are the center and the radius of the circle that the relative position of the two line segments tracks, and  $\Phi$  is the fixed relative orientation. In

this perspective, the image of all relative locations of two line segments in the projection plane is a set of ellipses, circles and lines.

Furthermore, it is helpful to investigate the situations when the image points are on the boundary of (NM). In the following, the lengths of the two line segments are represented by  $|AB|$  and  $|GH|$ . The possible situations for the image points to lie on the boundary of (NM) can be categorized into four types as follows,

- (a) The image point is at  $X = 0$  and  $0 \leq Y \leq |AB|$ . In this case, the line segment  $\overline{AB}$  touches the endpoint G of the line segment  $\overline{GH}$  (Fig. 2.2(a)).
- (b) The image point is at  $0 \leq X \leq |GH|$  and  $Y = |AB|$ . In this case, the endpoint B of the line segment  $\overline{AB}$  is on the line segment  $\overline{GH}$  (Fig. 2.2(b)).
- (c) The image point is at  $0 \leq X \leq |GH|$  and  $Y = 0$ . In this case, the endpoint A of the line segment  $\overline{AB}$  is on the line segment  $\overline{GH}$  (Fig. 2.2(c)).
- (d) The image point is at  $X = |GH|$  and  $0 \leq Y \leq |AB|$ . In this case, the line segment  $\overline{AB}$  touches the endpoint H of the line segment  $\overline{GH}$  (Fig. 2.2(d)).

## 2.2 Intersection of a Line Segment And a Circle

Suppose the equation of a line segment  $\overline{AB}$  is represented by Eq. (2.1) and the equation of a circle with center  $C(x_C, y_C)$  and radius  $r_C$  is given as follows

$$(x - x_C)^2 + (y - y_C)^2 = r_C^2 \quad (2.9)$$

The point of intersection of the line segment and the circle can be derived by solving  $s_1$  from Eqs. (2.1) and (2.9). Since the derived equation is a quadratic equation in  $s_1$ , two solutions for  $s_1$  are obtained which can be complex conjugate, distinct real or double real roots. If the quadratic equation has real roots between 0 and 1, the line



segment and the circle intersect, and Eq. (2.1) can be used to determine the point of intersection.

The position of a line segment with respect to a circle can be used to determine the intersection of a line segment and a circle. Suppose, at the outset, a fixed world coordinate (xy) system is specified. Then, a reference coordinate system ( $x'y'$ ) whose +x axis is the direction of  $\overline{AB}$  and whose origin is the center of the circle is selected. Let the circle be denoted by C. The relative position of the line segment  $\overline{AB}$  with respect to the circle C is represented by the coordinates of one endpoint, e.g.,  $A(x_A', y_A')$ , of the line segment in the reference coordinate system. Note that only the relative position of a line segment and a circle is defined, relative orientation is not defined.

Let the orientation of the line segment  $\overline{AB}$  with respect to the +x axis of the world coordinate frame be denoted by  $\Phi$ . The relative position ( $x_A', y_A'$ ) can be determined as follows,

$$\begin{bmatrix} x_A' \\ y_A' \end{bmatrix} = \begin{bmatrix} \cos\Phi & \sin\Phi \\ -\sin\Phi & \cos\Phi \end{bmatrix} \begin{bmatrix} x_A - x_C \\ y_A - y_C \end{bmatrix} \quad (2.10)$$

The necessary and sufficient condition for the line segment  $\overline{AB}$  to intersect the circle C is that the endpoint A of the line segment  $\overline{AB}$  lies inside a region of intersection (RI) as shown in Fig. 2.4. In other words, the relative position is inside (RI). The straight parts of (RI) are parallel to the line segment  $\overline{AB}$  and with length  $|\overline{AB}|$ . The other two parts of (RI) are semicircles with radius equal to that of the circle C. The boundary of (RI) can be expressed by

$$y' = \pm(r_C^2 - X^2)^{1/2}, \quad 0 \leq x' \leq r_C \quad (2.11a)$$

$$y' = \pm r_C, \quad -|AB| \leq x' \leq 0 \quad (2.11b)$$

$$y' = \pm(r_C^2 - (x' + |AB|)^2)^{1/2}, \quad -|AB| - r_C \leq x' \leq -|AB| \quad (2.11c)$$

Further, it is worthwhile to discuss the cases when the relative position lies on the boundary of (RI). Three cases can be categorized as follows:

- (a) The endpoint A of the line segment  $\overline{AB}$  touches the circle C. The relative position lies on the boundary given by Eq. (2.11a) (see Fig. 2.5(a)).
- (b) The endpoint B of the line segment  $\overline{AB}$  touches the circle C. The relative position lies on the boundary given by Eq. (2.11c) (see Fig. 2.5(b)).
- (c) The line segment  $\overline{AB}$  is tangent to the circle C. The relative position lies on the boundary given by Eq. (2.11b) (see Fig. 2.5(c)).

A point can be considered as a line segment with zero length or a circle with zero radius. In this perspective, the development in this and the previous sections can also be used to transform the relative position of a line segment with respect to a point. However, it is necessary to note that when the transformation for a pair of line segments is used, the relative orientation is expressed by the orientation of the line segment in the world coordinate system. This is because there is no relative orientation between a line segment and a point.

When the transformation for a pair of line segments is used for the transformation of a line segment and a point, the nonallowable manifold in the projection plane is  $X = 0$  and  $0 \leq Y \leq |AB|$ , where  $|AB|$  is the length of the line segment. In contrast, when the relative position of a line segment and a circle is used, the region of intersection is  $-|AB| \leq x' \leq 0$  and  $y' = 0$ .

### 2.3 Intersection of a Line Segment and an Ellipse

Analogous to the analysis in Section 2.2, the intersection of a line segment of Eq. (2.1) and an ellipse of the form

$$\frac{(x - x_E)^2}{a^2} + \frac{(y - y_E)^2}{b^2} = 1 \quad (2.12)$$

can be derived by computing the roots of a quadratic equation. Here  $(x_E, y_E)$  is the center and  $a, b$  are lengths of semi-major and semi-minor axes, respectively, of the ellipse.

Alternatively, a geometric transformation can be used to transform an isothetic ellipse of the following form

$$\frac{x^2}{a^2} + \frac{y^2}{b^2} = 1 \quad (2.13)$$

into a circle (Oommen and Reichstein 1987)(see Fig. 2.6). This transformation scales the dimensions along the major and minor axes of the ellipse by dividing them by  $\sigma_x$  and  $\sigma_y$  respectively, and these two scale factors satisfy the following relation

$$\frac{\sigma_x}{\sigma_y} = \frac{b}{a} \quad (2.14)$$

The parametric form of the ellipse after this transformation becomes

$$x = \sigma_x a \cos \theta \quad (2.15a)$$

$$y = \sigma_y b \sin \theta \quad (2.15b)$$

For convenience, it is assumed that the ellipse is transformed into a circle of radius  $R$ . This transformation, being linear, maps straight lines into straight lines. The

slope of a line in a plane is denoted by  $m$  and  $m'$  is the slope of the line after the transformation becomes  $(\sigma_y/\sigma_x)m$ .

The perpendicular distance between two parallel lines is denoted by  $d$  and  $d'$  is the perpendicular distance between the two transformed parallel lines (see Fig. 2.7). It is then desirable to find the relation between  $d$  and  $d'$ . Let  $E(x_E, y_E)$  and  $F(x_F, y_F)$  represent respective points on two parallel lines  $l_E$  and  $l_F$  of slope  $m$ , and the equations of the two parallel lines are given by

$$l_E : y = mx - mx_E + y_E \quad (2.16)$$

$$l_F : y = mx - mx_F + y_F \quad (2.17)$$

The perpendicular distance between these two lines is

$$d = |m(x_E - x_F) - (y_E - y_F)| / (m^2 + 1)^{1/2} \quad (2.18)$$

After the transformation, the equations of the two parallel lines become

$$l'_E : y = m'x - m'\sigma_x x_E + \sigma_y y_E \quad (2.19)$$

$$l'_F : y = m'x - m'\sigma_x x_F + \sigma_y y_F \quad (2.20)$$

and the perpendicular distance between these two lines is

$$d' = |m'\sigma_x(x_E - x_F) - \sigma_y(y_E - y_F)| / (m'^2 + 1)^{1/2} \quad (2.21)$$

Replacing  $m'$  by  $(\sigma_y/\sigma_x)m$ , Eq. (2.21) can be expressed as

$$\begin{aligned} d' &= |\sigma_x| |\sigma_y| |m(x_E - x_F) - (y_E - y_F)| / (\sigma_y^2 m^2 + \sigma_x^2)^{1/2} \\ &= d |\sigma_x| |\sigma_y| [(m^2 + 1) / (\sigma_y^2 m^2 + \sigma_x^2)]^{1/2} \end{aligned} \quad (2.22)$$

The midpoint of a line segment is preserved under this transformation. This can be realized by considering that the midpoint  $M$  of a line segment with end points  $A(x_A, y_A)$  and  $B(x_B, y_B)$  is represented by  $((x_A + x_B)/2, (y_A + y_B)/2)$ . Using the transformation, the coordinates of  $M$  become  $(\sigma_x(x_A + x_B)/2, \sigma_y(y_A + y_B)/2)$ , which is the

midpoint of  $(\sigma_{x_A}, \sigma_{y_A})$  and  $(\sigma_{x_B}, \sigma_{y_B})$ , the coordinates of points A and B after the transformation.

This transformation has been applied to determine the interference of elliptic objects (Oommen and Reichstein 1987). In this study, it is used to assist the determination of interference of a rectangle and an ellipse and can be found in Section 4.2.

## 2.4 Intersection of a Cone and a Sphere

This section is devoted to the detection and determination of the intersection of a right circular cone and a sphere. In this study, a circular cone ( $CN_1$ ) is traced by the end effector link of a manipulator with a endpoint fixed. This is the vertex of the cone while the other endpoint of the end effector link lies on a circle ( $C_b$ ) which is called the base of the cone and the plane where the base lies is called the base plane of the cone (see Fig. 2.8). The base plane of the cone  $CN_1$  is denoted by  $\pi$ . The orientation of the link in which it intersects a sphere is of interest.

The detection of intersection between a right circular cone and a sphere  $S_{ob}$  can be accomplished by firstly considering the plane which contains the axis of the cone and the center of the sphere (assume the axis of the cone does not pass through the center of the sphere). This plane intersects the cone in an isosceles triangle and intersects the sphere in a circle. It is observed that when the circle intersects either one of the two equal sides (PA or PB) of the triangle (see Fig. 2.9), the cone may intersect the sphere.

In order to find the intersection of the cone and the sphere  $S_{ob}$ , the polar plane of the vertex  $P$  of the cone with respect to the sphere  $S_{ob}$  is obtained (see Fig. 2.10). This polar plane intersects the sphere  $S_{ob}$  in a circle  $C_s$ , and any tangent from  $P$  to  $S_{ob}$  has a point contact with the circle  $C_s$ .

A perspective projection is then used to project the circle  $C_s$  onto the base plane of the cone. The image of the circle  $C_s$  under this projection is a conic which can be an ellipse, a hyperbola, or a parabola. This can be perceived by considering a plane section of a second right circular cone  $CN_2$  whose vertex is point  $P$  and all elements of this cone have a point contact with  $C_s$ .

Figure 2.11 shows the circular cone  $CN_2$  and a section  $IV_1J$  of the cone by the plane  $\pi$  which is the base plane of  $CN_1$ . Here,  $V_1$  and  $V_2$  are the points of the curve  $IV_1J$  on the intersection of  $\pi$  and the plane perpendicular to  $\pi$  through the line  $PG$ , where  $G$  is the center of circle  $C_s$ . Let  $G'$  be the intersection of  $\pi$  and  $PG$ , and  $C$  be the point in which the bisector of the angle  $G'V_1P$  meets  $PG$ . The point  $C$  is at the same distance  $r_1$  from  $PV_1$  and from the line of symmetry  $V_1G'$  of the curve  $IV_1J$ ; and the perpendicular from  $C$  upon  $V_1G'$  is normal to the plane  $\pi$ , being in a plane perpendicular to  $\pi$ . A sphere of radius  $r_1$  can be generated with center at  $C$ . Let  $F_1$  denote the point where the sphere is tangent to the plane of the section and  $B_1$  denote the point where the sphere is tangent to the line  $PV_1$ . Since the cone is right circular, this sphere is tangent to each element of the cone, and all the points of tangency are on a circle  $B_1E_1$ . Further,  $D_1H_1$  is the line of intersection of the plane of the circle and the plane  $\pi$  and is perpendicular to  $B_1D_1$ .

Let  $M$  be any point of the curve in which the plane cuts the cone, and  $PLM$  the element of the cone through  $M$ ,  $L$  being its point of tangency to the sphere. Since  $MF_1$  and  $ML$  are tangents to the sphere from the same outside point, they are equal. Further, all the elements of the cone make the same angle with the plane  $E_1B_1L$ . Therefore, the line  $ML$  makes with this plane an angle equal to  $V_1B_1D_1$ . It follows that (Lehmann, 1964)

$$\frac{MF_1}{MN} = \frac{ML}{MN} = \frac{\sin \angle V_1D_1B_1}{\sin \angle V_1B_1D_1} = \text{const.} \quad (2.23)$$

where  $N$  is the foot of the perpendicular from  $M$  on the line  $D_1H_1$ . Thus the curve is a conic,  $F_1$  being the focus and  $D_1H_1$  the directrix.

When the angle  $V_1D_1B_1$  is less than the angle  $V_1B_1D_1$ , in which case the ratio in Eq. (2.23) is less than 1, the plane intersects all the elements of the cone and the section is an ellipse. As the angle  $V_1D_1B_1$  is taken smaller and smaller, the eccentricity becomes smaller and approaches the value 0, in which case the plane is normal to the axis of the cone and the plane section is a circle.

When the angle  $V_1D_1B_1$  is equal to the angle  $V_1B_1D_1$ , that is, when the line  $D_1V_1G'$  is parallel to the element  $PE_1$ , in which case plane  $\pi$  is parallel to  $PE_1$ , the ratio in Eq.(2.23) is equal to +1, and the plane section is a parabola.

When the angle  $V_1D_1B_1$  is greater than the angle  $V_1B_1D_1$ , in which case the ratio in Eq. (2.23) is greater than +1, the plane intersects only some of the elements of the cone and the section is one branch of a hyperbola, the other branch being the section of the cone obtained by extending the elements through  $P$ . If we take a plane through  $P$  parallel to plane  $\pi$ , it intersects the two cones in two elements;

when these are projected orthogonally upon plane  $\pi$ , the resulting lines are the asymptotes of the hyperbola, and their point of intersection, that is, the projection of  $P$ , is the center of the hyperbola.

Since the perspective projection preserves the incidence relation, the intersection of the projected conic and the base of the cone determines the location where elements of the cone intersect the sphere  $S_{ob}$ . The projected conic is symmetric with respect to the plane which contains the axis of the cone and the center of the sphere  $S_{ob}$ . Thus, the conic is symmetric with respect to the line connecting its center and the center of the base  $C_b$  of the cone (see Fig. 2.12). This observation is important in finding intersection points of the projected conic and the base of the cone.

### 2.5 Intersection of a Cone and a Cylinder

In this section, the problems of detection and determination of intersection of a right circular cone and a cylinder is discussed. In this study, a right circular cone, as stated in the previous section, is traced by a link with a fixed end while the other end lies on a circle. A cylinder is used to model a robot link in later application.

As shown in Fig. 2.13, let  $\Gamma_2$  be a plane which passes through the axis of a cylinder and being parallel to the axis of a cone and  $\Gamma_1$  be a plane which passes through the axis of the cone and is perpendicular to  $\Gamma_2$ . Using the plane sections of the cylinder and the cone in  $\Gamma_1$ , it can be shown that if the distance of the center of the plane section (an ellipse) of the cylinder to a line passing through one foot and



perpendicular to the base of the plane section (an isosceles triangle) of the cone is less than the radius of the cylinder, the cylinder and the cone will not intersect. Further, if the plane section of the cylinder in  $\Gamma_2$  does not intersect with the perspective projection of the cone from a point at infinity onto  $\Gamma_2$ , the cylinder and the cone will not intersect.

If the possibility of intersection between the cone and the cylinder is positive, it is necessary to determine the locations of intersection. This can be done by first projecting the cylinder from the vertex of the cone onto the base plane of the cone. Then, finding the intersection of the boundary of the projection figure and the base of the cone.

The perspective projection of a cylinder from the vertex to the base plane of a cone can be performed in three steps. First, the section of the cylinder between the base plane of the cone and a parallel plane passing the vertex of the cone is identified. Second, the two conics on both ends of the identified cylinder are projected. This results in two conics on the projection planes. Finally, the trunk of the cylinder is projected. This results in two line segments on the projection plane, and they are tangent to the above two conics (see Fig. 2.14).

In order to find the projection of a conic, a transformation matrix which is associated with this projection is determined. A projection transformation of a plane onto the other plane is completely determined by four distinct pairs of corresponding points, no three are colinear. Let the projection transformation be represented by a  $3 \times 3$  matrix  $[M]$  which transforms a point of a plane  $\pi$  in homogeneous coordinates onto a point in the projection plane  $\bar{\pi}$ , thus

$$\begin{bmatrix} \sigma \bar{x}_1 \\ \sigma \bar{x}_2 \\ \sigma \bar{x}_3 \end{bmatrix} = [M] \begin{bmatrix} x_1 \\ x_2 \\ x_3 \end{bmatrix} \quad (2.24)$$

and which has the inverse,

$$\begin{bmatrix} \mu x_1 \\ \mu x_2 \\ \mu x_3 \end{bmatrix} = [M]^{-1} \begin{bmatrix} \bar{x}_1 \\ \bar{x}_2 \\ \bar{x}_3 \end{bmatrix} \quad (2.25)$$

A conic  $f(X)$  in the plane  $\pi$  of the form,

$$f(X) = a_{ij}x_i x_j = 0 \quad (2.26)$$

is mapped into a conic  $g(\bar{X})$  in  $\bar{\pi}$  under this transformation and

$$g(\bar{X}) = b_{ij}\bar{x}_i \bar{x}_j = 0 \quad (2.27)$$

where  $b_{ij}$  can be determined by replacing  $x_i$  and  $x_j$  in Eq. (2.26) by Eq. (2.25).

The projection of the trunk of the cylinder is bounded by two line segments. In fact, these two line segments lie on the intersections of the projection plane and two planes passing through the center of the projection and being tangent to the cylinder. Note that if the cylinder intersects with the plane passing through the vertex of the cone and being parallel to the base plane of the cone, these two line segments have endpoints which are points at infinity.

By computing the intersection of these two projection conics and line segments with the base of the cone, the locations of the intersection between the cone and the cylinder are determined.

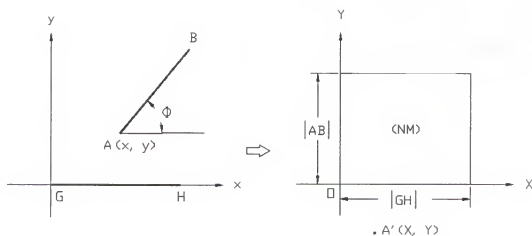


Fig. 2.1 Transformation of relative location of a pair of line segments.

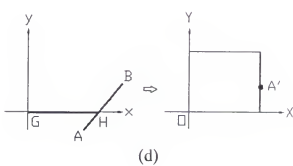
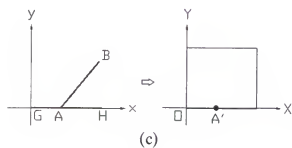
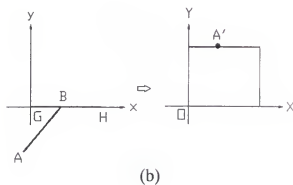
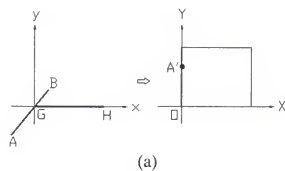


Fig. 2.2 possible cases for the image point being in the boundary of nonallowable manifold (NM).

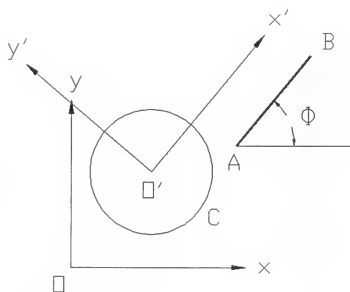


Fig. 2.3 Relative location of a line segment and a circle.

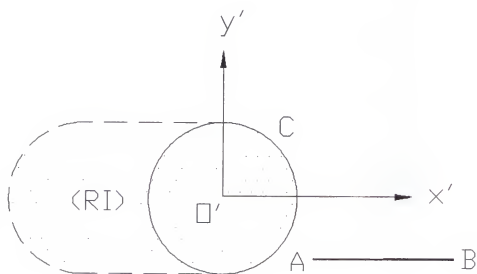
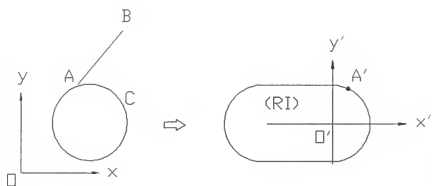
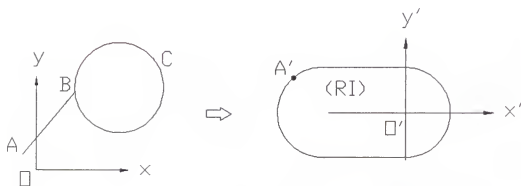


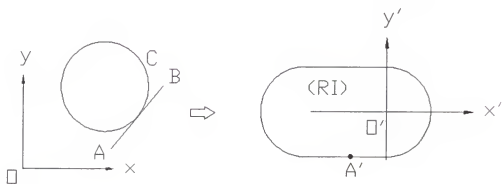
Fig. 2.4 Region of intersection.



(a)



(b)



(c)

Fig. 2.5 possible cases for the relative position being on the boundary of region of intersection (RI).



Fig. 2.6 Transform an ellipse into a circle.

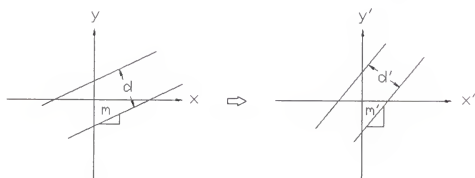


Fig. 2.7 Transformation of parallel lines.

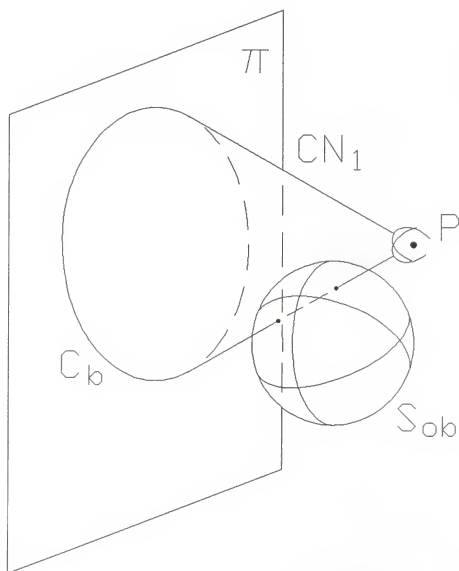


Fig. 2.8 A right circular cone and a sphere.

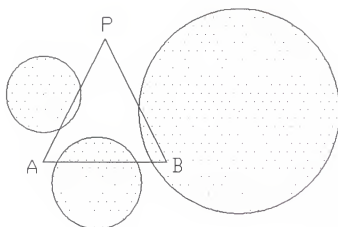


Fig. 2.9 Plane sections of cone and spheres.

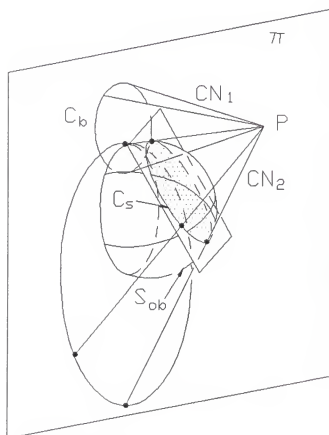


Fig. 2.10 Polar plane of P with respect to  $S_{ob}$ .



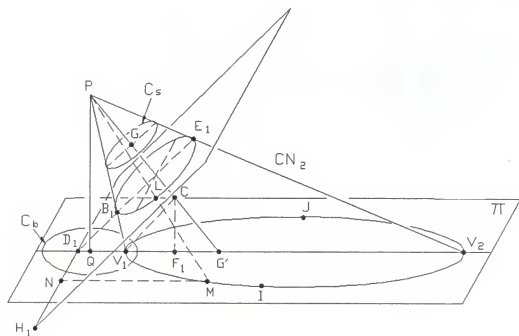


Fig. 2.11 Plane section of a cone.

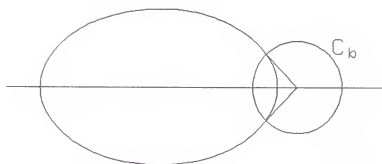


Fig. 2.12 Projection conic.

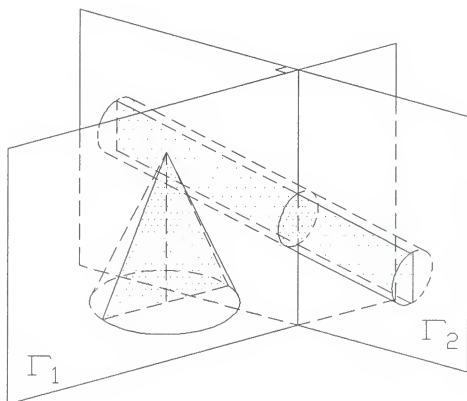


Fig. 2.13 A cone and a cylinder.

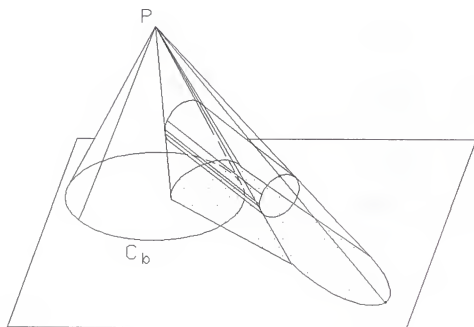


Fig. 2.14 Perspective projection of a cylinder.

### CHAPTER 3

#### INTERFERENCE AVOIDANCE OF LINE-SEGMENT-MODELED ROBOT MANIPULATORS

This chapter is devoted to the development of algorithms which are applied to a robot manipulator to avoid obstacles or a second robot manipulator in the workspace while following a prespecified path. The robot manipulators are modeled by a sequence of line segments connected by joints.

TRS robots and PUMA robots are considered in this study. The workspace of a TRS robot is bounded by two concentric spheres (Lovell, 1983). Due to the presence of the second joint offset, the workspace of the PUMA robot has a cylindrical inner boundary. The outer boundary is, however, a sphere (Krishnamurthy, 1985).

Permissible orientations which describe the geometric capability of a robot manipulator when its end effector is pinned at a point are discussed in Section 3.1. Then, the determination of allowable orientations of robot links in which they avoid interference with spherical and polyhedral obstacles is demonstrated in Section 3.2. In Section 3.3, a procedure for determining favorable orientations of the robot links is presented. It should be noted that the derivation of the allowable orientations and the favorable orientations of robot links are performed on a plane of operation which is the plane where the forearm of the robot lies. Finally, Section 3.4 discusses two types of operations that can be used for the coordination of two robot

manipulators working in a common workspace. The first type of operations is referred to as master-slave operations, and the second type of operations is referred to as parallel operations. Due to the complexity of the problem, the robots are restricted to rotary planar robots in the parallel operations.

In subsequent discussion, the analysis are mainly for the TRS robots unless otherwise specified. However, the analysis can be extended to the PUMA robots and can be found in separate sections.

### 3.1 Permissible Orientations of Robot Links

#### 3.1.1 Spatial Consideration

End effector. In order to determine the permissible orientations of the end effector of a TRS robot (Fig. 3.1) or a PUMA robot (Fig. 3.2), a reference coordinate system  $Oxyz$  can be selected such that its origin coincides with the intersection point of the first two joints of the robot, i.e., the shoulder of the robot. It is assumed that a path of the end effector has been specified. For a target point  $P(x_p, y_p, z_p)$  in the specified path, the end effector can be considered connected with the point P by a fixed hypothetical spherical joint. The wrist joint of the robot is thus free to move on a spherical surface which will be called constraint surface and can be determined by the intersection of the concentric spheres  $SP_{3\_i}$  and  $SP_{3\_o}$  centered at O and the sphere  $SP_3$  centered at P (see Fig. 3.3). For TRS robots (see Fig. 3.1), the radii of  $SP_3$ ,  $SP_{3\_i}$  and  $SP_{3\_o}$  are  $r_3 = S_{66}$ ,  $r_{3i} = |a_{23}S_{44}|$  and  $r_{3o} = a_{23} + S_{44}$ , respectively. For PUMA robots (see Fig. 3.2),  $r_3 = S_{66}$ ,  $r_{3i} = [(a_{23} - S_{44})^2 + (S_{22} - S_{33})^2]^{1/2}$  and  $r_{3o} = [(a_{23} + S_{44})^2 + (S_{22} - S_{33})^2]^{1/2}$ .

For convenience, a pair of transformations of coordinate system will be introduced (see Fig. 3.4). First the  $Ox'y'z'$  system is obtained by rotating the  $Oxyz$  system about the  $z$  axis through an angle  $\alpha$ . Next the  $Ox''y''z''$  system is derived by rotating the  $Ox'y'z'$  system about the  $y'$  axis through an angle  $(\pi/2-\beta)$ , where  $\alpha$  and  $\beta$  are given by

$$\alpha = \tan^{-1}(y_p / x_p) \quad (3.1)$$

and

$$\beta = \tan^{-1}(z_p / (x_p^2 + y_p^2)^{1/2}) \quad (3.2)$$

Using the  $Ox''y''z''$  coordinate system, the coordinates of the target point  $P$  become  $(0,0,d)$ , where  $d$  is the distance of the target point  $P$  to the origin  $O$ , i.e.,

$$d = (x_p^2 + y_p^2 + z_p^2)^{1/2} \quad (3.3)$$

The equations of the spheres  $SP_3$ ,  $SP_{3\_i}$  and  $SP_{3\_o}$  can be expressed in  $Oxyz$  system as follows

$$SP_3: x^2 + y^2 + (z - d)^2 = r_3^2 \quad (3.4)$$

$$SP_{3\_i}: x^2 + y^2 + z^2 = r_{3i}^2 \quad (3.5)$$

$$SP_{3\_o}: x^2 + y^2 + z^2 = r_{3o}^2 \quad (3.6)$$

The intersection of  $SP_3$  and  $SP_{3\_o}$  is a circle (assuming they intersect), the equation of which in parametric form is

$$\begin{aligned} x'' &= S_{66} \cos \delta_3 \cos u \\ y'' &= S_{66} \cos \delta_3 \sin u & 0 \leq u \leq 2\pi \\ z'' &= d + S_{66} \sin \delta_3 \end{aligned} \quad (3.7)$$

where  $\delta_3$  and  $u$  are latitude and longitude of the sphere  $SP_3$ . Analogously, the circle determined by the intersection of  $SP_3$  and  $SP_{3\_i}$  can be expressed in the same form by replacing  $\delta_3$  with  $\delta_4$  (see Fig. 3.5).

The permissible orientation of the end effector can be expressed in terms of the latitudes and longitudes of the sphere  $SP_3$ . Any point on the constraint surface can thus be represented in the  $Ox''y''z''$  coordinate system by

$$\begin{aligned}x'' &= S_{66}\cos v \cos u \\y'' &= S_{66}\cos v \sin u \\z'' &= d + S_{66}\sin v\end{aligned}\tag{3.8}$$

where  $\delta_4 \leq v \leq \delta_3$  and  $0 \leq u \leq 2\pi$ . Note that when  $SP_3$  and  $SP_{3\_0}$  do not intersect with each other,  $\delta_3 = \pi/2$  and when  $SP_3$  and  $SP_{3\_i}$  do not intersect with each other,  $\delta_4 = -\pi/2$ .

Upperarm and forearm. To determine the permissible orientations of the upperarm and the forearm, it is helpful to consider these two links together. Since the joint connecting the upperarm and the forearm of a TRS robot is a revolute joint, these two links will always lie on a plane passing through the  $z$  axis. In addition, this plane belongs to a pencil of planes with the  $z$  axis as the axis of the pencil (see Fig. 3.6). Two planes of this pencil which are tangent to the sphere  $SP_3$  determine the boundary of this pencil that the upperarm and the forearm can lie on. For convenience, these planes will be called planes of operation or  $\pi$  planes hereafter. In the work of Choi (1990) they are called the profile planes.

It is observed that each  $\pi$  plane intersects the sphere  $SP_3$  in a circle, with the exception of the pair of tangent planes which have a point contact with the sphere. The permissible orientation ranges of the upperarm and the forearm on a  $\pi$  plane depend upon where this  $\pi$  plane is located. In each  $\pi$  plane, the computation of the permissible orientations can be performed by considering the robot to be a planar 3R robot with three links. The lengths of the first two links are the same as those of the upperarm and the forearm of the TRS robot. Whereas, the length of the third link (the end effector) of the planar robot is equal to the radius of the circle of intersection of the  $\pi$  plane and the sphere  $SP_3$ . In addition, the center of the circle is the position where the reference point of the end effector of the planar robot is located (see Fig. 3.7).

Thus for each  $\pi$  plane, the permissible orientation ranges of the upperarm and the forearm can be computed by analyzing the motion capability of a planar 3R robot or a planar four-bar linkage which is presented in the next section. The permissible orientations of the upperarm and the forearm of the TRS robot can thus be determined by the union of the permissible orientations of these two links on each  $\pi$  plane.

### 3.1.2 Planar Consideration

When the position of a reference point on the end effector of a planar 3R robot is fixed, the mechanism of the planar robot becomes a four-bar linkage. The location of the wrist joint of the robot is restricted on a constraint curve which can be determined by the intersection of the concentric circle  $C_{3\_i}$  and  $C_{3\_o}$  centered at

the reference point  $P'$  and the circle  $C_3$  centered at shoulder  $O$  (see Fig. 3.8). In fact, this constraint curve is the intersection of the  $\pi$  plane where the robot links lie and the constraint surface described in Section 3.1.1. The constraint curve for the elbow joint can be derived analogously (see Fig. 3.9).

The permissible orientations of links for a planar four-bar mechanism are dependent upon its link lengths. A four-bar mechanism may be a so-called crank-rocker, double-crank or double-rocker linkage, depending on the range of motion of the two links connected to the ground link.

There are four possible types for the range of permissible end effector orientations according to whether the constraint circle  $C_3$  intersects the circles  $C_{3\_i}$  and  $C_{3\_o}$ . In other words, they depend upon the relationship between  $d + S_{66}$  and the radius of  $C_{3\_o}$ ,  $a_{23} + S_{44}$ , together with that between  $d - S_{66}$  and the radius of  $C_{3\_i}$ ,  $|a_{23} - S_{44}|$ , where  $d$ ,  $a_{23}$ ,  $S_{44}$ , and  $S_{66}$  are link lengths. These conditions are illustrated in Fig. 3.10(a) - (d). Similarly, four types can be obtained for the range of permissible upperarm orientations. However, for a given set of link lengths, the number of types is reduced. For instance, there are only three types for a robot with link lengths satisfying the conditions  $S_{44} > a_{23} > S_{66}$ . Each type is dependent upon the distance of the target point to the shoulder, viz.,  $d \geq a_{23} + S_{44} - S_{66}$ ,  $-a_{23} + S_{44} + S_{66} \leq d < a_{23} + S_{44} - S_{66}$  and  $d < -a_{23} + S_{44} + S_{66}$ . For each type, the configurations of the robot, i.e., elbow up (down) and wrist up (down), must be taken into account in order to determine the ranges of the permissible orientations of the upperarm and the end effector.

In conclusion, based upon the position of the target point and the desired configuration of the robot manipulator, ranges of permissible orientations for the upperarm and the end effector can be computed.



### 3.1.3 Permissible Orientations of PUMA Robots

Since there is an offset along the elbow joint, the upperarm and the forearm of a PUMA robot do not lie on the same plane. However, the upperarm and the forearm lie on a pair of parallel vertical planes separated by a fixed distance  $S_{33}$ , the offset of the elbow. Therefore, a pencil of pairs of vertical planes can be selected such that the upperarm lies on one, which is denoted by  $\pi_a$ , of the parallel planes and the forearm lies on the other, which is denoted by  $\pi_b$ , as shown in Fig. 3.11. The boundary of all possible plane pairs ( $\pi_a$  and  $\pi_b$ ) is determined by the two  $\pi_b$  planes which are tangent to the sphere  $SP_3$ . The upperarm and the forearm can lie on any plane pair between the boundary plane pairs.

In order to compute the permissible orientations of the upperarm and the forearm for a pair of specific  $\pi_a$  and  $\pi_b$  planes, it is necessary to introduce a hypothetical link  $a_{23}'$  which is a perspective projection of the upperarm onto the  $\pi_b$  plane from a center which is a point at infinity on a line normal to the planes  $\pi_a$  and  $\pi_b$ . The resulting mechanism in the plane  $\pi_b$  is a four-bar linkage, and the development for the TRS robots in the previous sections can be applied to the PUMA robots.

### 3.2 Allowable Orientations of Robot Links

The allowable orientations of a link are the orientations where the link does not collide with obstacles in the workspace. In this section, the upperarm and the forearm of a robot manipulator are assumed to be on a  $\pi$  plane. The computation

of allowable orientations of each link such that it avoids spherical and polyhedral obstacles is demonstrated.

### 3.2.1 Polyhedral Obstacles

If the  $\pi$  plane where the upperarm and the forearm lie intersects with an obstacle which is modeled by a convex polyhedron, the intersection is, in general, a polygon. Since the position of the shoulder of the manipulator is fixed, the upperarm sweeps a circular region in the  $\pi$  plane. The allowable orientations of the upperarm are then determined by a circular section with center O and radius  $a_{23}$  and which is outside the polygon.

The allowable orientations of the forearm are the orientations where the link does not intersect with the polygon. In order to find the allowable orientations, each side of the polygon needs to be considered in sequence. For each side of the polygon, a range of orientations within which the forearm does not intersect this side is determined by using the transformation for a pair of line segments. The intersection of these ranges of orientations for all sides of the polygon gives the allowable orientations of the forearm. However, if the endpoints of the forearm do not intersect with the polygon, in other words, the forearm is in a range of orientations where the upperarm and the end effector do not intersect the polygon, the forearm needs only to avoid all vertices of the polygon. This statement can be perceived by the description of possible boundary crossings in Section 2.1.

Refer to Fig. 3.12, the relation between the orientations of the forearm and the upperarm can be expressed in the form (Hunt 1978)

$$R_1 \cos \Phi_2 + R_2 \cos \Phi_3 - \cos(\Phi_2 - \Phi_3) + R_3 = 0 \quad (3.9)$$

where

$$R_1 = d / s_{44}$$

$$R_2 = d / a_{23}$$

$$R_3 = (s_{66}^2 - a_{23}^2 - s_{44}^2 - d^2) / 2a_{23}s_{44}$$

$a_{23}$ ,  $s_{44}$ , and  $s_{66}$  are link lengths,  $d$  is the distance of the fixed reference point on the end effector to the shoulder  $O$ , and  $\Phi_2$ ,  $\Phi_3$  are orientations of the upperarm and the forearm, respectively. For each  $\Phi_2$ , two values of  $\Phi_3$  can be computed which correspond to the wrist up and the wrist down configurations.

In order to check when the forearm intersects a line segment  $\overline{GH}$  in the same plane, the transformation presented in Section 2.1 can be applied. Suppose that the upperarm  $a_{23}$  rotates within an angular range, the relative locations of the forearm  $s_{44}$  and the line segment  $\overline{GH}$  can be transformed into a curve in a projection plane. The section of this curve outside the Nonallowable Manifold (NM) gives a range of orientations of the forearm within which the forearm does not intersect the line segment  $\overline{GH}$ . In Fig. 3.13, an illustration of image curve of relative location of the forearm with respect to a line segment is presented.

In order to find the image curve outside (NM), it is necessary to find the intersection point(s) of the image curve with the boundary of (NM). It is noted that if the upperarm and the end effector do not intersect line segment  $\overline{GH}$ , the image curve of the relative locations of the forearm and the line segment will not cross the

boundary of (NM) via cases (b) and (d) as described in Section 2.1. Therefore, only cases (a) and (c) are of interest.

When the image point is in the case (a), the following equation:

$$X = 0 \quad (3.10)$$

together with Eq. 3.9 must be satisfied simultaneously.

Replacing  $X$  by Eq. 2.6, Eq. 3.10 becomes

$$x - y \cot \Phi_3 = 0 \quad (3.11)$$

or

$$(a_{23} \cos \Phi_2 - x_G) - (a_{23} \sin \Phi_2 - y_G) \cot \Phi_3 = 0 \quad (3.12)$$

where  $(x_G, y_G)$  are coordinates of the endpoint  $G$  of the line segment  $\overline{GH}$ . Here, the line segment  $\overline{GH}$  is assumed to be parallel to the  $x$  axis of the reference coordinate system (see Fig. 3.12).

Equations 3.9 and 3.12 are both nonlinear with unknowns  $\Phi_2$  and  $\Phi_3$ . In order to solve a set of nonlinear equations, Newton's method (Conte and de Boor 1980) which has a quadratic convergence is used.

In order to find the allowable orientations of the end effector, it is necessary to consider the intersection of a circular cone and the polyhedral obstacle. For each face of the polyhedron, a perspective projection with center at the vertex of the cone can be used to project this face onto the base plane of the cone (see Fig. 3.14). The intersection of the projected polygon with the base of the cone can be used to determine the orientations of the end effector outside this face. The intersection of orientations of the end effector that do not collide with each face of the polyhedron gives the allowable orientations of the end effector.

It is necessary to identify the location of faces of a polyhedron before applying the projection. Let  $\Gamma$  be a plane passing through the vertex of the cone and parallel to the plane  $\pi$ , the base plane of the cone. Since intersection of a face and the cone may occur only at the section of the face that lies between the planes  $\pi$  and  $\Gamma$ , only this section of the face is of interest. As shown in Fig. 3.15, faces  $F_1$  and  $F_2$  do not lie between the planes  $\Gamma$  and  $\pi$ , thus these two faces will not intersect the cone and the projection is not necessary for them. In contrast, faces  $F_3$  and  $F_4$  intersect with  $\Gamma$  or  $\pi$ , and the projection is applied only to the sections of the faces which lie between the planes  $\Gamma$  and  $\pi$ .

### 3.2.2 Spherical Obstacles

In general, the intersection of a  $\pi$  plane and a spherical obstacle  $S_{ob}$  (assuming they intersect) is a circle which will be denoted by  $C_{ob}$  (Fig. 3.16). Therefore, the allowable orientation range of the upperarm is determined by a circular section with center O (shoulder) and radius  $a_{23}$  (upperarm length) which is outside the circle  $C_{ob}$ .

The endpoints of the forearm are constrained by the elbow and the wrist joints which are moving along circular arcs. In order to find the allowable orientations where the forearm avoids the circle  $C_{ob}$ , the transformation for the relative position of a line segment and a circle as described in Section 2.2 can be used. In Fig. 3.17, an illustration of image curve of relative positions of the forearm with respect to a circle is presented. In order to find the image curve outside (RI), the numerical procedure presented in the previous section is used.

When the upperarm and the forearm lie on a  $\pi$  plane, the end effector lies on a right circular cone. The vertex of this cone is the target point P and the base  $C_b$  of this cone lies on the  $\pi$  plane. The detection of intersection between a right circular cone and a sphere can then be accomplished by using the perspective projection described in Section 2.4.

### 3.3 Favorable Orientations

In the previous section, the ranges of allowable orientation of three links of the robot have been computed. In order to determine the favorable orientations of a robot with respect to a specific  $\pi$  plane, the following procedure will be used:

- (a) Determine the orientations of the upperarm corresponding to the allowable orientations of the end effector.
- (b) Determine the intersection of the allowable orientations of the upperarm and the orientations found in (a).
- (c) Determine the orientations of the upperarm in the region obtained in (b) such that the forearm is in its allowable orientation range.

This procedure yields an orientation range of the upperarm within which all links of the robot do not intersect the obstacles.

Finally, it is necessary to emphasize that the robot manipulator is to follow a prespecified path. At any instant, a target point is specified and a series of  $\pi$  planes is obtained based upon the location of the upperarm and the forearm at the previous instant and the velocity constraint on the base joint of the robot. For each  $\pi$  plane, a range of favorable orientations can be obtained. The location of the  $\pi$

plane where the robot has a local maximum favorable orientation range can be identified numerically, and the upperarm and the forearm of the robot is relocated at this  $\pi$  plane. The robot can have joint angles within the favorable orientations and is guaranteed to be free from collision.

### 3.4 Coordination of Two Robot Manipulators

Due to high complexity in the computation, two simplified operations are considered here, and strategies are proposed which are applied to the two types of operations.

The first type of operations is referred to as master-slave operations. In this type of operations, one robot manipulator is assigned as the master and the motion of which has precedence over that of the second robot manipulator (the slave). The slave robot must adapt its motion to the master robot.

The second type of operations is referred to as parallel operations. In this type of operations, both robot manipulators possess the same status, and they must accommodate to each other. Further, the manipulators are modeled by rotary planar manipulators. By a rotary planar manipulator we mean a manipulator whose links with revolute joints lie in a plane which can rotate around the vertical axis of the robot's base. It is assumed that the links of a robot manipulator always lie on the same plane during the motion.

#### 3.4.1 Master-Slave Operations

It is assumed that the motion of the master robot has been completely specified. In other words, the locations of links of the master robot are known at

any time during the motion. The slave robot is to avoid interference with the links of the master robot while tracking a specified trajectory.

Following the analysis in Section 3.1, when the upperarm and the forearm of the slave robot lie on a  $\pi$  plane, this plane will intersect the links of the master robot in points unless the links of the master robot lie on this plane. Therefore, in order to avoid interference with the master robot, the upperarm and the forearm of the slave robot must avoid intersecting these points.

The area swept by the upperarm is a circular region with radius equal to its link length. If a point lies within this circular region, the upperarm may intersect this point. To compute an allowable orientation range, it is necessary to find the orientation where the upperarm intersects the point. This orientation will divide the permissible orientations into two regions. Based upon the orientation of the upperarm at the previous time instant, one of the permissible orientation regions is selected as the allowable orientation region.

The end points of the forearm are constrained by the elbow joint and the wrist joint which are moving along circular arcs. Therefore, the forearm's orientation, as well as the positions of its end points, varies constantly. In order to determine where the forearm intersects a point, the transformation for relative locations of a line segment and a point can be used.

After finding the orientations where the forearm intersects a point, a range of orientations can be obtained which is consistent with the orientation of the forearm at the previous time instant to avoid interference.



As described in the previous section, the end effector encloses a right circular cone when the upperarm and the forearm lie on a specific  $\pi$  plane. In order to find the location where the end effector intersects a link of the master robot, a perspective projection can be applied. This projection projects each link of the master robot from the vertex of the cone into a line segment in the base plane of the cone. Since the end effector lies on one side of the base plane, only the section of the line segment that lies on the same side as the end effector is of interest. The intersection point(s) of the projected line segment and the base of the cone can be used to find the location where the end effector intersects the links of the master robot. Finally, the  $\pi$  plane where the robot manipulator has the largest favorable orientation range is computed numerically.

### 3.4.2 Parallel Operations

In this section, two robot manipulators are considered having the same status. To perform the operation, each robot manipulator has been assigned a trajectory regardless of orientation. One robot manipulator has to avoid interference with the other based upon the information of target positions and motion capability of links of both robot manipulators.

At any instant, in order to obtain a configuration for each robot manipulator to avoid interference, it is necessary to determine first a specific  $\pi$  plane where the upperarm and the forearm lie and then a set of joint angles that the manipulator holds. This will unavoidably bring significant complexity into analysis. In order to simplify the analysis, it is convenient to place the upperarm and the forearm of the

robot manipulator on a specific  $\pi$  plane, in particular, the plane which passes through the specified target point of the end effector. In this perspective, all three links of the robot manipulator will lie on this  $\pi$  plane. This implies that 2 degrees of freedom (DOF) in the wrist joint will become inactive and the robot manipulator becomes 4 DOF. Therefore, the interference avoidance problem between two TRS robots is reduced to that between two planar 3R robot manipulators on different planes in space.

Forbidden regions. When two robot manipulators lie on two different planes in the space, the only possible location for interference is at the intersection line of these two planes. As shown in Fig. 3.18, one TRS robot lies on the plane  $\pi_1$ , and the other TRS robot lies on the plane  $\pi_2$ . The line  $l$  is the intersection of the planes  $\pi_1$  and  $\pi_2$ . The points  $P_1$  and  $P_2$  are target points for the end effectors of two robot manipulators.

As the links of one robot manipulator move within the permissible orientation range, the links will intersect  $l$  in points which form one or two line segments. In the following analysis, only one line segment case is considered. The two line segments case can be analyzed similarly.

In order to find the endpoints of the line segment, it is convenient to discuss the intersection of  $l$  and each link of the robot manipulator separately. The union of the line segments determined from each link yields the positions where the robot links may intersect  $l$ .

The endpoints of a line segment generated by the intersection of  $l$  and the upperarm or the end effector can be obtained by considering the intersection of  $l$

and a circular sector. The endpoints of a line segment generated by the intersection of  $l$  and the forearm cannot be derived explicitly. Thus, an approximation for the endpoints will be obtained by the aid of intersection points of  $l$  and tangents from the circle  $C_2$  to the circle  $C_3$ . In Fig. 3.19, the approximated boundaries for the locations of the links of a robot manipulator are illustrated, where the robot manipulator has link lengths  $a_{23} = 44$ ,  $S_{44} = 55$ , and  $S_{66} = 15$  units.

At the elbow up and wrist up configuration, the upper bound of the forearm is approximated by a tangent from the elbow  $A_2$  to the circle  $C_3$ . At the elbow up and wrist down configuration, the lower bound of the forearm is approximated by a tangent from  $A_1$  or  $A_2$  to the circle  $C_3$ . The object of making an approximation is to confine the forearm by lines through extreme positions of the elbow joint or the wrist joint and tangent points on  $C_2$  and  $C_3$ . A comparison of the exact bound and the approximated bound of a region swept by the links of a robot manipulator is shown in Fig. 3.20.

The intersection of the bounded region and the line  $l$  represents the region where the links of a robot manipulator may traverse  $l$ . Thus, two robot manipulators determine two segments of  $l$  along which they are able to traverse. If these two segments intersect, the links of the two robot manipulators may interfere. In order to avoid interference, it is proposed to divide the overlapping region into two segments of same length. One robot manipulator must avoid moving along one segment while the other robot manipulator avoids moving along the other segment. The segment within which a robot manipulator cannot have motion is called the forbidden region of that robot manipulator. Using this concept, the allowable

orientations of a robot link can be defined as the orientations in which the link does not intersect the forbidden region.

Allowable orientations. The upperarm is connected to the shoulder which is fixed whilst the end effector is instantaneously joined to a fixed target point. Thus the area swept by the upperarm and the end effector are circular regions with radii equal to the link lengths. When the forbidden region lies within the circular region, the link may intersect the forbidden region. In this situation, the allowable orientation range is determined either by the intersection points of the forbidden region and the boundary of the circular region or by the endpoints of the forbidden region.

The endpoints of the forearm are constrained by the elbow joint and the wrist joint which are moving along circular arcs. In order to find the allowable orientations of the forearm, the affine transformation introduced in Section 2.1 can be applied.

After finding the allowable orientations, the procedure presented in Section 3.3 can be used to find the favorable orientations for each robot manipulator. The robot links can thus flex within their favorable orientation range and avoid interference with the links of the other robot manipulator.

### 3.4.3 PUMA Robots

Analogous to the TRS robots case, at any instant a specific pair of  $\pi_a$  and  $\pi_b$  planes can be chosen such that the complicated 3-D problem is reduced to an easier

2-D problem. In order to achieve this, the specific plane pair is selected as the one whose  $\pi_b$  plane containing the target point of the end effector. Thus, both the forearm and the end effector lie on the  $\pi_b$  plane.

For the master-slave operation, the master robot intersects the specific plane pairs of the slave robot in points. The allowable orientations of a link of the slave robot are the orientations where the link avoids intersecting these points.

For the parallel operation, in order to compute a range of allowable orientations for each link of the PUMA robots, forbidden regions are assigned to each robot. In order to determine the forbidden region for each PUMA robot, it is necessary to consider the intersection lines of the selected plane pair of one robot and that of the other robot. As a result, there are two forbidden regions on each selected plane and they lie on the intersection lines of this plane and the selected pair of planes of the other robot. The forbidden regions are line segments and the determination of the endpoints of them is analogous to that for the TRS robot.

In order to find the allowable orientations of the upperarm and the end effector, it is necessary to consider the plane containing each of them, i.e., the selected planes  $\pi_a$  and  $\pi_b$  respectively. The upperarm must lie outside the two forbidden regions in the plane  $\pi_a$  to avoid interference. Analogously, the end effector must lie outside the forbidden regions in the plane  $\pi_b$ . The procedure in Section 3.4.2 can be applied to each plane to find the corresponding allowable orientations of the upperarm and the end effector.

In order to find the allowable orientations of the forearm, the hypothetical link  $a_{23}'$  (which is the projection of the forearm on plane  $\pi_b$ ) introduced in Section

3.1.3 can be used. As a result, the mechanism formed becomes a four-bar linkage in the  $\pi_b$  plane and the allowable orientations of the forearm can be computed following the procedure in Section 3.4.2.

After computing the allowable orientations of each link of the PUMA robot, the favorable orientations can be determined by following the procedures in Section 3.3.

### 3.5 Computation of Joint Angles

In the previous sections, the orientations of links of a robot manipulator are determined which are measured with respect to a horizontal plane. However, in order to control the motion of a robot, it is necessary to determine the angular displacements of the joints of the robot. The purpose of this section is to derive the joint angular displacements from the orientations of robot links.

A kinematic model of a TRS robot is shown in Fig. 3.21. The notation used in the analysis is developed by Duffy (1980). Briefly stated, suppose a link of a manipulator is connected by two kinematic joints with axes  $\underline{S}_i$  and  $\underline{S}_j$ . The perpendicular distance between the joint axes is  $a_{ij}$  and the unit vector along the mutual perpendicular is  $\underline{a}_{ij}$ . The twist angle between the joint axes is represented by  $\alpha_{ij}$  and is measured in a right handed sense about the vector  $\underline{a}_{ij}$ .

Further, the perpendicular distance between two links connected by a revolute joint, specifically the perpendicular distance between the vectors  $\underline{a}_{ij}$  and  $\underline{a}_{jk}$ , is denoted by the offset distance  $S_{ij}$ . The relative angle between two links is represented by  $\theta_{ij}$  and is measured in a right handed sense about the unit vector  $\underline{S}_j$ .

A world coordinate system,  $x_0y_0z_0$ , is located with the z-axis coaxial with  $\underline{S}_1$  and the x- and y-axes are in the plane of rotation of  $\underline{a}_{12}$ . For a target point  $\underline{P}$  in the world frame, the orientations of links of the robot are derived and are given by four parameters  $\Phi_1$ ,  $\Phi_2$ ,  $\Phi_3$ , and  $\Phi_4$ .  $\Phi_1$  is the angle measured between the x-z plane in the world frame and the  $\pi$  plane where the upperarm and the forearm of the robot lie.  $\Phi_2$ , and  $\Phi_3$  are respectively the orientations of the upperarm and the forearm.  $\Phi_4$  is the orientation of the projection of the end effector on the  $\pi$  plane.  $\Phi_2$ ,  $\Phi_3$ , and  $\Phi_4$  are measured with respect to the x-y plane of the world coordinate system.

The joint angles  $\Theta_2$  and  $\Theta_3$  of the robot are given by the following:

$$\Theta_2 = \Phi_2 \quad (3.13)$$

$$\Theta_3 = \Phi_3 - \Phi_2 + \pi/2 \quad (3.14)$$

The determination of the joint angles  $\Theta_4$  and  $\Theta_5$  requires the derivation of the unit vector  $\underline{S}_6$  of the axis of the end effector. This can be accomplished by first finding the position of the wrist joint (the spherical joint) of the robot. Denoting this by  $\underline{Q}(x_q, y_q, z_q)$ , the position vector of the wrist joint in the world coordinate system is given by

$$\begin{bmatrix} x_q \\ y_q \\ z_q \end{bmatrix} = [R(z, -\Phi_1)] \begin{bmatrix} a_{23}\cos\Phi_2 + S_{44}\cos\Phi_3 \\ 0 \\ a_{23}\sin\Phi_2 + S_{44}\sin\Phi_3 \end{bmatrix} \quad (3.15)$$

where  $[R(z, -\Phi_1)]^1$  is the rotation matrix which rotates a coordinate frame about the  $z$ -axis by an angle  $-\Phi_1$  and is given by

$$[R(z, -\Phi_1)] = \begin{bmatrix} \cos\Phi_1 & -\sin\Phi_1 & 0 \\ \sin\Phi_1 & \sin\Phi_1 & 0 \\ 0 & 0 & 1 \end{bmatrix} \quad (3.16)$$

The unit vector of the axis of the end effector  $\underline{S}_6^{(0)}$  in the world coordinate system is then given by

$$\underline{S}_6^{(0)} = \frac{\underline{P} - \underline{Q}}{|\underline{P} - \underline{Q}|} \quad (3.17)$$

We associate with each joint of the robot a dextral coordinate system; the  $x_{ij}y_{ij}z_{ij}$  system has coordinate vectors  $\underline{a}_{ij}$ ,  $\underline{S}_i \times \underline{a}_{ij}$ ,  $\underline{S}_j$ , where  $ij = 12, 23, \dots, 67$ . The rotation matrix which transforms the coordinates of a vector in the  $x_{ij}y_{ij}z_{ij}$  system to those of the  $x_jy_jz_j$  system is denoted by  $[A_{ij}]$  and

$$[A_{ij}] = [R(z, \Theta_j)] [R(x, \alpha_{ij})]$$

$$= \begin{bmatrix} C_j & S_j & 0 \\ -S_j & C_j & 0 \\ 0 & 0 & 1 \end{bmatrix} \begin{bmatrix} 1 & 0 & 0 \\ 0 & C_{ij} & S_{ij} \\ 0 & -S_{ij} & C_{ij} \end{bmatrix} \quad (3.18)$$

where  $C_j = \cos\Theta_j$ ,  $S_j = \sin\Theta_j$ ,  $C_{ij} = \cos\alpha_{ij}$  and  $S_{ij} = \sin\alpha_{ij}$ .

---

<sup>1</sup>Rotation matrices which effect rotations about the  $x$ -axis and  $y$ -axis by an angle  $\Phi$  are represented by  $[R(x, \Phi)]$  and  $[R(y, \Phi)]$ .



The unit vector of the axis of the end effector  $\underline{S}_6^{(3)}$  in the  $x_3y_3z_3$  system which has coordinate vectors  $\underline{a}_{34}$ ,  $\underline{S}_3 \times \underline{a}_{34}$ ,  $\underline{S}_3$  is determined by transforming  $\underline{S}_6^{(0)}$  from the world coordinate system to the  $x_3y_3z_3$  system and is expressed by

$$\begin{aligned}\underline{S}_6^{(3)} &= [A_{03}]\underline{S}_6^{(0)} \\ &= [A_{23}][A_{12}][A_{01}]\underline{S}_6^{(0)}\end{aligned}\quad (3.19)$$

where  $[A_{01}] = R[(z, \Phi_1)]$ .

Further,  $\underline{S}_6^{(3)}$  can be derived by transformed the unit vector  $\underline{S}_6^{(6)} = (0, 0, 1)$  from the  $x_6y_6z_6$  system to the  $x_3y_3z_3$  system, and is given by

$$\underline{S}_6^{(3)} = (X_{54}, Y_{54}, Z_{54}) \quad (3.20)$$

where, by definition,

$$\begin{aligned}X_{54} &= \bar{X}_5 C_4 - \bar{Y}_5 S_4 \\ Y_{54} &= C_{34}(\bar{X}_5 S_4 + \bar{Y}_5 C_4) - S_{34} \bar{Z}_5 \\ Z_{54} &= S_{34}(\bar{X}_5 S_4 + \bar{Y}_5 C_4) + C_{34} \bar{Z}_5\end{aligned}\quad (3.21)$$

$$\begin{aligned}\bar{X}_5 &= S_{56} S_5 \\ \bar{Y}_5 &= -(S_{45} C_{56} + C_{45} S_{56} C_5) \\ \bar{Z}_5 &= C_{45} C_{56} - S_{45} S_{56} C_5\end{aligned}\quad (3.22)$$

Equating Eqs. (3.19) and (3.20), we can solve for  $\Theta_4$  and  $\Theta_5$ . In this work, since the orientation of the end effector is considered a free parameter,  $\Theta_6$  is undefined.

Similarly, the joint angles of a PUMA robot can be computed. Fig. 3.22 shows a kinematic model of a PUMA robot. Note that due to the offsets in the second and third joints, the position vector of the wrist joint of the robot is given by

$$\begin{bmatrix} x_q \\ y_q \\ z_q \end{bmatrix} = [R(z, -\Phi_1)] \begin{bmatrix} a_{23}\cos\Phi_2 + S_{44}\cos\Phi_3 \\ S_{22} - S_{33} \\ a_{23}\sin\Phi_2 + S_{44}\sin\Phi_3 \end{bmatrix} \quad (3.23)$$

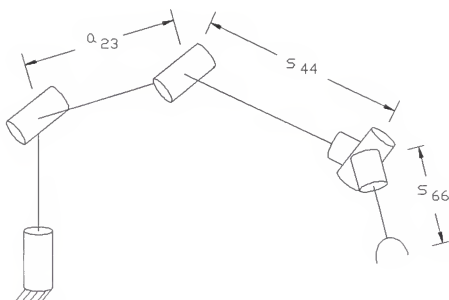


Fig. 3.1 TRS type robot.

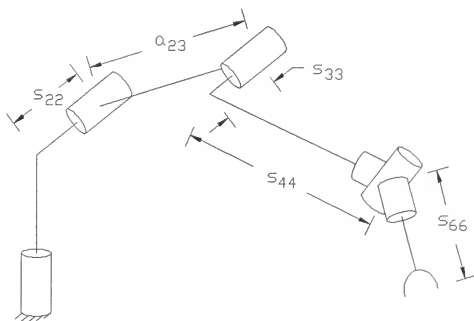


Fig. 3.2 PUMA robot.

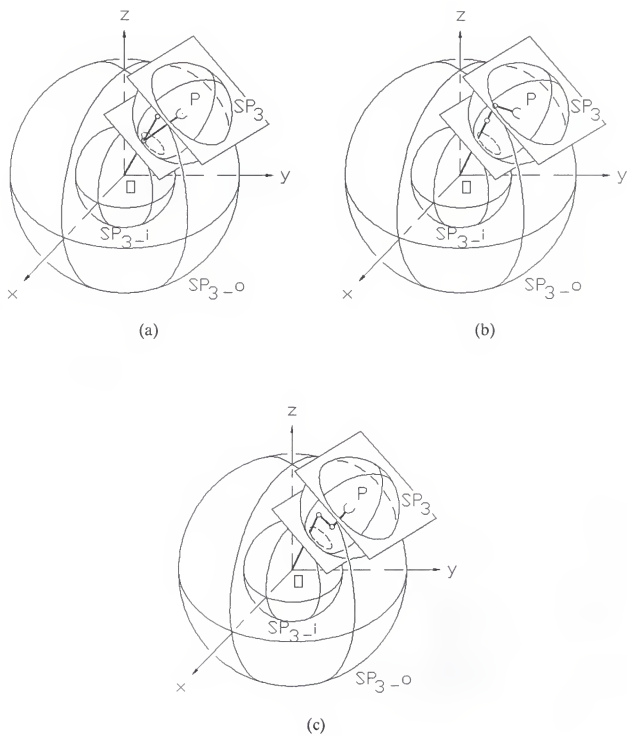


Fig. 3.3 Constraint surface of wrist joint.

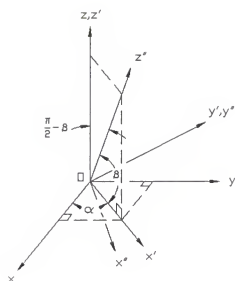
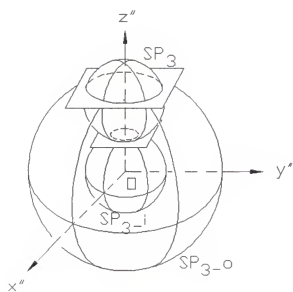
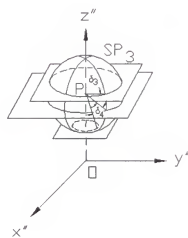


Fig. 3.4 Transformation of coordinate system.



(a)



(b)

Fig. 3.5 Permissible orientations of end effector.

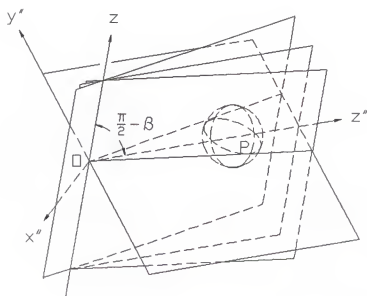


Fig. 3.6 A pencil of planes.

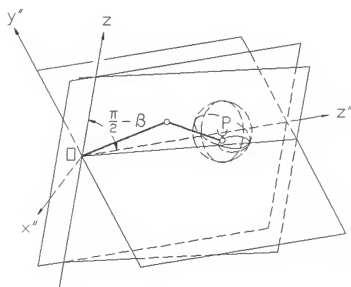


Fig. 3.7 The upperarm and the forearm are on a  $\pi$  plane.

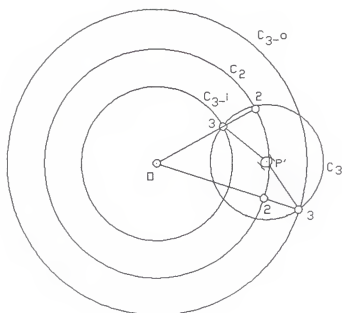


Fig. 3.8 Constraint curve of wrist.

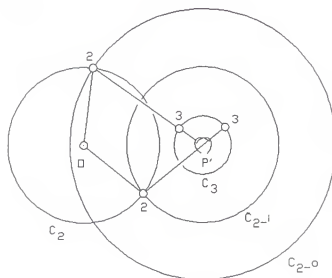
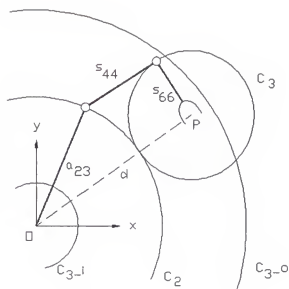
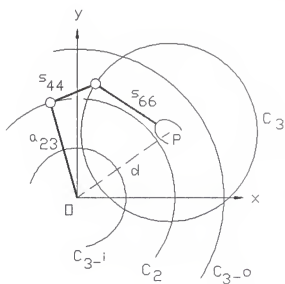


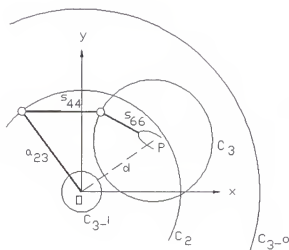
Fig. 3.9 Constraint curve of elbow.



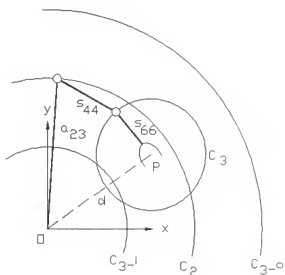
$$(a) \begin{aligned} d + s_{66} &\geq a_{23} + s_{44} \\ d - s_{66} &> |a_{23} - s_{44}| \end{aligned}$$



$$(b) \begin{aligned} d + s_{66} &\geq a_{23} + s_{44} \\ d - s_{66} &\leq |a_{23} - s_{44}| \end{aligned}$$



$$(c) \begin{aligned} d + s_{66} &< a_{23} + s_{44} \\ d - s_{66} &> |a_{23} - s_{44}| \end{aligned}$$



$$(d) \begin{aligned} d + s_{66} &< a_{23} + s_{44} \\ d - s_{66} &\leq |a_{23} - s_{44}| \end{aligned}$$

Fig. 3.10 Permissible orientations of end effector.



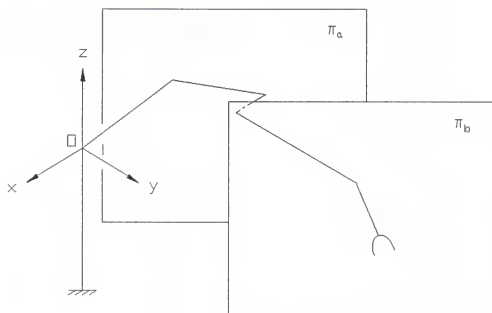


Fig. 3.11 The upperarm and forearm of a PUMA robot lie on two parallel vertical planes.

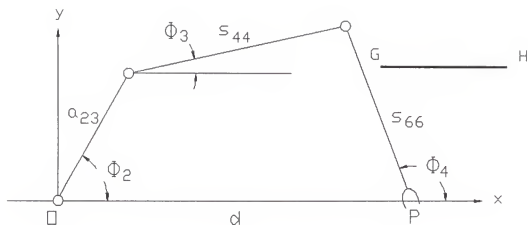


Fig. 3.12 Planar 3R robot and a line segment GH.

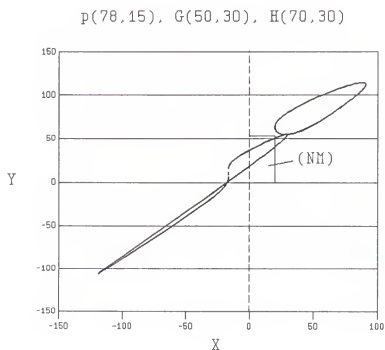


Fig. 3.13 Image curve of relative location of the forearm and a line segment.

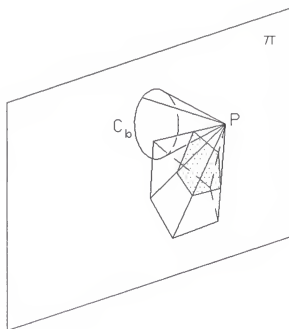


Fig. 3.14 Perspective projection of a face onto the  $\pi$  plane.

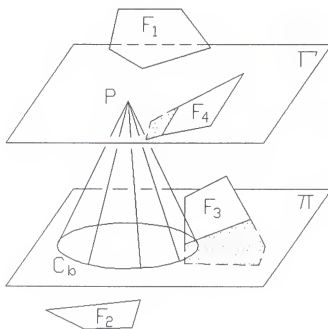


Fig. 3.15 Sections of faces between planes  $\Gamma$  and  $\pi$  are effective.

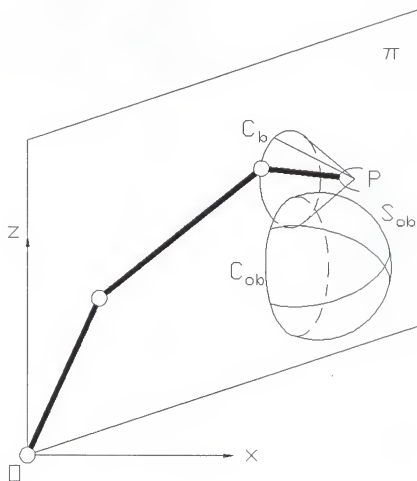
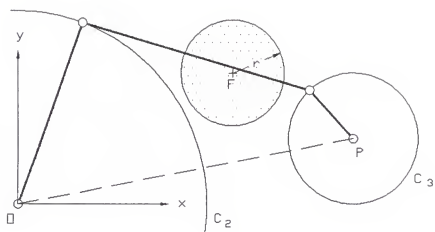


Fig. 3.16 Intersection of  $\pi$  plane and a sphere.



$$P = (78, 15); F = (50, 30)$$

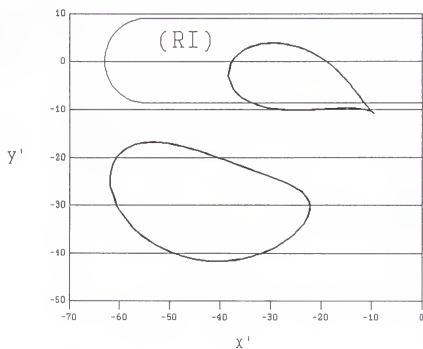


Fig. 3.17 Image curve of relative positions of the forearm and a circle.

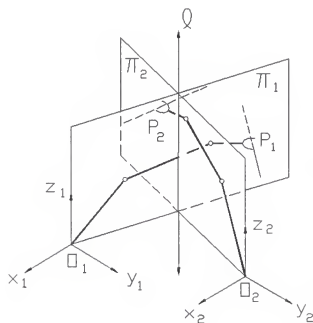
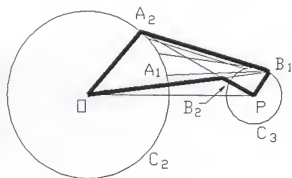
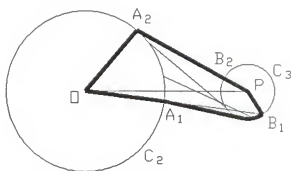


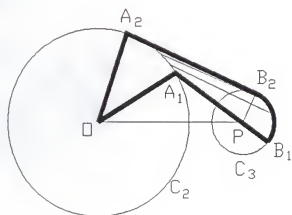
Fig. 3.18 Two robot manipulators lie on different planes.



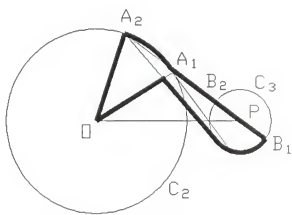
(a)  $P(90,0)$ , elbow up,  
wrist up



(b)  $P(90,0)$ , elbow up,  
wrist down



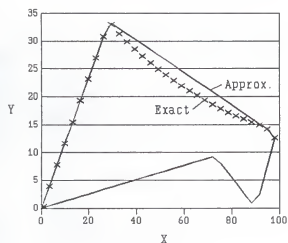
(c)  $P(70,0)$ , elbow up,  
wrist up



(d)  $P(70,0)$ , elbow up,  
wrist down

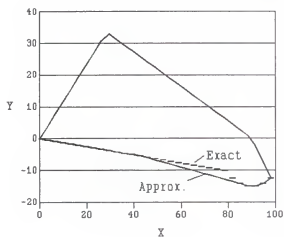
Fig. 3.19 Approximated boundaries of links of a robot.

P:(90,0), Elbow up, Wrist up



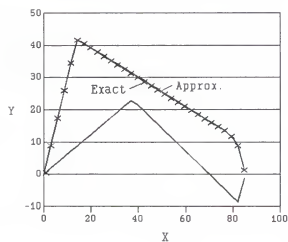
(a)

P:(90,0), Elbow up, Wrist down



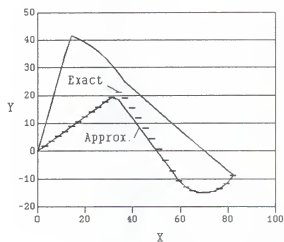
(b)

P:(70,0), Elbow up, Wrist up



(c)

P:(70,0), Elbow up, Wrist down



(d)

Fig. 3.20 Exact bound and approximated bound.



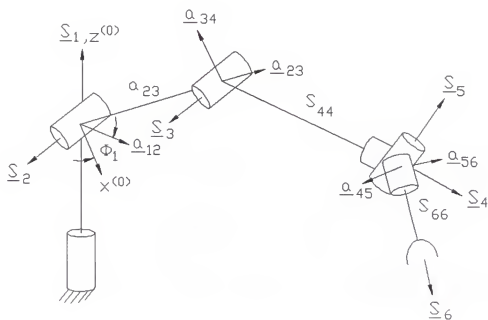


Fig. 3.21 Kinematic model of a TRS robot.

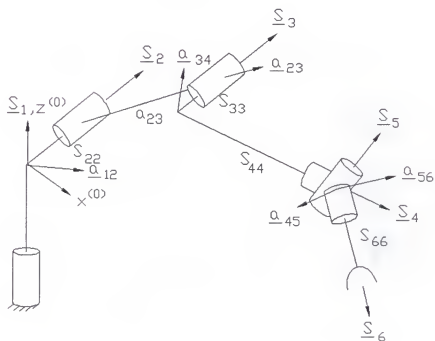


Fig. 3.22 Kinematic model of a PUMA robot.

## CHAPTER 4

### INTERFERENCE AVOIDANCE OF ROBOT MANIPULATORS WITH SOLID LINKS

In the previous chapter, the manipulator's links are modeled by line segments. However, all industrial robot manipulators have solid links with cross section dimensions. Therefore, to be practical, it is essential to consider the manipulators as consisting of a sequence of solid links connected by joints. In this chapter, the upperarm and the forearm of a manipulator are modeled by parallelepipeds, and the end effector is modeled by a cylinder.

In order to extend the interference avoidance algorithms developed in Chapter 3 to manipulators with solid links, it is desirable to expand the obstacles to compensate for the cross section dimensions of the links. The links can then be treated as line segments. For the problems of coordination of two robot manipulators, the master-slave operations are solved by considering the master robot as obstacles consisting of parallelepipeds and cylinders; the parallel operations are solved by modifying forbidden regions from line segments to rectangles.

#### 4.1 Expansion of Obstacles

The idea of expanding obstacles to compensate for the size of links appeared first in the work of Udupa [1977]. Lozano-Perez and Wesley [1979] then used this

idea to compute a configuration space of an object translating in space. The expansion of obstacles to compensate for the cross sections of links of a spatial robot can be found in Tseng [1987], where a thorough discussion of the expansion of obstacles with vertical sides and flat top and bottom is presented. The method used for expanding a convex polygon is to expand each side of the polygon and then introduces new sides to complete the expanded polygon. The amount of expansion is  $(W^2 + T^2)^{1/2}/2$ , where  $W$  and  $T$  are the width and the thickness, respectively, of a link of the robot. This is equivalent to treating the robot links as cylinders with radius  $(W^2 + T^2)^{1/2}/2$ .

In this work, the links of a TRS robot are modeled by two parallelepipeds and one cylinder as shown in Fig. 4.1. The upperarm is modeled by a parallelepiped of width  $W_u$  and thickness  $T_u$ . Similarly, the cross section dimensions of the forearm are represented by  $W_f$  and  $T_f$ . Since the upperarm can rotate about the base and shoulder joints while the forearm can rotate about the elbow joint, the vertical sides of these two links will remain vertical whatever the locations of these links are. The end effector is modeled by a cylinder of radius  $r_e$ , and can rotate about the wrist joint which is a spherical joint.

In the following, a supplemental discussion of obstacles expansion to compensate for the links of a robot manipulator is presented. Consider first a polyhedral obstacle with vertical sides and horizontal top and bottom. It can be seen from Fig. 4.2 that if the vertical sides of the obstacle are expanded horizontally along their normal directions by an amount  $W/2$ , a link will not intersect the obstacle if the central line of the link does not intersect the vertical sides of the expanded

obstacle, where  $W$  is the transverse dimension of the link. For the upperarm and the forearm  $W$  is the width of the arm, for the end effector  $W$  is the radius of the end effector. Similarly, the expansion of the top and bottom faces is performed by translating the faces vertically along their normal directions by an amount  $T/2$ , where  $T$  can be the thickness of the upperarm, the thickness of the forearm or the radius of the end effector.

If the faces of a polyhedral obstacle are neither vertical nor horizontal, the normal vector of each face has components on both vertical and horizontal directions. In this case, the amount of expansion along the plane normal is  $(W_u^2 + T_u^2)^{1/2}/2$ ,  $(W_f^2 + T_f^2)^{1/2}/2$ , or  $r_e$ , depending on which link is under consideration (see Fig. 4.3).

The expansion of a spherical obstacle is performed by increasing the radius of the sphere by an amount determined by the cross section dimensions of robot links. When computing the orientations of the upperarm and the forearm, the increment used is  $(W_u^2 + T_u^2)^{1/2}/2$  and  $(W_f^2 + T_f^2)^{1/2}/2$ , respectively. For the end effector, the increment is the radius of the cylindrical model,  $r_e$ .

#### 4.2 Master-Slave Operations of Two Robot Manipulators

As described in Section 3.4, two types of operations for the coordinated motions of two robot manipulators have been considered. In this section, allowable orientations of robot manipulators with solid links performing master-slave operations are discussed. The motion of the master robot is assumed completely specified. The motion of the slave robot is to be determined in order to avoid interference with the links of the master robot.

### 4.2.1 Allowable Orientations of Upperarm

Consider that the central lines of the upperarm and the forearm of the slave robot lie on a plane of operation or a  $\pi$  plane (see Fig. 4.4) as described in Chapter 3. In order to avoid interference with the links of the master robot, these two links need to avoid interference with two parallelepipeds, which are used to model the upperarm and the forearm of the master robot, and one cylinder, which is used to model the end effector of the master robot.

When the central line of the upperarm is constrained to lie on a  $\pi$  plane, the region swept by the upperarm is a circular region with radius equal to the distance from the axis of rotation to the end of the link and thickness equal to the width of the link. This region is denoted by  $\Omega_u$  (Fig. 4.5). If the links of the master robot lie within this region, the upperarm of the slave robot may interfere with the master robot.

In order to compute the allowable orientations of the upperarm of the slave robot, it is essential to find the intersection of the links of the master robot and the circular region  $\Omega_u$ . In the following, the determination of intersection regions of  $\Omega_u$  and the links of the master robot is presented.

#### 4.2.1.1 Parallelepipeds

When a parallelepiped intersects with the circular region  $\Omega_u$  as shown in Fig. 4.6, the intersection region can be bounded by a box with length  $L_b$ , width  $W_b$  and height  $H_b$ . A top view of the intersection is shown in Fig. 4.7. It is worth to recall

that the vertical sides of the upperarm and the forearm of the robots remain vertical whatever the locations of the links are. Let  $W_u$  represent the width of the upperarm of the slave robot and  $W_p$  represent the width of the parallelepiped. The length of the intersection box is then given by

$$L_b = \frac{W_u}{\tan\alpha} + \frac{W_p}{\sin\alpha} \quad (4.1)$$

where  $\alpha$  is the angle between the  $\pi$  plane and a vertical plane passing through the central line of the parallelepiped. Analogously, the height of the intersection region can be derived and is given by

$$H_b = W_u \tan\beta + \frac{T_p}{\cos\beta} \quad (4.2)$$

where  $T_p$  is the thickness of the parallelepiped and  $\beta$  is the angle of the parallelepiped with respect to a horizontal plane.  $W_b$  is equal to  $W_u$ .

In order to determine the allowable orientations of the upperarm in the presence of the parallelepiped, consider first the sections of the intersection box and the upperarm of the slave robot on the  $\pi$  plane. The section of the intersection box on the  $\pi$  plane is a rectangle with dimensions  $L_b$  and  $H_b$ . The section of the upperarm of the slave robot on the  $\pi$  plane is also a rectangle with dimensions  $a_{12}$  and  $T_w$ , where  $a_{12}$  is the link length of the upperarm. As shown in Fig. 4.8, the rectangle ABCD represents the section of the intersection box on the  $\pi$  plane and the rectangle GHIJ represents the section of the upperarm of the slave robot on the  $\pi$  plane. A reference coordinate system is chosen such that the  $x$ - $z$  plane coincides with the  $\pi$  plane, and the  $x$  axis is parallel to a horizontal plane.

Further, the section of  $\Omega_u$  in the  $\pi$  plane is a circle centered at the shoulder O and with radius  $[a_{12}^2 + (T_u/2)^2]^{1/2}$  and is denoted by  $C_u$ . The section of  $C_u$  outside rectangle ABCD can be expressed in terms of an angular range  $[\alpha_1, \alpha_2]$ , where  $\alpha_1, \alpha_2$  are the angles between the x axis and the points of intersection of  $C_u$  and rectangle ABCD (Fig. 4.9) or the angles between the x axis and the vertices of rectangle ABCD (Fig. 4.10).

Finally, the angular range  $[\alpha_1, \alpha_2]$  is narrowed to compensate for the thickness of the upperarm (rectangle GHIJ) and is given by  $[\alpha_1 + \delta_1, \alpha_2 - \delta_2]$ , where  $\delta_1$  and  $\delta_2$  can have values of  $\tan^{-1}[(T_u/2) / a_{12}]$  or  $\tan^{-1}[(T_u/2) / d_v]$ , depending on how  $\alpha_1$  and  $\alpha_2$  are determined. If  $\alpha_1$  (or  $\alpha_2$ ) is determined by the angle between the x axis and a point of intersection of  $C_u$  and rectangle ABCD,  $\delta_1$  (or  $\delta_2$ ) =  $\tan^{-1}[(T_u/2) / a_{12}]$ . Otherwise,  $\delta_1$  (or  $\delta_2$ ) is determined by the angle between the x axis and a vertex of rectangle ABCD,  $\delta_1$  (or  $\delta_2$ ) =  $\tan^{-1}[(T_u/2) / d_v]$ , where  $d_v$  is the distance of the vertex of rectangle ABCD to the origin O.

$[\alpha_1 + \delta_1, \alpha_2 - \delta_2]$  gives the orientation range of rectangle GHIJ in which it does not intersect with rectangle ABCD. The allowable orientations of the upperarm are given by the intersection of the permissible orientations of the upperarm and the angular region  $[\alpha_1 + \delta_1, \alpha_2 - \delta_2]$ .

#### 4.2.1.2 Cylinders

When a cylinder intersects with the circular region  $\Omega_u$  (see Fig. 4.11), it is convenient to consider the intersections of the cylinder and the two vertical sides of

$\Omega_u$ . Denoted by  $\pi_1$  and  $\pi_2$  the two planes containing the two vertical sides of  $\Omega_u$ . It is desirable to find the intersection of the cylinder with the planes  $\pi_1$  and  $\pi_2$ .

The intersection of a cylinder and a plane is, in general, an ellipse. The ellipse can be considered as a perspective projection of a circle from a point at infinity onto the plane. The equation of the ellipse can be derived in a similar manner to the derivation of the plane section of a cone given in Section 2.4.

In the following, the orientations of the upperarm in which it does not intersect with the ellipses on the  $\pi_1$  and  $\pi_2$  planes are computed. As shown in Fig. 4.12, the rectangle GHJ with dimensions  $a_{12}$  and  $T_u$  represents the section of the upperarm of the slave robot in the  $\pi_1$  (or  $\pi_2$ ) plane. The ellipse represents a section of a cylinder in the  $\pi_1$  (or  $\pi_2$ ) plane. Using a translation followed by a rotation of the coordinate system, the ellipse can be transformed into an isothetic ellipse centered at the origin of the new coordinate system.

In order to determine the intersection of a rectangle and an ellipse, two methods are presented. The first method uses an expansion of ellipses so that a rectangle can be treated as a line segment. The second method uses an expansion of circles after applying a linear transformation to map ellipses into circles.

Expansion of ellipses. An ellipse centered at the origin whose major and minor axes are isothetic can be expressed by

$$\frac{x^2}{a^2} + \frac{y^2}{b^2} = 1 \quad (4.3)$$



where  $a$  and  $b$  are the lengths of the semi-major and semi-minor axes respectively, and its parametric form is

$$x = a \cos \theta \quad (4.4a)$$

$$y = b \sin \theta \quad (4.4b)$$

In order to determine if a rectangle with dimensions  $a_{12}$  and  $T$  and varying orientations will intersect an ellipse of the form in Eq. (4.3), the ellipse is expanded by an amount  $T/2$  and the rectangle is treated as a line segment. This expansion is equivalent to an actual physical space covered by a circle of radius  $T/2$  when the center of the circle is on the ellipse (Fig. 4.13). The expanded figure, denoted by  $EF$ , thus obtained has the parametric form

$$x = a \cos \theta + \frac{(T/2) \cdot b \cos \theta}{(a^2 \sin^2 \theta + b^2 \cos^2 \theta)^{1/2}} \quad (4.5a)$$

$$y = b \sin \theta + \frac{(T/2) \cdot a \sin \theta}{(a^2 \sin^2 \theta + b^2 \cos^2 \theta)^{1/2}} \quad (4.5b)$$

where  $0 \leq \theta \leq 2\pi$ .

A complete derivation of the above figure together with some important characteristics of this figure can be found in the work of Oommen and Reichstein (1987). Some characteristics of this figure which are useful for this work are summarized in the following,

- (1) For any parameter  $\theta$ , the slope of the tangent line to the ellipse in Eq. (4.4) has exactly the same value as the slope of the tangent to the expanded figure in Eq. (4.5) at the corresponding point.

- (2) For the parameter  $\Theta$ , the equation for the tangent line to the expanded figure has the form

$$\frac{x \cos \Theta}{a} + \frac{y \sin \Theta}{b} = 1 + \frac{(T/2) \cdot (a^2 \sin^2 \Theta + b^2 \cos^2 \Theta)^{1/2}}{ab} \quad (4.6)$$

- (3) The slope  $m$  of the tangent to the expanded figure passing through the point  $(x, y)$  has the value  $-1/t$ , where  $t$  is a root of the quartic equation:

$$k_4 t^4 + k_3 t^3 + k_2 t^2 + k_1 t + k_0 = 0 \quad (4.7)$$

where, if  $F(p, q, r) = p^2 - q^2 - r^2$ , and  $G(p, q) = 2pq$ ,

$$k_4 = F^2(y, b, T/2) - G^2(b, T/2)$$

$$k_3 = 2 \cdot F(y, b, T/2) \cdot G(x, y)$$

$$k_2 = 2 \cdot F(y, b, T/2) \cdot F(x, a, T/2) + G^2(x, y) - G^2(a, T/2) - G^2(b, T/2)$$

$$k_1 = 2 \cdot F(x, a, T/2) \cdot G(x, y)$$

$$k_0 = F^2(x, a, T/2) - G^2(a, T/2)$$

By using the expansion of the ellipse in the  $\pi_1$  (or  $\pi_2$ ) plane, the problem of interest becomes finding the orientations of a line segment fixed in one end point to avoid intersection with the expanded figure **EF**. When one end point of a line segment is fixed, the area swept by the line segment is a circular region  $C_u$  (Fig. 4.14). The orientations of the line segment in which it intersects **EF** are determined either by tangents of **EF** passing through the fixed end point or the intersection points of  $C_u$  and **EF**.

When the points of tangency of **EF** are outside  $C_u$ , the orientation range of interference is determined by the points of intersection of **EF** and  $C_u$ . Otherwise, it is determined by the points of tangency of **EF**. The tangents of **EF** passing

through the fixed end point can be determined by solving Eq. (4.7). However, the intersection of  $C_u$  and EF cannot be obtained analytically. Therefore, if the points of tangency of EF are outside  $C_u$ , the orientations of the intersection points of  $C_u$  and EF are approximated by the orientations of the tangent lines of EF passing through the center of  $C_u$ . The applicability of this approximation is due to the fact that  $C_u$  which has a radius equal to a link length is substantially bigger than EF which has axes lengths in the orders of the cross section dimensions of a link.

Transformation of ellipses. Using the transformation of ellipses described in Section 2.4, the problem of determining the intersection of a rectangle and an ellipse can be transformed into the problem of determining the intersection of a parallelogram and a circle. This problem is further reduced to the problem of finding the intersection of a line segment and a circle and can be solved by using the method presented in Section 2.2. Note that using this transformation, the orientation  $\theta$  of a line segment with respect to the x axis of the reference frame is transformed into  $\theta'$ , and they are related by

$$\tan \theta' = (\sigma_y / \sigma_x) \tan \theta \quad (4.8)$$

where  $\sigma_x$  and  $\sigma_y$  are as those defined in Section 2.3. As far as the orientation of the line segment is concerned, this conversion should be applied appropriately.

After finding the intersection of the upperarm and the plane sections of the cylinder in the  $\pi_1$  and  $\pi_2$  planes, it is necessary to find the intersection of the upperarm and the cylinder itself. Suppose the orientation ranges of the upperarm within which it has intersection with the plane sections of a cylinder in the  $\pi_1$  and  $\pi_2$  planes are given by  $[\mu_1, \mu_2]$  and  $[\mu_3, \mu_4]$ , respectively. The orientation range of the

upperarm within which it intersects with the cylinder is given by  $[\mu_1, \mu_4]$ . The allowable orientations of the upperarm is then obtained by excluding  $[\mu_1, \mu_4]$  from the permissible orientations.

#### 4.2.2 Allowable Orientations of Forearm

Since the forearm and the upperarm always lie on the same plane, the central line of the forearm remains in the  $\pi$  plane where the central line of the upperarm locates (see Fig. 4.4). In addition, the end points of the forearm are constrained by the elbow and wrist joints which move in circular arcs. In order to find the allowable orientations of the forearm, the analysis for the upperarm described above can be applied with some modifications. In the following, the determination of allowable orientations of the forearm with respect to the links of the master robot which are modeled by parallelepipeds and cylinders are presented.

##### 4.2.2.1 Parallelepipeds

When the central line of the forearm lies on a  $\pi$  plane, the two vertical sides of the forearm lie on two vertical planes which are denoted by  $\pi_1$  and  $\pi_2$ . Denoted by  $\Omega_f$  the region between planes  $\pi_1$  and  $\pi_2$  (see Fig. 4.15). The intersection of  $\Omega_f$  and a parallelepiped can be bounded by a box with dimensions  $L_b$ ,  $W_b = W_f$  and  $H_b$ , and  $L_b$  and  $H_b$  are given by

$$L_b = \frac{W_f}{\tan \alpha} + \frac{W_p}{\sin \alpha} \quad (4.9)$$

$$H_b = W_f \tan \beta + \frac{T_p}{\cos \beta} \quad (4.10)$$

where  $W_f$  is the width of the forearm,  $W_p$  and  $T_p$  are width and thickness of the parallelepiped,  $\alpha$  is the angle between the  $\pi$  plane and a vertical plane passing through the central line of the parallelepiped, and  $\beta$  is the angle of the parallelepiped with respect to a horizontal plane.

In order to determine the allowable orientations of the forearm, it is helpful to consider the plane sections of the above bounding box and the forearm of the slave robot on the  $\pi$  plane. As a result, the forearm is represented by a rectangle with dimensions  $a_{34}$ ,  $T_p$  and the parallelepiped is reduced to a rectangle with dimensions  $L_b$  and  $H_b$ .

The allowable orientations of the forearm can be obtained by considering the forearm as a line segment while the rectangle is expanded by  $T_f/2$  along the normal direction of each side to compensate for the thickness of the forearm. Using the method described in Section 3.2.1, the allowable orientations of the forearm with respect to the expanded rectangle can be obtained.

#### 4.2.2.2 Cylinders

A cylinder intersects with the  $\pi_1$  and  $\pi_2$  planes in two ellipses (see Fig. 4.16). In order to determine the allowable orientations of the forearm in the presence of a cylinder, the orientations of the forearm in which it does not intersect with the ellipses on the  $\pi_1$  and  $\pi_2$  planes are determined.

The intersections of the forearm and an ellipse on the  $\pi_1$  (or  $\pi_2$ ) plane is equivalent to the intersections of the plane section of the forearm on the  $\pi_1$  (or  $\pi_2$ ) plane and the ellipse on the same plane. The determination of these intersections can be accomplished by a transformation of ellipse followed by a determination of intersections of line segments and a circle as described in Section 4.2.1.2.

#### 4.2.3 Allowable Orientations of End Effector

When the upperarm and the forearm of the slave robot lie on a plane, its end effector lies on a circular cone. The allowable orientations of the end effector of the slave robot are determined by considering the intersection of a cone and the links of the master robot.

Before finding the intersection of the end effector of the slave robot and the links of the master robot, it is necessary to detect whether the intersection is possible or not. In order to detect the possibility of intersection between the end effector of the slave robot and the links of the master robot, it is convenient to consider the links of the master robot as cylinders. The radii of the cylinders are as small as possible while the cylinders encompass the links. Further, these cylinders are expanded by the radius of the end effector of the slave robot. The detection of the possibility of intersection of the end effector of the slave robot and the links of the master robot can then be performed by finding the relative location of a cone and a cylinder as described in Section 2.5.

The upperarm and the forearm of the master robot are modeled by parallelepipeds. In order to compute the allowable orientations of the end effector

of the slave robot with respect to the upperarm and the forearm of the master robot, the intersection of a cone and a parallelepiped is considered, which can be found in Section 3.2.1. However, before applying that algorithm, it is essential to expand the parallelepiped along the normal direction of each side by the radius of the end effector of the slave robot. Similarly, in order to compute the allowable orientations with respect to the end effector of the master robot, the intersection of a cone and a cylinder is needed, which can be found in Section 2.5.

Consequently, by computing the intersection of allowable orientations with respect to each link of the master robot, the allowable orientations of the end effector of the slave robot can be obtained.

#### 4.3 Parallel Operations of Two Robot Manipulators

In this section, the problem of interference avoidance of two manipulators operating in parallel is investigated. Recall that in Section 3.4.2, robot manipulators are considered having 4 DOF, and their links remain in a plane as their motion proceeds. And the problem was solved by using forbidden regions which were represented by line segments. This section modifies the development in Section 3.4.2 so it can be applied to robot manipulators with solid links.

At any instant, the links of a robot manipulator are restricted in a vertical region. Let the regions where the two robots lie be denoted by  $\Omega_1$  and  $\Omega_2$ . The respective widths of these two regions are represented by  $W_1$  and  $W_2$ . Further, two vertical planes which lie in the center of  $\Omega_1$  and  $\Omega_2$  are represented by  $\pi_1$  and  $\pi_2$ , respectively. It is clear that the only possible location for interference is somewhere

within the intersection prism,  $\Sigma$ , of these two regions as shown in Fig. 4.17. It is thus necessary to determine a forbidden region for each robot within the intersection prism  $\Sigma$ .

The intersection prism  $\Sigma$  on the regions  $\Omega_1$  and  $\Omega_2$  can be bounded by boxes  $B_1$  and  $B_2$  with lengths  $L_{b1}$  and  $L_{b2}$  and widths  $W_{b1}$  and  $W_{b2}$ ,

$$L_{b1} = \frac{W_1}{\tan\alpha} + \frac{W_2}{\sin\alpha} \quad (4.11)$$

$$L_{b2} = \frac{W_2}{\tan\alpha} + \frac{W_1}{\sin\alpha} \quad (4.12)$$

$$W_{b1} = W_1 \quad (4.13)$$

$$W_{b2} = W_2 \quad (4.14)$$

where  $\alpha$  is the angle between  $\pi_1$  and  $\pi_2$  planes. The plane sections of  $B_1$  on the plane  $\pi_1$  is a rectangle with width  $L_{b1}$ . Similarly, the plane section of  $B_2$  on the plane  $\pi_2$  is a rectangle with width  $L_{b2}$ .

The forbidden regions of two robot manipulators can be determined by considering the plane sections of  $B_1$  and  $B_2$  and the links of the two manipulators on the planes  $\pi_1$  and  $\pi_2$ , respectively. The procedure for determining the forbidden regions is described in the following.

First, determine forbidden regions of two line-segment-modeled manipulators lying on the  $\pi_1$  and  $\pi_2$  planes by using the procedure described in Section 3.4.2. This will yield two disjoint forbidden regions which are line segments in the intersection line,  $l$ , of  $\pi_1$  and  $\pi_2$  planes. However, before applying this procedure, a modification has to be made in order to compensate for the thicknesses of robot links. This is



because when a link of a robot manipulator passes through the end points of the bounded region in the intersection line  $l$ , the bounded region needs to contain the thickness of the link. The length of the additional bounded region in the line  $l$  is dependent on the orientation of the link and can be expressed as follows:

$$d = T / (2\cos\beta) \quad (4.15)$$

where  $d$  is the length of additional bounded region,  $T$  is the thickness of the link and  $\beta$  is its orientation with respect to the horizontal plane (see Fig. 4.18). It is important to recognize that the bounded region in line  $l$  are union of regions of intersection of links of the manipulator with line  $l$ . Therefore, in order to find the new bounded regions in  $l$ , each link's thickness has to be considered.

Second, the two line-segment forbidden regions on the  $\pi_1$  and  $\pi_2$  planes are expanded to rectangles which have widths of  $L_{b1}$  and  $L_{b2}$ , respectively. The heights of the rectangles are the same as the lengths of the two line-segment forbidden regions.

Finally, the problem reduces to the determination of the orientations of links, which are rectangles, of a manipulator such that the links do not interfere with a rectangular forbidden region. The method used for solving this problem can be found in the discussion of master-slave operations of two robot manipulators in the previous section.

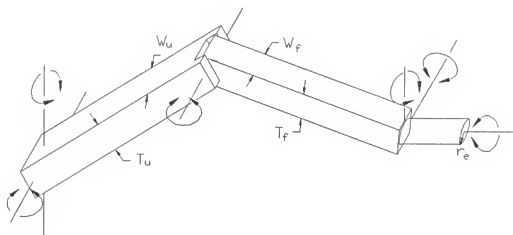


Fig. 4.1 Robot manipulators with solid links.

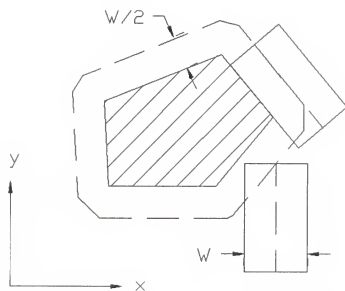


Fig. 4.2 Expansion of vertical sides.

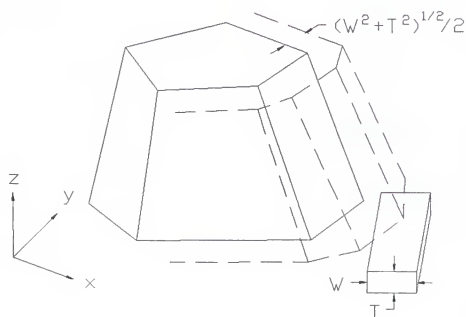


Fig. 4.3 Expansion of oblique sides.

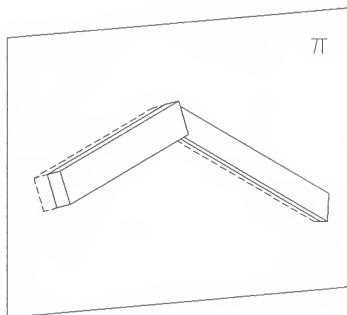


Fig. 4.4 The central lines of the upperarm and the forearm lie on the  $\pi$  plane.

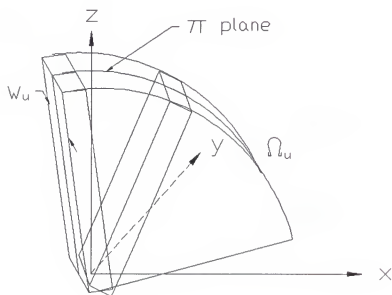


Fig. 4.5 The upperarm sweeps a region  $\Omega_u$ .

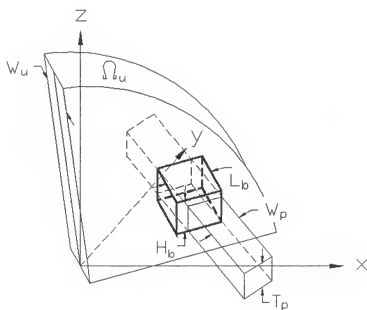


Fig. 4.6 Intersection region of  $\Omega_u$  and a parallelepiped.

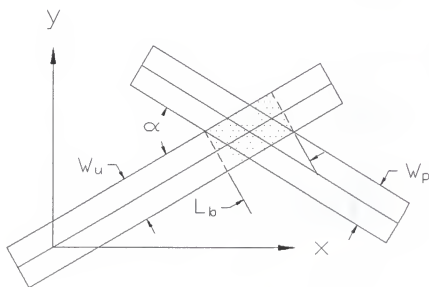


Fig. 4.7 Top view.

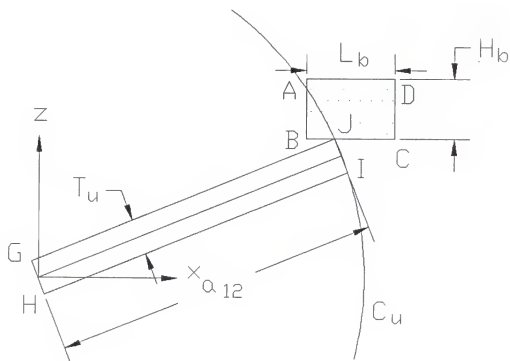


Fig. 4.8 Plane section of the upperarm and an intersection box.

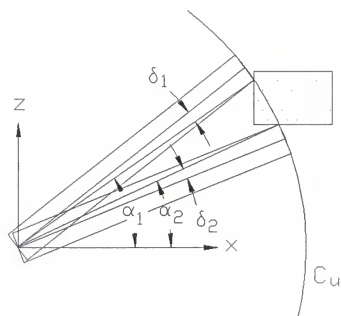


Fig. 4.9 Vertices of rectangle outside  $C_u$ .

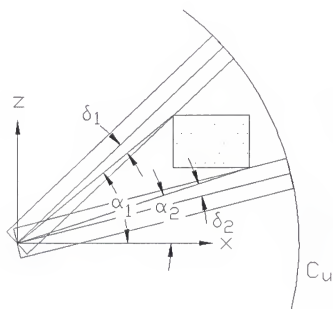


Fig. 4.10 Vertices of rectangle inside  $C_u$ .

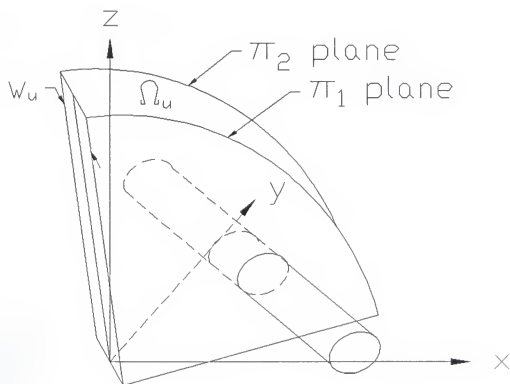


Fig. 4.11 A cylinder intersects with  $\Omega_u$ .



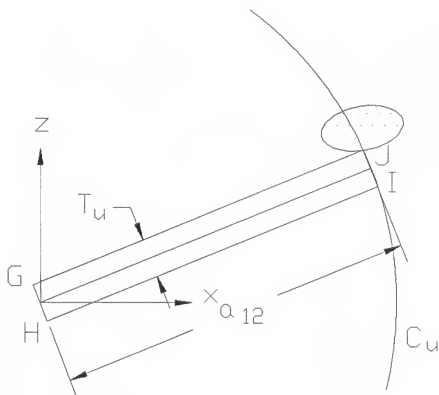


Fig. 4.12 Plane sections of the upperarm and a cylinder.

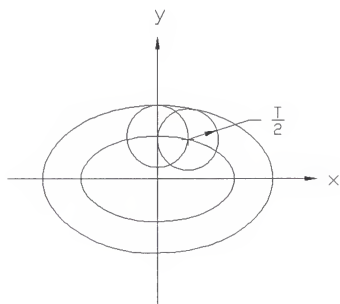


Fig. 4.13 Expansion of an ellipse.

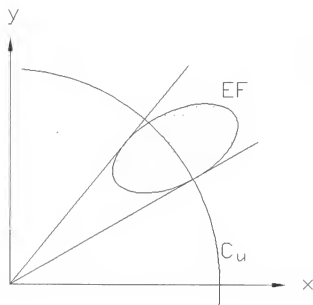


Fig. 4.14 Intersection of the expanded figure (EF) and  $C_u$ .

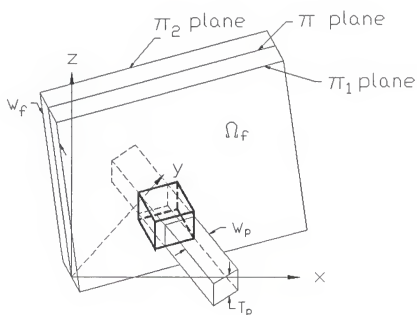


Fig. 4.15 Intersection of a parallelepiped and  $\Omega_f$  is bounded by a box.

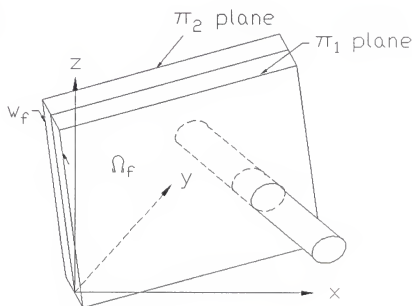


Fig. 4.16 Intersection of a cylinder and  $\Omega_f$ .

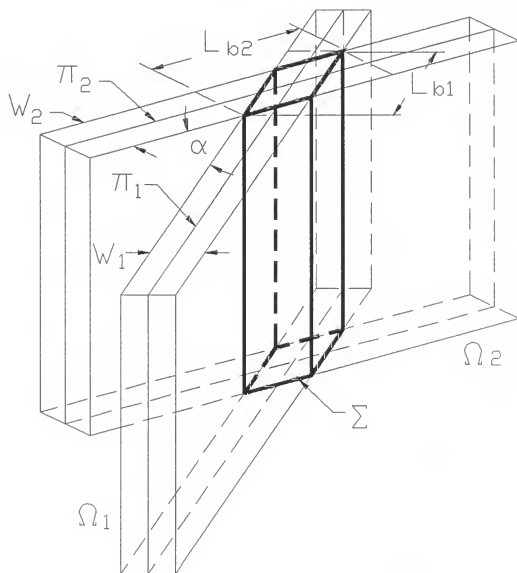


Fig. 4.17 Possible location of interference of two robot manipulators.

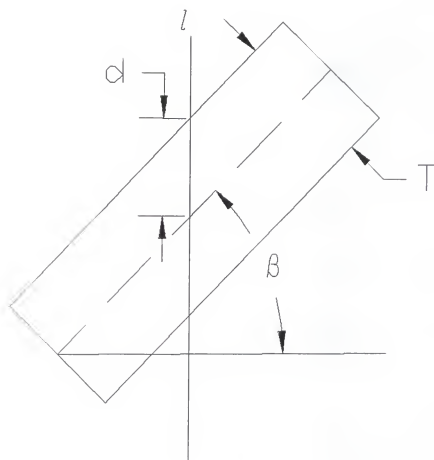


Fig. 4.18 Determination of the length of the additional bounded region.

## CHAPTER 5

### TIME SCHEDULING OF TWO ROBOT MANIPULATORS

In Chapters 3 and 4, the determination of favorable orientation ranges of two robot manipulators, which is based on the predefined trajectories of the manipulators, has been discussed. However, it is possible that the robot manipulators may not have favorable orientations at some instants during the motion. This implies that the two manipulators cannot avoid each other while tracking their specified trajectories. In this situation, the trajectories should be modified such that the robot manipulators can arrive at their goal positions successfully.

In this section, it is proposed to use speed reduction or time delay of either one of the two robot manipulators without changing its path to generate an interference-free motion. In order to do this, two tasks must be performed:

1. determine potential collisions between the links of the two robot manipulators according to the specified paths.
2. modify the trajectories of the manipulators such that the potential collisions can be avoided.

In the following, potential collisions between the links of a pair of robot manipulators are discussed. The potential collisions are assumed to happen only between the end effectors which are moving on straight line paths. Strategies for

modifying trajectories of robot manipulators for the purpose of avoiding potential collisions are then proposed.

The approach presented here is somewhat similar to the work of Lee and Lee (1987). It is important to recognize that in their work, the boundary of the potential collision region was not described analytically and was approximated by a bounding box. However, here a complete novel analysis is presented where the potential collision region is described precisely.

### 5.1 Potential Collision Regions

Since the end effector is instantaneously joined to a fixed target point, the permissible locations of an end effector lie within a sphere and it is reasonable to model the end effector by a sphere. The center of the sphere coincides with the target point on the specified path and the radius of the sphere is equal to the length of the end effector (see Fig. 5.1). Using this model, the interference problem is reduced to determining the intersection of a pair of spheres.

Let the parametric equations of two straight lines which represent the paths of the end effectors of two manipulators be given by

$$\underline{P}_1 = \underline{U}_1 + s_1(\underline{V}_1 - \underline{U}_1) \quad 0 \leq s_1 \leq 1 \quad (5.1)$$

$$\underline{P}_2 = \underline{U}_2 + s_2(\underline{V}_2 - \underline{U}_2) \quad 0 \leq s_2 \leq 1 \quad (5.2)$$

where  $\underline{U}_i$  and  $\underline{V}_i$  are beginning and end points of the  $i$ th manipulator. It is assumed that there is no interference between the two end effectors when they are at the beginning and end points of the straight line paths.

The intersection of a pair of spheres occurs when the distance between the centers of the spheres is less than the sum of radii of the two spheres. Thus, a potential collision region can be obtained and the boundary of the potential collision region is determined by the following equation:

$$|\underline{P}_1 - \underline{P}_2| = r_1 + r_2 \quad (5.3)$$

where  $r_1$  and  $r_2$  are link lengths of the two end effectors. Replacing  $\underline{P}_1$  and  $\underline{P}_2$  by Eqs. (5.1) and (5.2) yields

$$|(\underline{U}_1 - \underline{U}_2) + s_1(\underline{V}_1 - \underline{U}_1) - s_2(\underline{V}_2 - \underline{U}_2)| = r_1 + r_2 \quad (5.4)$$

Square both sides of Eq. (5.4) yields

$$\begin{aligned} & |\underline{V}_1 - \underline{U}_1|^2 s_1^2 - 2(\underline{V}_1 - \underline{U}_1) \cdot (\underline{V}_2 - \underline{U}_2) s_1 s_2 + |\underline{V}_2 - \underline{U}_2|^2 s_2^2 \\ & + 2(\underline{U}_1 - \underline{U}_2) \cdot (\underline{V}_1 - \underline{U}_1) s_1 - 2(\underline{U}_1 - \underline{U}_2) \cdot (\underline{V}_2 - \underline{U}_2) s_2 \\ & + |\underline{U}_1 - \underline{U}_2|^2 - (r_1 + r_2)^2 = 0 \end{aligned} \quad (5.5)$$

which can be expressed in the form

$$A s_1^2 - 2B s_1 s_2 + C s_2^2 + 2D s_1 - 2E s_2 + F = 0 \quad (5.6)$$

which is a quadratic equation in  $s_1$  and  $s_2$ . The discriminant of the second-degree equation is given by

$$\begin{aligned} B^2 - AC &= [(\underline{V}_1 - \underline{U}_1) \cdot (\underline{V}_2 - \underline{U}_2)]^2 - |\underline{V}_1 - \underline{U}_1|^2 |\underline{V}_2 - \underline{U}_2|^2 \\ &= |\underline{V}_1 - \underline{U}_1|^2 |\underline{V}_2 - \underline{U}_2|^2 (\cos^2 \alpha - 1) \\ &\leq 0 \end{aligned}$$

where  $\alpha$  is the angle between the vectors  $\underline{V}_1 - \underline{U}_1$  and  $\underline{V}_2 - \underline{U}_2$ .

When  $B^2 - AC < 0$ , the trace of the second-degree equation in the parametric space, i.e., the  $s_2$ - $s_1$  plane, is an ellipse. When  $B^2 - AC = 0$ , i.e.  $\cos \alpha = \pm 1$ , the trace



is, in general, a parabola. However, in the present case, when  $B^2 - AC = 0$ , the equation is degenerate and reduces to two parallel lines which are represented by

$$\begin{aligned} & (|\underline{V}_1 - \underline{U}_1| s_1 - \cos\alpha |\underline{V}_2 - \underline{U}_2| s_2 + |\underline{U}_1 - \underline{U}_2| \cos\beta)^2 \\ & = (r_1 + r_2)^2 - (|\underline{U}_1 - \underline{U}_2| \sin\beta)^2 \end{aligned} \quad (5.7)$$

where

$$\beta = \cos^{-1} \frac{(\underline{U}_1 - \underline{U}_2) \cdot (\underline{V}_1 - \underline{U}_1)}{|\underline{U}_1 - \underline{U}_2| |\underline{V}_1 - \underline{U}_1|} \quad (5.8)$$

In the following discussion, ellipses will be used to represent the potential collision regions.

It is further assumed that the robot manipulators are performing motions which involve three stages: acceleration, constant velocity, and deceleration, and the velocity vs. time graph is shown in Fig. 5.2. For this analysis, the acceleration and deceleration of each manipulator are assumed to be the same in magnitude.

Using these velocity profiles, the position of each robot at a given time can be determined. The traveled distances of the robots in terms of the parameters  $s_1$  and  $s_2$  at each time interval can be expressed as follows:

(A) Robot 1

$$(1) \ t_0 \leq t \leq t_1$$

$$s_1 = \frac{a_1 t^2}{2 |\underline{V}_1 - \underline{U}_1|} \quad (5.9a)$$

$$(2) \ t_1 < t \leq t_4$$

$$s_1 = s_1(t_1) + \frac{a_1 t_1 (t - t_1)}{|\underline{V}_1 - \underline{U}_1|} \quad (5.9b)$$

where

$$s_1(t_1) = \frac{a_1 t_1^2}{2|\underline{Y}_1 - \underline{U}_1|}$$

(3)  $t_4 < t \leq t_r$

$$s_1 = 1 - \frac{a_1(t_r - t)^2}{2|\underline{Y}_1 - \underline{U}_1|} \quad (5.9c)$$

(B) Robot 2

(1)  $t_0 \leq t \leq t_2$

$$s_2 = \frac{a_2 t^2}{2|\underline{Y}_2 - \underline{U}_2|} \quad (5.10a)$$

(2)  $t_2 < t \leq t_3$

$$s_2 = s_2(t_2) + \frac{a_2 t_2(t - t_2)}{|\underline{Y}_2 - \underline{U}_2|} \quad (5.10b)$$

where

$$s_2(t_2) = \frac{a_2 t_2^2}{2|\underline{Y}_2 - \underline{U}_2|}$$

(3)  $t_3 < t \leq t_r$

$$s_2 = 1 - \frac{a_2(t_r - t)^2}{2|\underline{Y}_2 - \underline{U}_2|} \quad (5.10c)$$

According to the above trajectories, the corresponding positions between the two robots at various time intervals are computed by eliminating the time from Eqs. (5.9) and (5.10) and are shown in the following:

$$(1) \ t_0 \leq t \leq t_1$$

$$s_2 = \frac{a_2 |\underline{V}_1 - \underline{U}_1|}{a_1 |\underline{V}_2 - \underline{U}_2|} s_1 = A_1 s_1 \quad (5.11a)$$

$$(2) \ t_1 < t \leq t_2$$

$$s_2 - s_2(t_1) = B_1[s_1 - s_1(t_1)] + B_2[s_1 - s_1(t_1)]^2 \quad (5.11b)$$

where

$$s_2(t_1) = \frac{a_2 t_1^2}{2 |\underline{V}_2 - \underline{U}_2|}$$

$$B_1 = A_1$$

$$B_2 = a_2 \frac{|\underline{V}_1 - \underline{U}_1|^2}{2(a_1 t_1)^2 |\underline{V}_2 - \underline{U}_2|}$$

$$(3) \ t_2 < t \leq t_3$$

$$s_2 - s_2(t_2) = C_1[s_1 - s_1(t_2)] \quad (5.11c)$$

where

$$s_1(t_2) = s_1(t_1) + \frac{a_1 t_1(t_2 - t_1)}{|\underline{V}_1 - \underline{U}_1|}$$

$$C_1 = \frac{a_2 t_2 |\underline{V}_1 - \underline{U}_1|}{a_1 t_1 |\underline{V}_2 - \underline{U}_2|}$$

$$(4) \ t_3 < t \leq t_4$$

$$s_2 - s_2(t_3) = D_1[s_1 - s_1(t_3)] + D_2[s_1 - s_1(t_3)]^2 \quad (5.11d)$$

where

$$s_1(t_3) = s_1(t_2) + \frac{a_1 t_1(t_3 - t_2)}{|\underline{V}_1 - \underline{U}_1|}$$

$$s_2(t_3) = s_2(t_2) + \frac{a_2 t_2 (t_3 - t_2)}{|\underline{V}_2 - \underline{U}_2|}$$

$$D_1 = C_1$$

$$D_2 = -B_2$$

$$(5) \ t_4 < t \leq t_f$$

$$s_2 - 1 = E_1(s_1 - 1) \quad (5.11e)$$

$$\text{where } E_1 = A_1$$

Consequently, a curve in the parametric space is obtained and is illustrated in Fig. 5.3. If this curve is outside the potential collision region, the two end effectors will not collide with each other. Otherwise, the intersection points of this curve with the potential collision region must be identified.

In order to visualize the effect of modification of robot trajectories, it is convenient to map the potential collision region from  $s_1$ - $s_2$  plane to either  $s_1$ - $t$  or  $s_2$ - $t$  plane. This is performed by replacing  $s_2$  or  $s_1$  in Eqs. (5.11) by Eqs. (5.10) or (5.9) for each time interval. As a result, a closed region is obtained, and the boundaries of this region at different time intervals are given as follows:

(A)  $s_1$ - $t$  plane

$$(1) \ t_0 \leq t \leq t_2$$

$$As_1^2 - 2Bp_1s_1t^2 + C(p_1t^2)^2 + 2Ds_1 - 2Ep_1t^2 + F = 0 \quad (5.12a)$$

$$\text{where } p_1 = \frac{a_2}{2|\underline{V}_2 - \underline{V}_1|}$$

$$(2) \ t_2 < t \leq t_3$$

$$As_1^2 - 2Bp_2s_1t + C(p_2t)^2 + 2(D - Bq_2)s_1 - 2p_2(E - Cq_2)t$$

$$+ F + Cq_2^2 - 2Eq_2 = 0 \quad (5.12b)$$

$$\text{where } p_2 = \frac{a_2 t_2}{|\underline{V}_2 - \underline{U}_2|}$$

$$q_2 = s_2(t_2) - \frac{a_2 t_2^2}{|\underline{V}_2 - \underline{U}_2|}$$

$$(3) \ t_3 < t \leq t_f$$

$$\begin{aligned} & A s_1^2 - 2B s_1(p_3 t^2 + q_3 t + r_3) + C(p_3 t^2 + q_3 t + r_3)^2 \\ & + 2D s_1 - 2E(p_3 t^2 + q_3 t + r_3) + F = 0 \end{aligned} \quad (5.12c)$$

$$\text{where } p_3 = - \frac{a_2}{|\underline{V}_2 - \underline{U}_2|}$$

$$q_3 = \frac{a_2 t_f}{|\underline{V}_2 - \underline{U}_2|}$$

$$r_3 = 1 - \frac{a_2 t_f^2}{2|\underline{V}_2 - \underline{U}_2|}$$

(B)  $s_2$ - $t$  plane

$$(1) \ t_0 \leq t \leq t_1$$

$$A(p_4 t^2)^2 - 2B p_4 s_2 t^2 + C s_2^2 + 2D p_4 t^2 - 2E s_2 + F = 0 \quad (5.13a)$$

$$\text{where } p_4 = \frac{a_1}{2|\underline{V}_1 - \underline{U}_1|}$$

$$(2) \ t_1 < t \leq t_4$$

$$\begin{aligned} & A(p_5 t)^2 - 2B p_5 s_2 t + C s_2^2 + 2p_5(D + A q_5)t \\ & - 2(E + B q_5)s_2 + F + A q_5^2 + 2D q_5 = 0 \end{aligned} \quad (5.13b)$$

$$\text{where } p_5 = \frac{a_1 t_1}{|\underline{Y}_1 - \underline{U}_1|}$$

$$q_5 = s_1(t_1) - \frac{a_1 t_1^2}{|\underline{Y}_1 - \underline{U}_1|}$$

$$(3) \ t_4 < t \leq t_r$$

$$\begin{aligned} & A(p_6 t^2 + q_6 t + r_6)^2 - 2B(p_6 t^2 + q_6 t + r_6)s_2 + Cs_2^2 \\ & + 2D(p_6 t^2 + q_6 t + r_6) - 2Es_2 + F = 0 \end{aligned} \quad (5.13c)$$

$$\text{where } p_6 = -\frac{a_1}{2|\underline{Y}_1 - \underline{U}_1|}$$

$$q_6 = \frac{a_1 t_r}{|\underline{Y}_1 - \underline{U}_1|}$$

$$r_6 = 1 - \frac{a_1 t_r^2}{2|\underline{Y}_1 - \underline{U}_1|}$$

The modification of the robots trajectories can be done conveniently either in the  $s_1$ - $t$  plane or in the  $s_2$ - $t$  plane, depending upon which robot trajectory is to be modified (see Fig. 5.4).

## 5.2 Modification of Trajectories

When the distance curve of two end effectors in the parametric space intersects with the potential collision region, these two end effectors will collide with each other while tracking their specified trajectories. In order to avoid collision, the trajectory of either one of the two robot manipulators can be modified.

Two methods for modifying the trajectories of robots are discussed here. The first method is to delay the motion of a robot to avoid potential collisions, and the second method uses a speed reduction concept.

Before discussing in detail about these methods, it is helpful to know which robot trajectory can be modified. In general, both robot trajectories are considered modifiable. In some cases, however, it is preferable to alter the trajectory of one robot rather than the other.

Consider different locations of the potential collision region in Figs. 5.5(a) - (g). The rectangular region bounded by  $s_1 = 0$ ,  $s_1 = 1$ ,  $s_2 = 0$ , and  $s_2 = 1$  is the valid locations of potential collisions when the two robots move in the prespecified line segment trajectories.

When the potential collision region intersects with the border  $s_2 = 1$  or  $s_1 = 0$  as shown in Figs. (5.5a) and (5.5d), it is preferable to modify the trajectory of robot 2. In contrast, when the potential collision region intersects with the border  $s_1 = 1$  or  $s_2 = 0$  as shown in Figs. (5.5b) and (5.5c), it is preferable to modify the trajectory of robot 1. When the potential collision region does not intersect with the borders as shown in Fig. (5.5e), both robot trajectories can be modified. Finally, when the potential collision region intersects with two opposite sides of the valid region as in Figs. (5.5f) and (5.5g), collision can not be avoided by the proposed methods.

### 5.2.1 Time Delay

In this section, it is assumed that the trajectory of robot 2 is to be modified using time delay at the beginning of the trajectory. According to the velocity profile

of robot 2 in Fig. 5.2, a distance vs. time ( $s_2$ - $t$ ) curve, which represents the displacement profile of robot 2, is obtained (see Fig. 5.6). In addition, the potential collision region in the  $s_2$ - $s_1$  plane is mapped onto the  $s_2$ - $t$  plane a closed region as shown in Fig. 5.4. In order for robot 2 to avoid potential collisions, its distance vs. time curve must lie outside the potential collision region in the  $s_2$ - $t$  plane.

The time delay strategy considered here is to delay the motion of robot 2 at the beginning point of its path. This has the effect of shifting the distance vs. time curve to the right.

The amount of time that the motion of robot 2 must be delayed can be determined as follows. Let the intersection point of the distance vs. time curve and the potential collision region in the  $s_2$ - $t$  plane be denoted by M and N. The corresponding traveled distances and time of robot 2 at these two points are denoted by  $s_{2M}$ ,  $s_{2N}$ , and  $t_M$ ,  $t_N$  (see Fig. 5.7). The time required for the motion of robot 2 to be delayed is determined by the maximum time difference between the distance vs. time curve and the potential collision region in  $s_2$ - $t$  plane with  $s_{2M} \leq s_2 \leq s_{2N}$ . Fig. 5.8 illustrates the result of the distance vs. time curve of robot 2 after a time delay.

### 5.2.2 Speed Reduction

In this section, another approach for modifying the trajectories of robots by using the concept of speed reduction is discussed. Speed reduction has the effect of decreasing the slope of the distance versus time curve. If the curve is modified such that it is outside the potential collision region, no collision will occur. In the work of Lee and Lee [1987], the potential collision region in the distance vs. time domain



is approximated by a bounding box. In other words, the potential collision region is expanded into a box to simplify the problem.

In the following, the potential collision region is expressed explicitly, and is used to determine the location of collision and to modify the trajectories of robots. The method applied here is based upon the assumption that a velocity constraint on the end effector is imposed. Therefore, the slope the distance vs. time curve is limited to a value which is denoted by  $v_m$ . This suggests that two lines with a slope equal to the constrained velocity  $v_m$  and being tangent to the potential collision region to be obtained. Of these two lines, only the one which has a smaller intercept is of interest and is denoted by  $l_v$ . This line together with a horizontal tangent line of the potential collision region, i.e.,  $s_1 = s_{1,\min}$  or  $s_2 = s_{2,\min}$  is used to bound the potential collision region (see Fig. 5.9).

In the following discussion, it is assumed that the trajectory of robot 1 is to be modified while the trajectory of the other robot remains unchanged. The line with a slope of the limiting velocity and having point contact with the potential collision region is obtained using the following procedure. First, tangent lines of the potential collision region with the specified slope are derived for each time interval. Among these tangent lines, the one with a smallest intercept is selected as the line  $l_v$ . Let the line  $l_v$  be expressed as

$$s_1 = s_{1,0} + v_m t \quad (5.14)$$

It is then necessary to determine the value of  $s_{1,0}$ .

According to the velocity profile of robot 2, the distance versus time curve of robot 2 consists of segments of curves of two different types which can be expressed in the following forms:

$$s_2 = pt + q \quad (5.15a)$$

and

$$s_2 = pt^2 + qt + r \quad (5.15b)$$

For the type of curve in Eq. (5.15a), the mapped potential collision region in  $s_1$ - $t$  plane remains a quadratic form. In this case, the tangent line with slope  $v_m$  is derived first by replacing  $s_1$  in the boundary equation of the mapped potential collision region by Eq. (5.14). This results in a second order polynomial in  $t$ . If a line is tangent to the potential collision region, a double root can be found at the point contact. In other words, the discriminant of the second order equation in  $t$  must equal zero. This can be used to find the values of  $s_{1,0}$  such that the line in Eq. (5.14) is tangent to the potential collision region.

When the displacement profile of robot 2 is in the form of Eq. (5.15b), the corresponding potential collision region in  $s_1$ - $t$  plane becomes a fourth order curve,

$$\begin{aligned} &As_1^2 - 2Bs_1(pt^2 + qt + r) + C(pt^2 + qt + r)^2 \\ &+ 2Ds_1 - 2E(pt^2 + qt + r) + F = 0 \end{aligned} \quad (5.16)$$

or

$$A_0s_1^2 + (B_0t^2 + B_1t + B_2)s_1 + C_0t^4 + C_1t^3 + C_2t^2 + C_3t + C_4 = 0 \quad (5.17)$$

where

$$A_0 = A$$

$$B_0 = -2Bp, B_1 = -2Bq, B_2 = -2(Br - D)$$

$$C_0 = Cp^2, C_1 = 2Cpq, C_2 = C(q^2 + 2pr) - 2Ep,$$

$$C_3 = 2q(Cr - E), C_4 = Cr^2 - 2Er + F$$

For each value of  $t$ , two values of  $s_1$  can be computed. The lower part of the potential collision region is derived by solving Eq. (5.17) for  $s_1$  and is expressed as follows (assume  $A_0 > 0$ ),

$$s_1 = \{-(B_0t^2 + B_1t + B_2) - [(B_0t^2 + B_1t + B_2)^2 - 4A_0(C_0t^4 + C_1t^3 + C_2t^2 + C_3t + C_4)]^{1/2}\} / (2A_0) \quad (5.18)$$

The slope of the above curve is the derivative with respect to time and is given by

$$\begin{aligned} ds_1 / dt = \{ & -(2B_0t + B_1) - 0.5[(B_0t^2 + B_1t + B_2)^2 - \\ & 4A_0(C_0t^4 + C_1t^3 + C_2t^2 + C_3t + C_4)]^{1/2} \\ & [2(B_0t^2 + B_1t + B_2)(2B_0t + B_1) \\ & - 4A_0(4C_0t^3 + 3C_1t^2 + 2C_2t + C_3)] \} / (2A_0) \end{aligned} \quad (5.19)$$

When a line with slope  $v_m$  is tangent to the curve of Eq. (5.17), the slope of the curve at the point of tangency is equal to the slope of the line. This suggests that at the point of tangency, the following function must be satisfied:

$$f(t) = (ds_1 / dt) - v_m = 0 \quad (5.20)$$

which can be used to solve for the time when a point contact may occur between the line and the curve.

From the above discussion, the tangent line of the potential collision region at each time interval can be identified. If the time for the points of tangency are outside the range of the potential collision region or outside the time interval under consideration, it will not be counted. After all valid tangent lines are found, the one having the smallest intercept is chosen as the line  $l_v$ .

The line  $l_v$  intersects with the line  $s_1 = s_{1,\min}$  in a point G. It is proposed to plan the motion of robot 1 such that its distance vs. time curve passes through point G with a velocity as high as possible.

When the distance vs. time curve of robot 1 passes through point G, a collision-free motion is guaranteed. This is because robot 1 cannot exceed the limiting velocity, and the distance vs. time curve will have a slope less than the limiting velocity and will not intersect the potential collision region.

The trajectory planning of robot 1 involves the planning of two segments of the path. The first segment is for the traveled distance  $s_1 \in [0, s_G]$  and it occurs at  $t \in [t_0, t_G]$ . The second segment is for the traveled distance  $s_1 \in [s_G, 1]$  and it occurs at  $t \in [t_G, t_c]$ . It is necessary to have a smooth transition at  $t = t_G$ .

Suppose the trajectory in the first segment involves an acceleration part followed by a constant velocity part. Denoted by  $t_{acc1}$  the time for the acceleration part, and  $t_{vel1}$  the time for the constant velocity part. It follows that

$$t_{acc1} + t_{vel1} = t_G \quad (5.21)$$

$$\frac{a_1 t_{acc1}^2}{2|\underline{V}_1 - \underline{U}_1|} + \frac{a_1 t_{acc1} t_{vel1}}{|\underline{V}_1 - \underline{U}_1|} = s_G \quad (5.22)$$

where  $a_1$  is the magnitude of the acceleration. Solving Eqs. (5.21) and (5.22) yields

$$t_{acc1} = t_G \pm \left( t_G^2 - \frac{2s_G |\underline{V}_1 - \underline{U}_1|}{a_1} \right)^{1/2} \quad (5.23)$$

Since  $t_{acc1}$  must be less than or equal to  $t_G$ , so

$$t_{acc1} = t_G - \left( t_G^2 - \frac{2s_G |\underline{V}_1 - \underline{U}_1|}{a_1} \right)^{1/2} \quad (5.24)$$

and

$$t_{vel1} = t_G - t_{acc1} = (t_G^2 - \frac{2s_G |\underline{Y}_1 - \underline{U}_1|}{a_1})^{1/2} \quad (5.25)$$

Note that if  $t_{acc1} = t_G$ , only the acceleration part is contained in the first segment of the trajectory and the velocity  $v_G$  of the end effector at  $t_G$  is  $a_1 t_{acc1}$ .

In order to determine the second segment of the trajectory, it is assumed that the trajectory contains three parts, viz., acceleration, constant velocity, and deceleration. The magnitude of acceleration and deceleration is  $a_1$ . The time of duration in each part is denoted by  $t_{acc2}$ ,  $t_{vel2}$ , and  $t_{dec}$ , respectively. The robot 1 is accelerated from  $v_G$  to  $v_m$  during the acceleration part. Then, the velocity of the end effector remains constant before being decelerated to a complete stop at the end point  $V_1$ . If the end effector reaches the velocity  $v_m$  at  $s_1 = s_G$ , it cannot be accelerated any further. In this case, the acceleration part in the second segment of the trajectory vanishes. Otherwise, we have

$$1 = s_G + \frac{1}{|\underline{Y}_1 - \underline{U}_1|} [(v_G t_{acc2} + a_1 t_{acc2}^2/2) + (v_G + a_1 t_{acc2})t_{vel2} + a_1 t_{dec}^2/2] \quad (5.26)$$

Since the end effector is accelerated from  $v_G$  to  $v_m$ , thus the time of duration in the acceleration part is given by

$$t_{acc2} = \frac{v_m - v_G}{a_1} \quad (5.27)$$

Next, the end effector is decelerated from  $v_m$  to zero, thus the time of duration in the deceleration part is given by

$$t_{\text{dec}} = \frac{v_m}{a_1} \quad (5.28)$$

Substituting Eqs. (5.27) and (5.28) into Eq. (5.26), one can solve for  $t_{\text{vel2}}$ . However, if  $t_{\text{vel2}} < 0$ , the trajectory in the second segment contains only an acceleration part followed by a deceleration part. In this case, the time of duration  $t_{\text{acc2}}$  and  $t_{\text{dec}}$  are determined by the following equations:

$$1 = s_G + \frac{1}{|\underline{V}_1 - \underline{U}_1|} [(v_G t_{\text{acc2}} + a_1 t_{\text{acc2}}^2/2) + a_1 t_{\text{dec}}^2/2] \quad (5.29)$$

and

$$v_G + a_1 t_{\text{acc2}} = a_1 t_{\text{dec}} \quad (5.30)$$

Substituting  $t_{\text{dec}}$  in (5.30) into (5.29) yields

$$a_1 t_{\text{acc2}}^2 + 2v_G t_{\text{acc2}} + (s_G - 1)|\underline{V}_1 - \underline{U}_1| + \frac{v_G^2}{2a_1} = 0 \quad (5.31)$$

The above quadratic equation can be used to solve for two values of  $t_{\text{acc2}}$ . However, only the positive one is of interest which is expressed as follows:

$$t_{\text{acc2}} = \frac{1}{a_1} \{-v_G + [v_G^2/2 + a_1(1 - s_G)|\underline{V}_1 - \underline{U}_1|]^{1/2}\} \quad (5.32)$$

and  $t_{\text{dec}}$  can be obtained from Eq. (5.30).

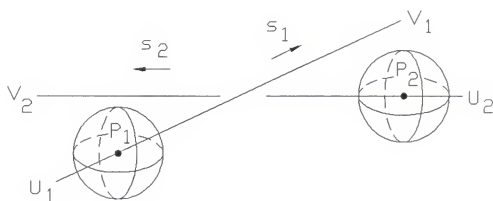


Fig. 5.1 Two spheres move on two rectilinear paths.

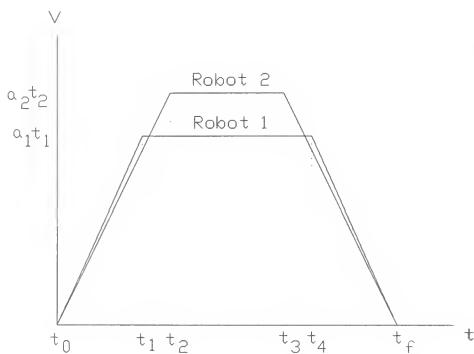


Fig. 5.2 Velocity profiles of two robots.

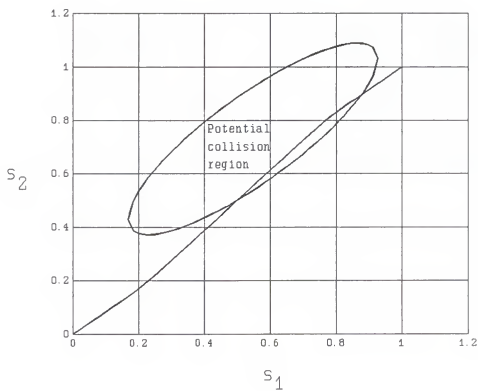


Fig. 5.3 Potential collision region and displacement curve.



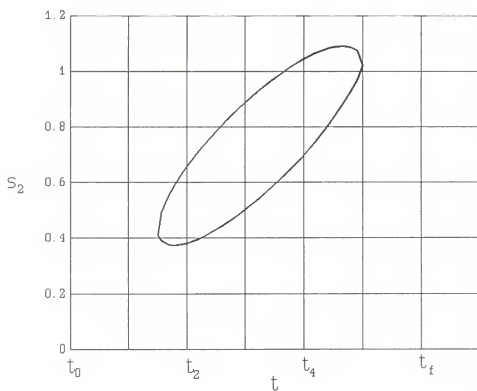
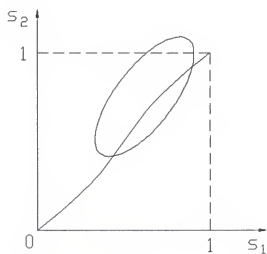
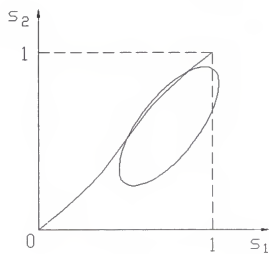


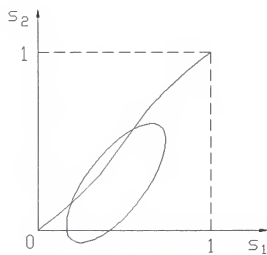
Fig. 5.4 Potential collision region in  $s_2$ - $t$  plane.



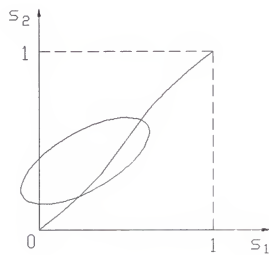
(a)



(b)

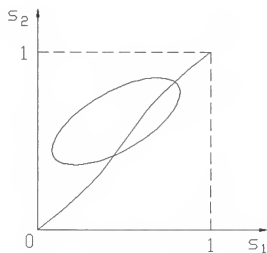


(c)

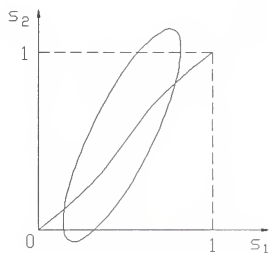


(d)

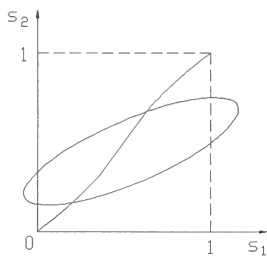
Fig. 5.5 Possible locations of potential collision region. (continued)



(e)



(f)



(g)

Fig. 5.5 Possible locations of potential collision region.

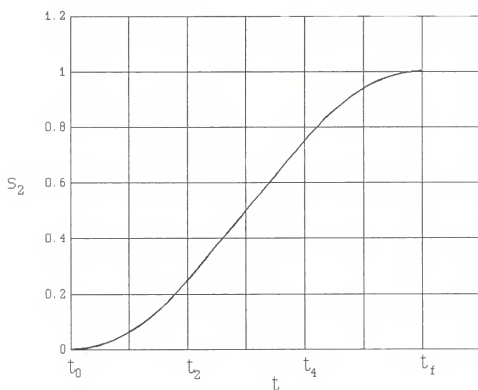


Fig. 5.6 Displacement profile of robot 2.

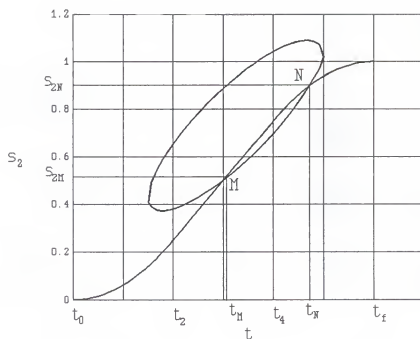


Fig. 5.7 Traveled distance vs. time curve intersects with the potential collision region at M and N.

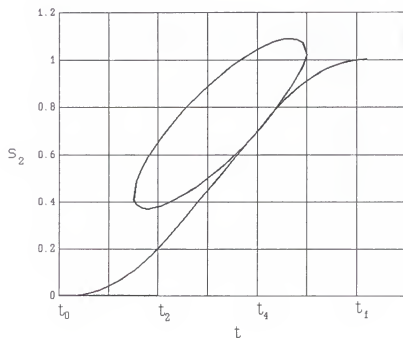


Fig. 5.8 Displacement curve of robot 2 after a time delay.

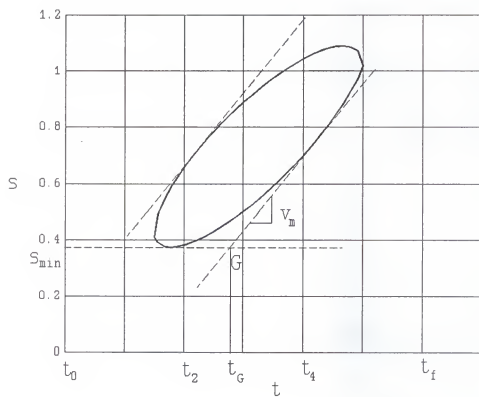


Fig. 5.9 Potential collision region is bounded by tangent lines.

## CHAPTER 6

### NUMERICAL EXAMPLES

The purpose of this chapter is to demonstrate the development in the previous chapters by numerical examples of industrial robots such as the Cincinnati Milacron T<sup>3</sup>-776 and PUMA robots. At first, the permissible orientations of robot links are demonstrated with the end effectors of the robots pinned at a target point. It is assumed that the joints of the robots have no angular limitations. Then examples of favorable orientations of robot links are displayed with the end effector pinned at a given point or following a prespecified path and the links avoiding spherical and polyhedral obstacles in the work environment. This is followed by demonstrations of favorable orientations of a pair of robot manipulators moving in coordination within a common workspace. Finally, the example of the time scheduling of two robot manipulators moving on a pair of rectilinear paths is demonstrated.

#### 6.1 Permissible Orientations

In order to illustrate the permissible orientations of robot links, a Cincinnati Milacron T<sup>3</sup>-776 robot and a PUMA robot are used as examples. Skeletal models of the robots are shown in Figs. 6.1 and 6.2, and the dimensions of the robots are given in Tables 6.1 and 6.2.

The permissible orientation ranges of the upperarm and the end effector of a T<sup>3</sup>-776 robot when the end effector is pinned at target points P(70°,0°,0°) and P(90°,0°,0°) are shown in Figs. 6.3 and 6.4, respectively. They describe the motion capability of the robot links with the end effector pinned at P. In these figures, the abscissa  $\Phi_1$  represents the locations of the planes of operation or the  $\pi$  planes as described in Section 3.1, and the ordinate represents the orientations of robot links with respect to a horizontal plane. The links orientations  $\Phi_1$ ,  $\Phi_2$ , and  $\Phi_4$  are as defined in Section 3.2.1 and are measured in radian.

In Fig. 6.3(a), the permissible orientations of the upperarm are shown to lie within two nonintersecting regions which represent respectively the elbow up and elbow down configurations. For each  $\Phi_1$ , two sectors of permissible orientations of the upperarm are obtained. Fig. 6.3(b) shows that the end effector is capable of a complete rotation ( $0 - 2\pi$ ) with respect to the target point P regardless the location of the  $\pi$  plane. In Fig. 6.4(a), the permissible orientations of the upperarm are shown to lie within a symmetric region which consists, in fact, of two intersecting regions representing the elbow up and elbow down configurations, respectively. Fig. 6.4(b) shows that a void exists within the permissible orientation range of the end effector. When the orientations of the end effector lie within this void, the wrist joint is outside the constraint surface as described in Section 3.1. Therefore, they are nonpermissible.

Analogously, the permissible orientation ranges of the upperarm and the end effector of a PUMA robot with respect to target points P(25°,0°,0°) and P(30°,0°,0°) are shown in Figs. 6.5 and 6.6, respectively.



In Fig. 6.5(a), the permissible orientations of the upperarm are shown to lie within two nonintersecting regions which represent respectively the elbow up and elbow down configurations. Fig. 6.5(b) shows that the end effector is capable of a complete rotation ( $0 - 2\pi$ ) with respect to the target point P regardless the location of the  $\pi$  plane. In Fig. 6.6(a), the permissible orientations of the upperarm are shown to lie within a region which consists of two intersecting regions representing the elbow up and elbow down configurations, respectively. Fig. 6.6(b) shows that a void exists within the permissible orientation range of the end effector. When the orientations of the end effector lie within this void, the wrist joint is outside the constraint surface. Therefore, they are nonpermissible.

## 6.2 Spherical Obstacles

In this section, favorable orientation ranges of robot links are demonstrated which direct the links avoiding collision with a spherical obstacle. At first, the favorable orientations of robot links are shown when the end effector link is pinned at a specific point. In this case, the favorable orientation ranges are determined for various  $\pi$  planes where the upperarm and forearm lie.

Then, the favorable orientations of the robot links when the end effector follows a prespecified path are demonstrated. In this case, two approaches for the determination of the favorable orientations are used. The first approach is to determine the favorable orientation range for each point on the path by using the  $\pi$  plane which contains the forearm and the end effector of the robot. In contrast, the second approach is to determine the favorable orientation range for each point

on the path by using the  $\pi$  plane where the upperarm has a maximum orientation ranges.

The permissible orientation range of the upperarm of a T<sup>3</sup>-776 robot with respect to a target point P(60",30",4") in a world coordinate system is shown in Fig. 6.7, which describes the motion capability of the robot link when the end effector is pinned at P. The world coordinate system is located at the intersection of axes of the base joint and shoulder joint of the robot. Here, the robot is assumed maintaining an elbow up and wrist up configuration. In this figure, the abscissa  $\phi_1$  is the angle between a  $\pi$  plane and a vertical plane containing the z-axis and the target point P. When  $\phi_1 = 0$ , i.e., the  $\pi$  plane passes through the point P, the upperarm has a maximum permissible orientation range. Fig. 6.8 shows the favorable orientation ranges of the upperarm with respect to a spherical obstacle with center (60",20",30") and radius 10". This demonstrates the capability of the robot links to move without colliding with the spherical obstacle. It can be seen that there is a void within the favorable orientation ranges. This implies that when the orientation of the upperarm is inside this void, the robot links will interfere with the spherical obstacle.

Next, the end effector of the robot is to move along a rectilinear path which can be expressed in the parametric form as follows

$$\underline{P} = \underline{U} + s(\underline{V} - \underline{U}) \quad 0 \leq s \leq 1 \quad (6.1)$$

where  $\underline{U}$  and  $\underline{V}$  are the starting and final points, respectively, and their coordinates are (85",0",10") and (60",30",4") in the world coordinate system. In addition, the

robot must avoid a spherical obstacle with center  $(60^{\circ}, 20^{\circ}, 30^{\circ})$  and radius  $10^{\circ}$ . For each point on the path, an analysis of the favorable orientations of the robot links can be performed according to the relative location of the robot and the obstacle. This analysis is repeated for a sequence of points on the path and any orientation within the favorable orientation range can be used to direct robot links to avoid interference. Fig. 6.9 illustrates the favorable orientation range of the robot links along the straight line path. In this example, the links of the robot remain on the same plane throughout the motion. In other words, the robot is moving as a planar 3R robot rotating about the first vertical axis. In the figure, the abscissa  $s$  is the displacement parameter along the path and the ordinate  $\Phi_2$  is the orientations of the upperarm. It can be seen that the favorable orientations of the upperarm lie within the upper and lower curves which are essentially the same as the permissible orientations. However, there is a void in the figure of favorable orientation ranges, which means that the links of the robot will interfere with the spherical obstacle when the orientation of the upperarm is inside the void.

In contrast, Fig. 6.10 illustrates the optimum favorable orientation range of the robot links along the straight line path. The optimum favorable orientation range is obtained by computing the favorable orientations for a specific target point. The location of the  $\pi$  plane where the upperarm has a maximum favorable orientation range is identified and the corresponding favorable orientation range is said to be optimum. This procedure is repeated for a sequence of target points along the path. Fig. 6.11 shows the locations of  $\pi$  planes where the upperarm has a maximum favorable orientation range. The locations of  $\pi$  planes are illustrated

by the ordinate  $\phi_1$  which represents the angle between the  $\pi$  plane and the x-z plane of the world coordinate system.

Similarly, the permissible orientation range of the upperarm of a PUMA robot with respect to a target point  $P(20", 5", 0")$  in a world coordinate system is shown in Fig. 6.12. The world coordinate system is located at the intersection of the axes of the base joint and the shoulder joint of the robot. In this figure, the abscissa  $\phi_1$  is the angle between a  $\pi$  plane and a vertical plane containing the z-axis and the target point P. At  $\phi_1 = 0$ , the  $\pi$  plane passes through the point P. Here, the robot is assumed maintaining an elbow up and wrist up configuration. Fig. 6.13 shows the favorable orientation range with respect to a spherical obstacle with center  $(18", 10", 0")$  and radius 5". It can be seen that no favorable orientation exists when  $\phi_1$  is greater than 0.1 and part of permissible orientations are not favorable when  $\phi_1$  is between -0.06 and 0.1.

Next, the end effector of a robot is to move along a rectilinear path which is expressed in the form of Eq. (6.1). The coordinates of the starting and final points of the path are given by  $U(30", -5", -1")$  and  $V(25", 10", -5")$ , respectively. In addition, the robot must avoid a spherical obstacle with center  $(34", 0", 13")$  and radius 11". Fig. 6.14 illustrates the favorable orientation range of the robot links along the straight line path. In this example, the forearm and the end effector of the robot remain on the same plane throughout the motion. In the figure, the abscissa  $s$  is the displacement parameter along the path and the ordinate  $\phi_2$  is the orientations of the upperarm. The favorable orientations of the upperarm lie between the upper and lower curves and when  $s$  is between 0 and 0.4, the favorable orientation range is small due to the presence of the spherical obstacle.

In contrast, Fig. 6.15 illustrates the optimum favorable orientation range of the robot links along the straight line path. The optimum favorable orientation range is obtained by computing the favorable orientations for a specific target point. The location of the  $\pi$  plane where the upperarm has a maximum favorable orientation range is identified and the corresponding favorable orientation range is said to be optimum. This procedure is repeated for a sequence of target points along the path. Fig. 6.16 shows the locations of  $\pi$  planes where the upperarm has a maximum favorable orientation range. The locations of  $\pi$  planes are determined by the values in the ordinate  $\phi_1$  which represents the angle between the  $\pi$  plane and the x-z plane of the world coordinate system.

### 6.3 Polyhedral Obstacles

In this section, favorable orientation ranges of robot links are determined which direct the links avoiding collision with a polyhedral obstacle. At first, the favorable orientations of robot links are shown when the end effector link is pinned at a specific point. Then, the favorable orientations of the robot links when the end effector follows a prespecified path are demonstrated.

The permissible orientation range of the upperarm of a T<sup>3</sup>-776 robot with respect to a target point P(80",40",0") in a world coordinate system is derived and is shown in Fig. 6.17, which describes the motion capability of the robot link when the end effector is pinned at P. In this figure, the abscissa  $\phi_1$  is the angle between the  $\pi$  plane and a vertical plane containing the z-axis and the target point P. The maximum and minimum permissible orientations are represented by the upper and

lower curves in the figure. Here, the robot is assumed maintaining an elbow up and wrist up configuration. Fig. 6.18 displays the favorable orientation ranges which describe the capability of the robot links to move without interfering a polyhedral obstacle whose vertices are A(75",30",30"), B(75",15",30"), C(112",15",30"), D(112",30",30"), E(75",30",12"), F(75",15",12"), G(112",15",12"), and H(112",30",12"). It can be seen that the favorable orientations of the upperarm lie within the upper and lower curves which are essentially the same as the permissible orientations. However, there is a void in the figure of favorable orientation ranges, which means that the links of the robot will interfere with the polyhedral obstacle when the orientation of the upperarm is inside the void.

Further, the end effector of the robot is assumed moving along a rectilinear path which is expressed in the form of Eq. (6.1). The coordinates of the starting and final points of the path are given by U(85",0",10") and V(60",30",4"), respectively. In addition, the robot must avoid a polyhedral obstacle with vertices A(75",30",30"), B(75",15",30"), C(112",15",30"), D(112",30",30"), E(75",30",12"), F(75",15",12"), G(112",15",12"), and H(112",30",12").

For each point on the path, an analysis of the favorable orientations of the robot links can be performed according to the relative location of the robot and the obstacle. This analysis is repeated for a sequence of discrete points on the path and any orientation within the favorable orientation range can be used to direct the robot links to avoid interference. The favorable orientation range of the robot is shown in Fig. 6.19. The locations of the  $\pi$  planes for this derivation are obtained by using a linear interpolation of the locations of the  $\pi$  planes at the starting and

final points of the path which are assumed given. In the figure, the abscissa  $s$  is the displacement parameter along the path and the ordinate  $\Phi_2$  is the orientations of the upperarm. It can be seen that there is a void in the figure of favorable orientation ranges, which means that the links of the robot will interfere with the polyhedral obstacle when the orientation of the upperarm is inside the void. Fig. 6.20 shows the locations of the  $\pi$  planes along the path. In this figure,  $\Phi_1$  is the angle between the selected  $\pi$  plane and the x-z plane of the world coordinate system, and  $\Delta\Phi_1$  is the angle between the selected  $\pi$  plane and the vertical plane which passes through the z-axis and the target point. The  $\Phi_1$  curve is linear due to the use of the linear interpolation approach.

Similarly, the permissible orientation range of the upperarm of a PUMA robot with respect to a target point  $P(30^\circ, 9^\circ, -4^\circ)$  in a world coordinate system is derived and is shown in Fig. 6.21, which describes the motion capability of the robot link when the end effector is pinned at P. In this figure, the abscissa  $\Phi_1$  is the angle between the  $\pi$  plane and a vertical plane containing the z-axis and the target point P. Here, the robot is assumed maintaining an elbow up and wrist up configuration. Fig. 6.22 shows the favorable orientation range which direct the robot links to move without interfering a polyhedral obstacle whose vertices are  $A(20^\circ, 5^\circ, -1^\circ)$ ,  $B(34^\circ, -5^\circ, -1^\circ)$ ,  $C(39^\circ, 2^\circ, -1^\circ)$ ,  $D(27^\circ, 10^\circ, -1^\circ)$ ,  $E(20^\circ, 5^\circ, -12^\circ)$ ,  $F(34^\circ, -5^\circ, -12^\circ)$ ,  $G(39^\circ, 2^\circ, -12^\circ)$ , and  $H(27^\circ, 10^\circ, -12^\circ)$ . Comparing the favorable orientation ranges with the permissible orientation ranges, we can find that, for the orientations of  $\Phi_1$  between  $-0.1$  and  $-0.18$ , part of the permissible orientations are not favorable due to the presence of the polyhedral obstacle.

In the following example, the end effector of a solid-link-modeled PUMA robot is to move along a rectilinear path which is expressed in the form of Eq. (6.1). The coordinates of the starting and final points of the path are given by  $U(32",5",-3")$  and  $V(24",22",-4")$ , respectively. In addition, the robot must avoid a polyhedral obstacle with vertices  $A(18",5",-1")$ ,  $B(22",-5",-1")$ ,  $C(25",-2",-1")$ ,  $D(22",7",-1")$ ,  $E(18",5",-52")$ ,  $F(22",-5",-52")$ ,  $G(25",-2",-52")$ , and  $H(22",7",-52")$ . The robot is assumed moving in an elbow up and wrist down configuration.

Fig. 6.23 shows the favorable orientation ranges of the robot links. The locations of the  $\pi$  planes for this derivation are obtained by using a linear interpolation of the locations of the  $\pi$  planes at the starting and final points of the path. In the figure, the abscissa  $s$  is the displacement parameter along the path and the ordinate  $\Phi_2$  is the orientations of the upperarm. When the orientations of the upperarm lie between the upper and lower curves of the figure, the links of the robot will not interfere with the polyhedral obstacle. Fig. 6.24 shows the locations of the  $\pi$  planes along the path. In the figure,  $\Phi_1$  is the angle between the selected  $\pi$  plane and the  $x$ - $z$  plane of the world coordinate system, and  $\Delta\Phi_1$  is the angle between the selected  $\pi$  plane and the vertical plane which passes through the  $z$ -axis and the target point.

#### 6.4 Coordination of Two Robot Manipulators

This section is devoted to the coordinations of two robot manipulators under parallel operations and master-slave operations. For the parallel operations, an example of coordination of two T<sup>3</sup>-776 robots modeled by line segments is presented.



At first, the permissible orientation ranges of each robot with the end effector following a prespecified trajectory are shown. Further, favorable orientation ranges which are obtained using the method described in Section 3.4 are illustrated. Finally, sets of joint angle displacements for the two robots throughout the trajectory are displayed. Similar results are also shown for two PUMA robots with solid links. In addition, computer graphics animation of two PUMA robots are used to verify the robots' motions.

For the master-slave operations, an example of coordination of two PUMA robots with solid links is presented.

#### 6.4.1 Parallel Operations

Suppose the end effectors of two T<sup>3</sup>-776 robots are moving along rectilinear trajectories as in Eq. (6.1) with starting points  $U_1(36", 66.5", 30")$ ,  $U_2(47", 40", 10")$  and final points  $V_1(72", 57.5", 10")$ ,  $V_2(38", 77", 20")$ , respectively, in a world coordinate system. The world coordinate system is located at the intersection of the axes of the base joint and the shoulder joint of the first robot, and the coordinates of the shoulder joint of the second robot in this coordinate system are  $(104", 108", 0")$ . The end effectors of two robots are assumed moving with an acceleration followed by a deceleration and they arrive the goal point at the same time. The displacements of the end effectors of the two robots are expressed in terms of the parameters  $s_1$  and  $s_2$  as follows:

$$(1) \quad t_0 \leq t < t_1 \quad s_i = \frac{a_i t^2}{2|\underline{V}_i - \underline{U}_i|} \quad (i = 1, 2) \quad (6.2)$$

$$(2) \quad t_1 \leq t \leq t_f \quad s_i = 1 - \frac{a_i(t_f - t)^2}{2|\underline{Y}_i - \underline{U}_i|} \quad (6.3)$$

It is assumed that the links of the robots remain on the same plane during the motion. Figs. 6.25 and 6.26 show the permissible orientation ranges of the two robots along their trajectories when they are in elbow up and wrist up configurations. In the figures, the abscissas are the displacement parameters along the trajectories and the ordinates are the orientations of the upperarms of the two robots. For each point in the trajectory of a robot, a range of permissible orientations can be found. The favorable orientation ranges of these two robots which avoid interference between the two robots are computed and are displayed in Figs. 6.27 and 6.28. It can be seen that when  $s_1$  is between 0.3 and 0.5 and  $s_2$  is between 0.25 and 0.5, parts of permissible orientations are not favorable, which means that in those orientations the two robots may interfere with each other. Also shown in the figures are orientations of the two upperarms that can be selected for interference-free motion of the two robots.

Analogously, Figs. 6.29 and 6.30 show the permissible orientation ranges of two solid-modeled PUMA robots moving along rectilinear trajectories with starting points  $U_1(26", 20", -3")$ ,  $U_2(31", -1", 3")$  and final points  $V_1(32", 5", -3")$ ,  $V_2(28", 23", 6")$ , respectively, in a world coordinate system which is located at the intersection of the axes of the base joint and shoulder joint of the first robot, and the coordinates of the shoulder joint of the second robot in this coordinate system are  $(60", 0", 0")$ . The displacements of the end effectors of the robots are represented by Eqs. (6.2) and

(6.3). In this example, the forearm and end effector of the robots are assumed remaining on the same plane throughout the motion.

The favorable orientation ranges of these two robots which avoid interference between the two robots are computed and are shown in Figs. 6.31 and 6.32. It can be seen the two robots may interfere with each other when  $s_1$  is between 0.6 and 0.8 and  $s_2$  is between 0.5 and 0.7. Finally, sets of joint angle displacements of the two robots which lie within the favorable orientation range are illustrated in Figs. 6.33 and 6.34. The resulting motion of the two robots were then verified by using computer graphics animation in a Silicon Graphics IRIS 4D/70GT Workstation as shown in Fig. 6.35.

#### 6.4.2 Master-Slave Operations

In this section, an example of coordination of two solid-modeled PUMA robots operating in a master-slave manner is demonstrated. At first, the motion of the master robot is determined such that it follows a desired trajectory. It is assumed that the end effector of the master robot moves in a rectilinear path with starting point  $U_1(26", 20", 0")$  and final point  $V_1(32", 5", 0")$  with a constant orientation  $a_6(0, 0, 1)$  and  $S_7(0, 1, 0)$  in a world coordinate system which is located at the intersection of the axes of the base joint and the shoulder joint of the first robot, and the coordinates of the shoulder joint of the second robot in this coordinate system are  $(62", 0", 0")$ . A set of joint angles can then be obtained by a reverse analysis and is shown in Fig. 6.36. Here, the end effector of the robot is assumed moving with a constant velocity.

The slave robot is to follow a rectilinear path with starting point  $U_2(33", -1", -6")$  and final point  $V_2(30", 20", -8")$  with a constant velocity. At each time instant, the target point of the slave robot is known and the favorable orientation ranges of the slave robot are computed such that the links of the slave robot do not interfere with the links of the master robot. Fig. 6.37 shows the favorable orientation ranges of the upperarm of the slave robot along the path. In this figure, the slave robot is in elbow up and wrist up configuration. It can be seen that when  $s_2$  is between 0.45 and 0.7, the links of the slave robot may interfere with the master robot, and the favorable orientation ranges in this segment of trajectory are smaller than the permissible orientation ranges. Also shown in the figure are orientations of the upperarm of the slave robot that can be selected to avoid interference with the master robot. A set of joint angles of the slave robot which lie within the favorable orientation ranges are illustrated in Fig. 6.38. The resulting motion of the two robots were then verified by using computer graphics animation in a Silicon Graphics IRIS 4D/70GT Workstation as shown in Fig. 6.39.

### 6.5 Time Scheduling of Two Robot Manipulators

Consider that the end effectors of two robot manipulators move along straight line paths with beginning points  $U_1(17", 17.5", 0")$ ,  $U_2(1.5", 45", 0")$  and final points  $V_1(87", 37", 0")$ ,  $V_2(75", 22", 0")$ , respectively. The sum of link lengths of these two end effectors is 15". Using this information, the potential collision region of two robot manipulators moving in the above straight line paths is determined by Eq. 5.5 and is illustrated in Fig. 6.40.

Further, the velocity profile of the robot manipulators are given in Fig. 6.41. Robot 1 accelerates from  $t = 0$  to  $t = 3$  sec with magnitude of acceleration  $a_1 = 2.7$  in/sec<sup>2</sup>, followed by a constant velocity until  $t = 9$  sec and finally decelerates with magnitude  $-2.7$  in/sec<sup>2</sup> until a complete stop at point  $V_1$ . Robot 2 has a similar velocity profile but the magnitudes of acceleration and deceleration are  $a_2 = 2.4$  in/sec<sup>2</sup> and  $-2.4$  in/sec<sup>2</sup>, the maximum velocity is 9.6 in/sec, and the time of transition are  $t = 4$  sec and  $t = 8$  sec. The total distances traveled for the two robots are 73" and 77", respectively.

Using the velocity profile, the corresponding positions of the two robots throughout the motion are obtained and are described in the parametric space as shown in Fig. 6.42. Also shown in the figure is the potential collision region. It can be seen that the curve of corresponding positions of two robots intersects with the potential collision region, which implied that the two robots will interfere with each other while tracking the specified trajectories. Further, the positions where the interference starts and ends are respectively  $s_1 = 0.503$ ,  $s_2 = 0.504$  and  $s_1 = 0.876$ ,  $s_2 = 0.896$ . Since the potential collision region in the parametric space intersects with the line  $s_2 = 1$ , it is therefore desirable to modify the trajectory of robot 2 to avoid interference.

In order to modify the trajectory of robot 2, the potential collision region is mapped into a space-time ( $s_2$ - $t$ ) domain as shown in Fig. 6.43. The traveled distance versus time curve for the original trajectory of robot 2 is also displayed in the figure. The time when the interference starts and ends are computed as 6.0 sec and 9.4 sec, respectively.

The time difference between the traveled distance versus time curve and the potential collision region in the interval of  $s_2 = [0.504, 0.896]$  is shown in Fig. 6.44. The maximum time difference is 0.43 sec, which is used as a time delay in the starting point of robot 2. The resulting trajectory can be realized by the traveled distance versus time curve in Fig. 6.45. The curve is shifted to the right by an amount of  $dt_{\max}$  ( $= 0.43$  sec), thus it moves out of the potential collision region and no interference will occur. The total travel time of the new trajectory is 12.43 sec.

Another method of modifying the trajectory of robot 2 is to reduce the speed of the robot to avoid the potential collision region. First, a transition point G outside the potential collision region in the space-time domain is located. The transition point G is the intersection point of two lines (see Fig. 6.46). One line has a slope of a limiting velocity  $v_m$  ( $= 10$  in/sec) and has a point contact with the potential collision region. The other line is horizontal and is tangent to the potential collision region at the point with minimum  $s_2$ . The new trajectory is to pass through the point G. The traveled distance versus time curve of the new trajectory is shown in Fig. 6.47. The curve consists of five segments, i.e., acceleration, constant velocity, acceleration, constant velocity and deceleration, and can be expressed in five time intervals as follows:

$$(1) \quad 0 \leq t \leq t_{\text{acc1}}$$

$$s_2 = \frac{a_2 t^2}{2|V_2 - U_2|} \quad (6.4)$$

$$(2) \quad t_{\text{acc1}} < t \leq t_G$$

$$s_2 = s_{2a} + \frac{a_2 t_{acc1}(t - t_{acc1})}{|\underline{V}_2 - \underline{U}_2|} \quad (6.5)$$

where

$$s_{2a} = \frac{a_2 t_{acc1}^2}{2|\underline{V}_2 - \underline{U}_2|}$$

$$(3) \quad t_G < t \leq t_b$$

$$s_2 = s_G + \frac{a_2 t_{acc1}(t - t_G)}{|\underline{V}_2 - \underline{U}_2|} + \frac{a_2(t - t_G)^2}{2|\underline{V}_2 - \underline{U}_2|} \quad (6.6)$$

$$(4) \quad t_b < t \leq t_c$$

$$s_2 = s_{2b} + \frac{v_m(t - t_G)}{|\underline{V}_2 - \underline{U}_2|} \quad (6.7)$$

where

$$s_{2b} = s_G + \frac{a_2 t_{acc1}(t_b - t_G)}{|\underline{V}_2 - \underline{U}_2|} + \frac{a_2(t_b - t_G)^2}{2|\underline{V}_2 - \underline{U}_2|}$$

$$(5) \quad t_c < t \leq t_d$$

$$s_2 = 1 - \frac{a_2(t_d - t)^2}{2|\underline{V}_2 - \underline{U}_2|} \quad (6.8)$$

where  $t_{acc1} = 2.95$  sec,  $t_G = 5.53$  sec,  $t_b = 6.74$  sec,  $t_c = 8.44$  sec, and  $t_d = 12.60$  sec.

The total travel time of the new trajectory after a speed reduction is 12.60 sec.

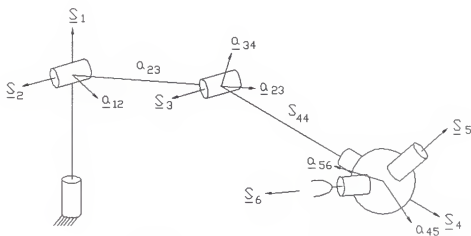


Fig. 6.1 Skeletal model of a Cincinnati Milacron T<sup>3</sup>-776 robot.

Link Length	Value (in)	Offset	Value (in)	Twist Angle	Value (deg)
$a_{12}$	0	$S_{11}$		$\alpha_{12}$	90
$a_{23}$	44	$S_{22}$	0	$\alpha_{23}$	0
$a_{34}$	0	$S_{33}$	0	$\alpha_{34}$	90
$a_{45}$	0	$S_{44}$	55	$\alpha_{45}$	61
$a_{56}$	0	$S_{55}$	0	$\alpha_{56}$	61
$a_{67}$	0	$S_{66}$	15	$\alpha_{67}$	

Table 6.1 Dimensions of Cincinnati Miracron T<sup>3</sup>-776 robot.



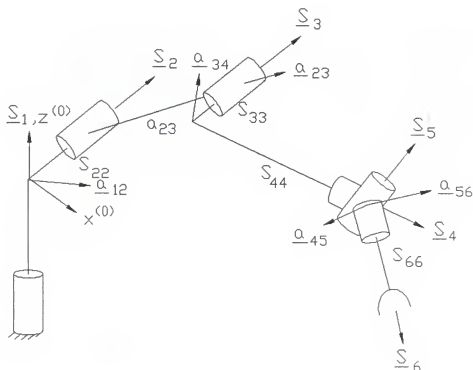
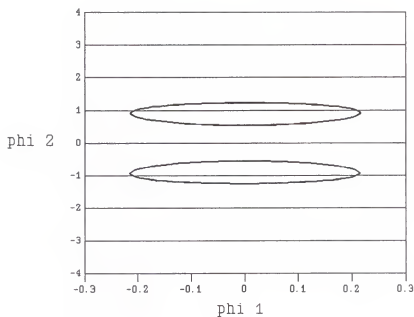


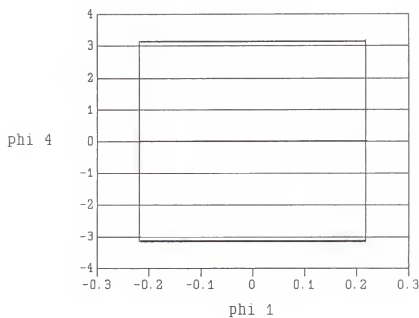
Fig. 6.2 Kinematic model of a PUMA robot.

Link Length	Value (in)	Offset	Value (in)	Twist Angle	Value (deg)
$a_{12}$	0	$S_{11}$		$\alpha_{12}$	270
$a_{23}$	17	$S_{22}$	9.545	$\alpha_{23}$	0
$a_{34}$	0	$S_{33}$	3.675	$\alpha_{34}$	270
$a_{45}$	0	$S_{44}$	17.05	$\alpha_{45}$	90
$a_{56}$	0	$S_{55}$	0	$\alpha_{56}$	270
$a_{67}$	0	$S_{66}$	6	$\alpha_{67}$	90

Table 6.2 Dimensions of PUMA robot.

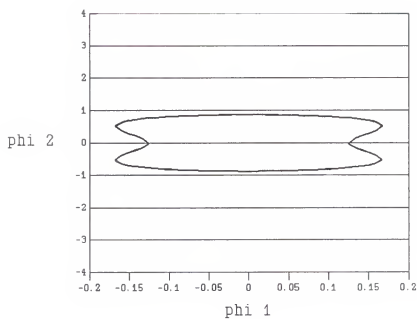


(a)

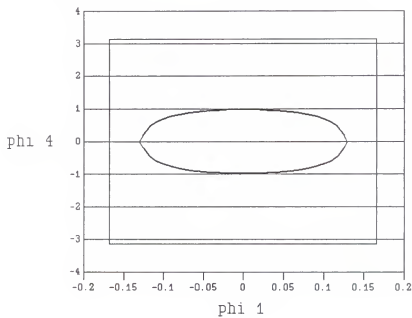


(b)

Fig. 6.3 Permissible orientations, target point  $P = (70'', 0'', 0'')$   
 (a) upperarm, (b) end effector

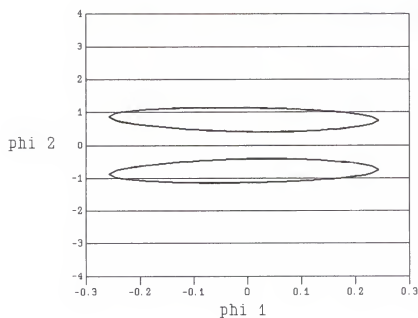


(a)

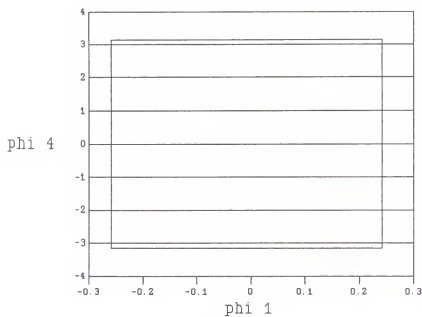


(b)

Fig. 6.4 Permissible orientations, target point  $P = (90^\circ, 0^\circ, 0^\circ)$   
 (a) upperarm, (b) end effector

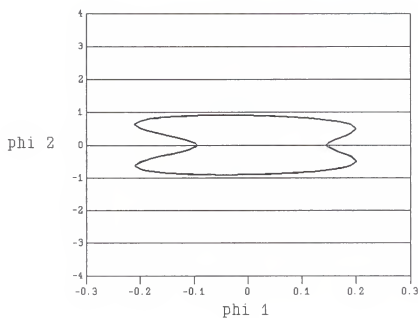


(a)

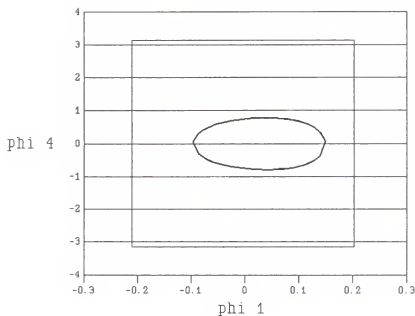


(b)

Fig. 6.5 Permissible orientations, target point  $P = (25'', 0'', 0'')$   
(a) upperarm, (b) end effector



(a)



(b)

Fig. 6.6 Permissible orientations, target point  $P = (30^\circ, 0^\circ, 0^\circ)$   
 (a) upperarm, (b) end effector

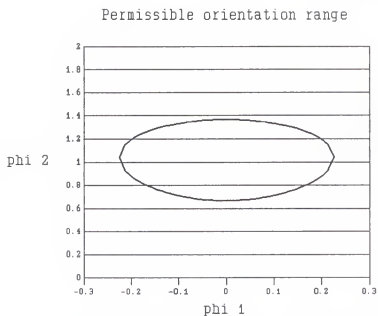


Fig. 6.7 Permissible orientation ranges of a T<sup>3</sup>-776 robot.

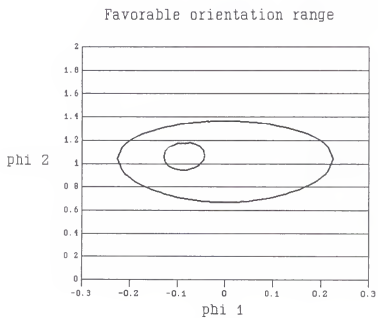


Fig. 6.8 Favorable orientation ranges of a T<sup>3</sup>-776 robot.

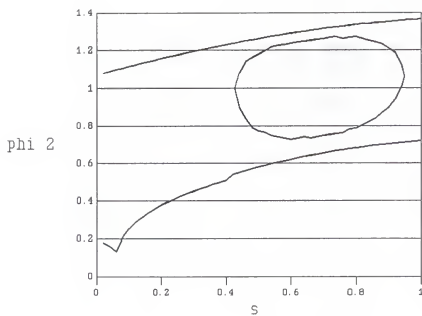


Fig. 6.9 Favorable orientation range along a straight line path.

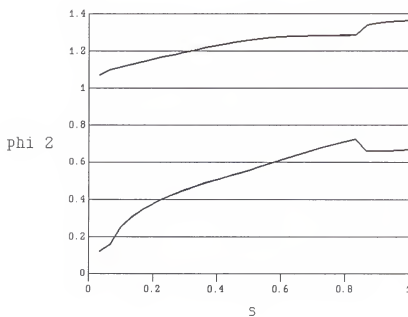


Fig. 6.10 Optimum favorable orientation range along a straight line path.

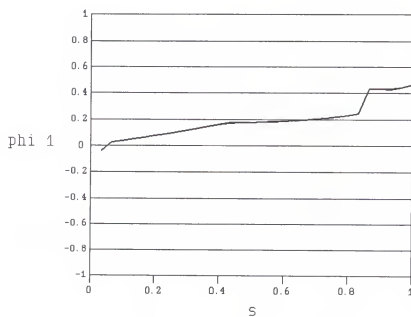


Fig. 6.11 Optimum location of  $\pi$  plane ( $\Phi_1$ ) along a straight line path.



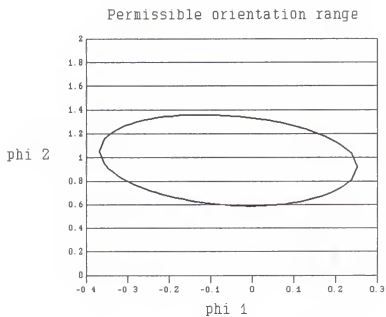


Fig. 6.12 Permissible orientation ranges of a PUMA robot.

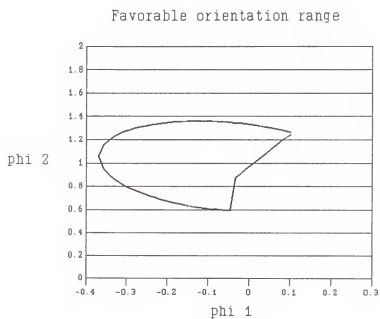


Fig. 6.13 Favorable orientation ranges of a PUMA robot.

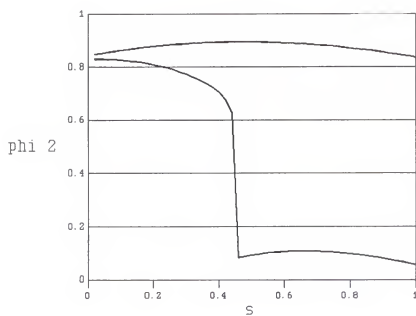


Fig. 6.14 Favorable orientation range along a straight line path.

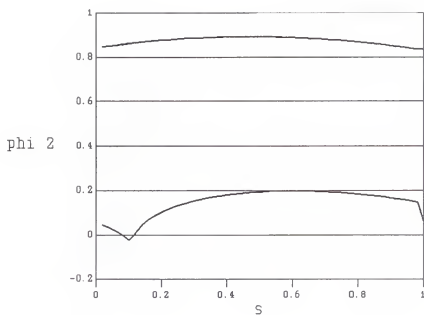


Fig. 6.15 Optimum favorable orientation range along a straight line path.

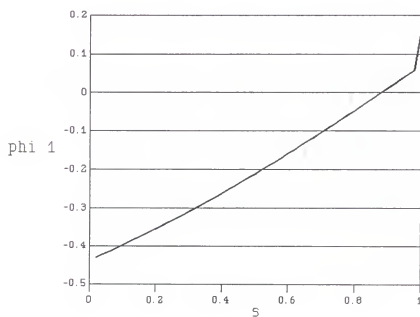


Fig. 6.16 Optimum location of  $\pi$  plane ( $\phi_1$ ) along a straight line path.

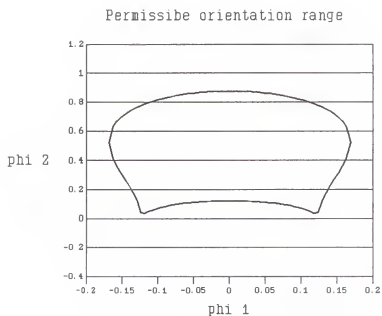


Fig. 6.17 Permissible orientation ranges of a T<sup>3</sup>-776 robot.

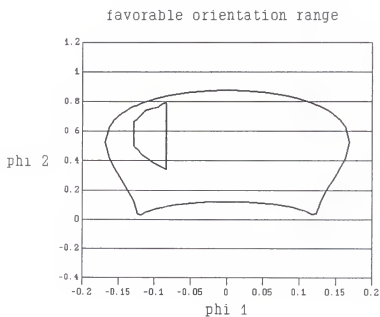


Fig. 6.18 Favorable orientation ranges of a T<sup>3</sup>-776 robot.

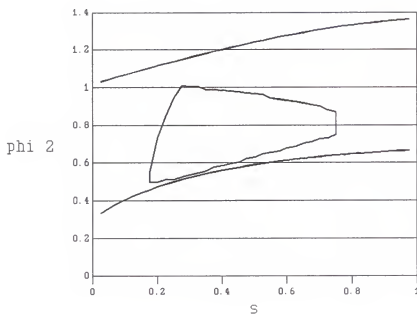


Fig. 6.19 Favorable orientation ranges along a straight line path.

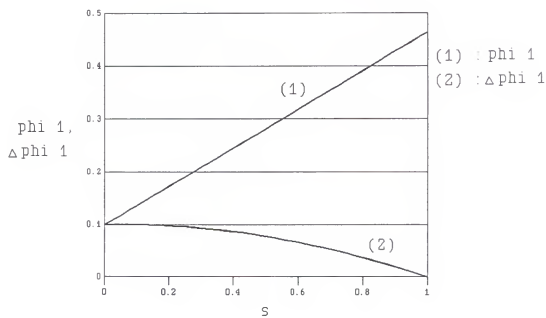


Fig. 6.20 Orientations of selected  $\pi$  planes along the path.

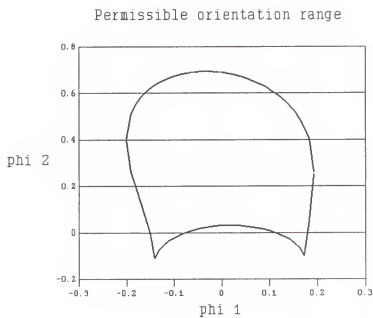


Fig. 6.21 Permissible orientation ranges of a PUMA robot.

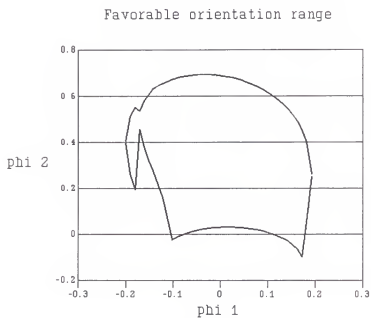


Fig. 6.22 Favorable orientation ranges of a PUMA robot.

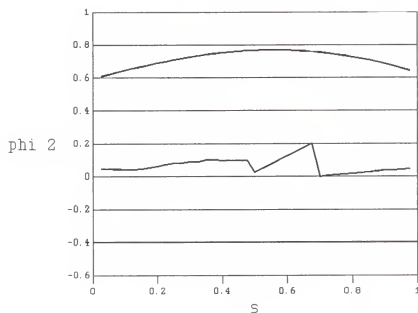


Fig. 6.23 Favorable orientation ranges along a straight line.

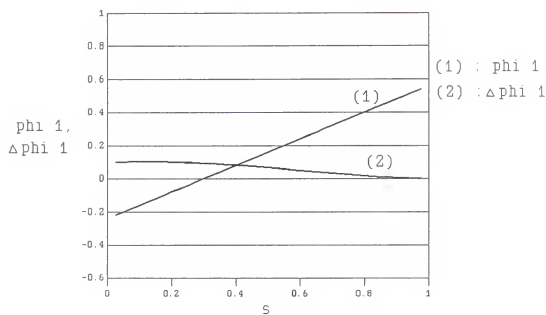


Fig. 6.24 Orientations of selected  $\pi$  planes along the path.

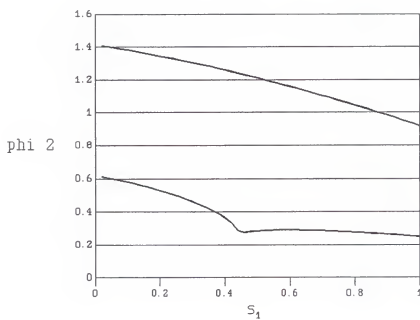


Fig. 6.25 Permissible orientation ranges of robot 1.

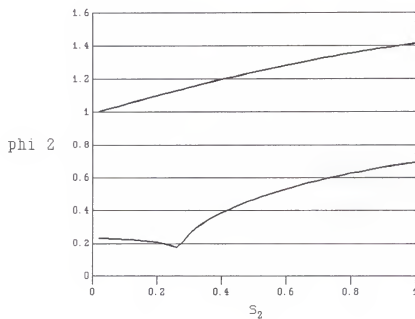


Fig. 6.26 Permissible orientation ranges of robot 2.



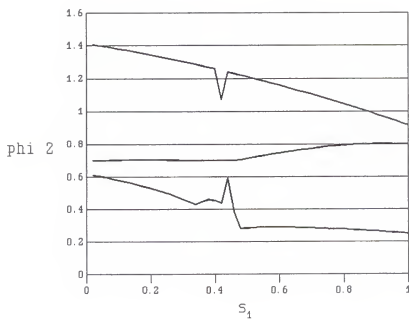


Fig. 6.27 Favorable orientation ranges of robot 1.

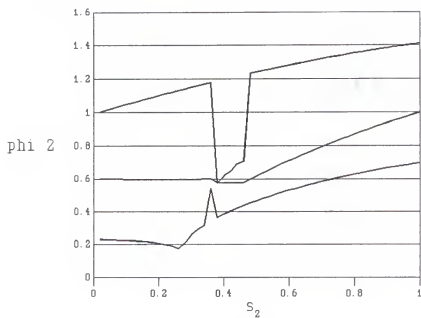


Fig. 6.28 Favorable orientation ranges of robot 2.

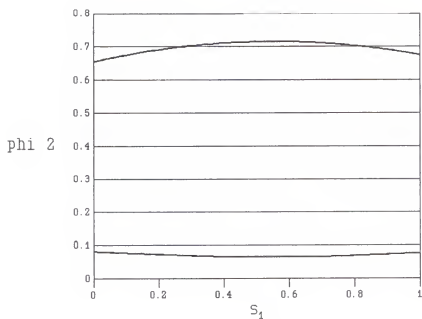


Fig. 6.29 Permissible orientations ranges of robot 1.

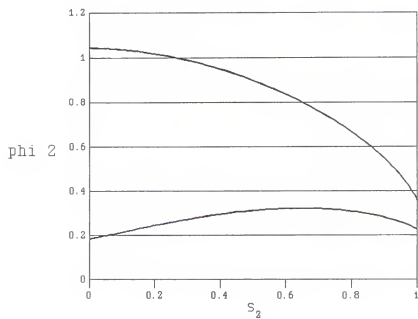


Fig. 6.30 Permissible orientation ranges of robot 2.

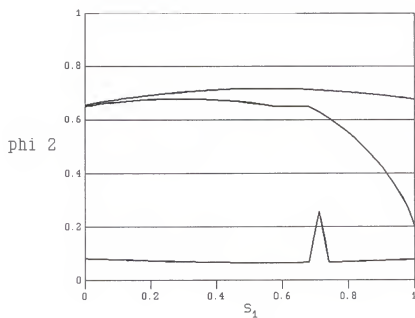


Fig. 6.31 Favorable orientation ranges of robot 1.

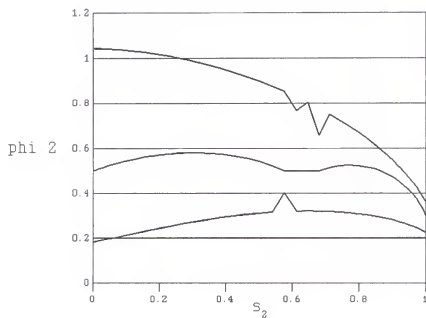


Fig. 6.32 Favorable orientation range of robot 2.

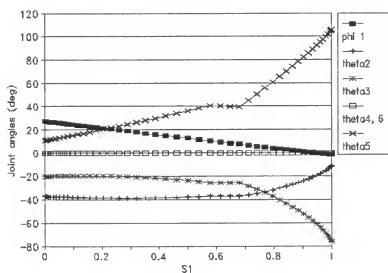


Fig. 6.33 Joint angles of robot 1.

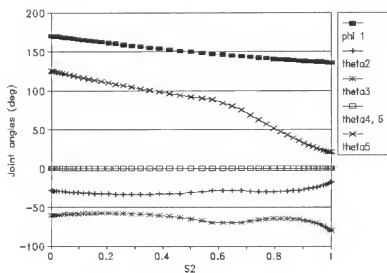


Fig. 6.34 Joint angles of robot 2.

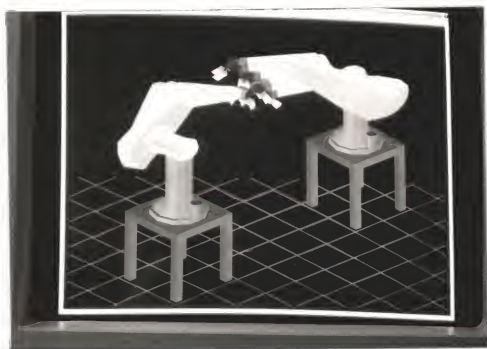


Fig. 6.35 Simulation of robots' motions.

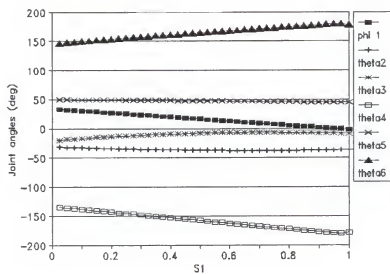


Fig. 6.36 Joint angles of the master robot.

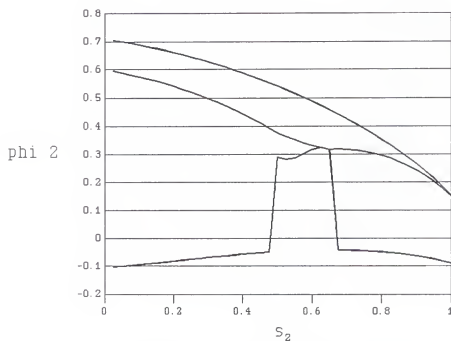


Fig. 6.37 Favorable orientation ranges of the slave robot.

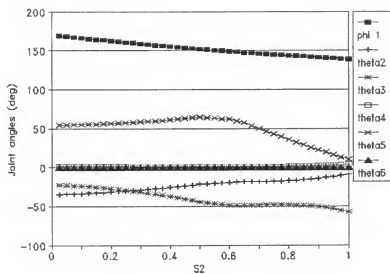


Fig. 6.38 Joint angles of the slave robot.

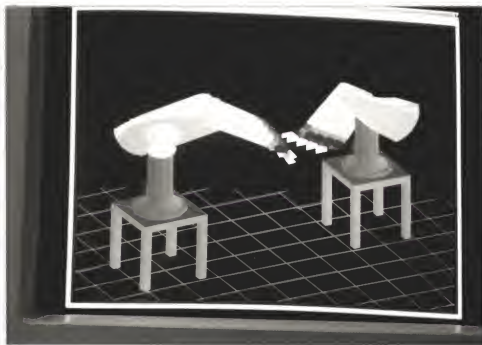


Fig. 6.39 Simulation of robots' motions.

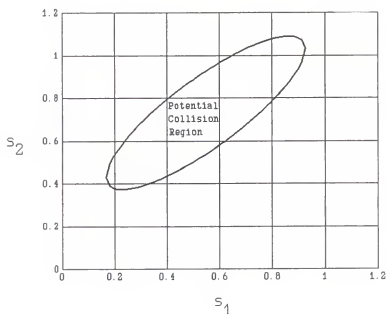


Fig. 6.40 Potential collision region.

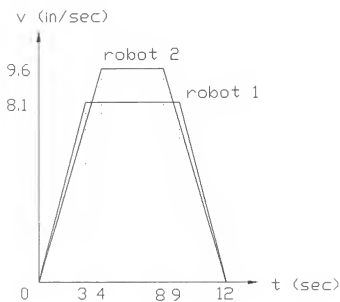


Fig. 6.41 Velocity profiles of two robots.



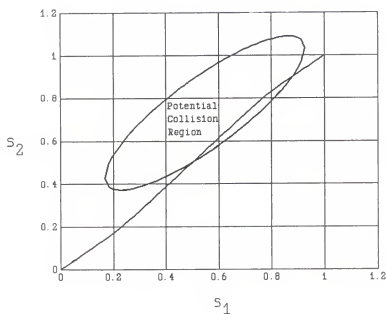


Fig. 6.42 Distances curve in parametric space.

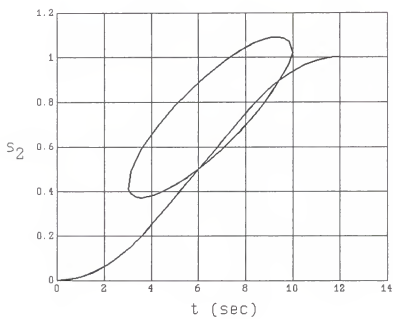


Fig. 6.43 Distance vs. time curve of robot 2.

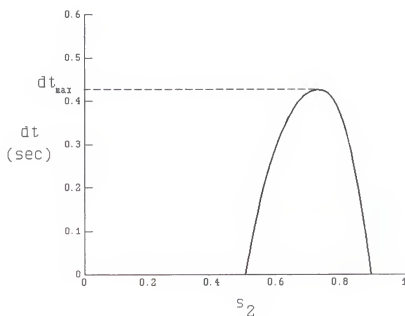


Fig. 6.44 Time difference between the distance vs. time curve and the potential collision region

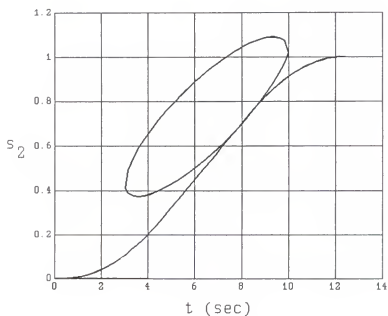


Fig. 6.45 Distance vs. time curve after a time delay.

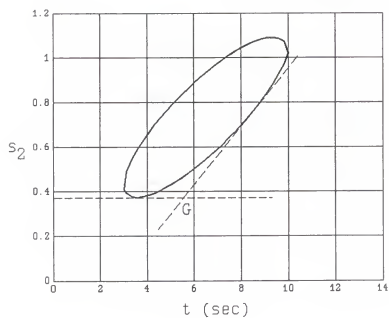


Fig. 6.46 Transition point G.

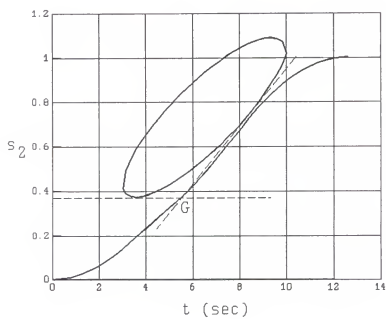


Fig. 6.47 Distance vs. time curve after a speed reduction.

## CHAPTER 7

### CONCLUSIONS AND RECOMMENDATIONS

In this research, the determination of the capability of a robot manipulator to follow a prespecified path while avoiding obstacles and a second robot manipulator has been demonstrated. This analysis considers first the motion capabilities of the links of a robot manipulator while its end effector is pinned at a target point. Then, the motion capabilities of the links of a robot manipulator while its end effector follows a prespecified path are determined. Permissible orientation ranges, allowable orientation ranges and favorable orientation ranges are used to describe the capabilities of the links to avoid interference. The joint angles of the robot links are then chosen within the favorable orientation range to guarantee a interference-free motion.

The efforts of this work are summarized in the followings.

(1) The determination of orientation ranges of links of a robot manipulator avoiding spherical obstacles while its end effector follows a prespecified path is shown.

(2) The determination of orientation ranges of links of a robot manipulator avoiding polyhedral obstacles while its end effector follows a prespecified path is presented.

(3) The determination of orientation ranges of links of a robot manipulator avoiding the links of a second robot manipulator while their end effectors follow prespecified trajectories is demonstrated.

(4) Trajectories planning of two robot manipulators using time scheduling scheme such that the two manipulators do not collide with each other is illustrated.

This study provides an understanding of dexterity of robot manipulators subject to constraint due to the presence of obstacles. It also provides a decision-making tool for off-line motion planning of spatial robot manipulators. When a path for a spatial robot is designated, the analysis in this work determines whether the robot is capable of tracking this path and how to control the robot to track the path. Further, the time scheduling schemes for the coordinations of two robot manipulators provide an effective way for planning the trajectories of the two manipulators to avoid interference. Finally, it is worth to mention that the joint displacement limitations of robots can be easily implemented into the analysis by reducing the permissible orientation ranges of robot links.

This research may also find applications for the motion planning of kinematically redundant robots which can be divided into non-redundant segments with ends constrained by joints. The motion capabilities of links of the robot in each segment can then be determined by the method presented in this work.

In this research, the problem of the trajectories planning for the coordination of two robot manipulators is discussed where each robot is assumed to have a trajectory with acceleration and deceleration of the same magnitude. This can be extended to the problem where the robot has different magnitudes of acceleration

and deceleration. Further, the problem can be extended to consider alternative tactics such as changing the path of one robot or altering the trajectories of both robots. It should be remembered that in the trajectory planning analysis, the collision is considered to occur only between the end effectors of the two robots. The cases where other links of the robots may involve in the collision worth further investigation. Finally, this analysis can be applied to the collision avoidance of mobile robots or automatically guided vehicles. In this case, the trajectory of a robot or vehicle is planned according to the relative motions of other robots or vehicles.

## REFERENCES

- Basta, R. A., Mehrotra, R. and Varanasi, M. R. 1988. Collision detection for planning collision-free motion of two robot arms. Proc. IEEE Conference on Robotics and Automation, Philadelphia, PA, pp. 638-640.
- Brady, M., Hollerbach, J. M., Johnson, T. L., Lozano-Pérez, T. and Mason, M. T. (eds.) 1982. Robot motion: planning and control. MIT Press, Cambridge, Mass.
- Brooks, R. A. 1983. Solving the find-path problem by good representation of free space. IEEE Trans. on System, Man, and Cybernetics, Vol. SMC-13, No. 3, pp. 190-197.
- Brooks, R. A. 1984. Planning collision free motions for pick and place operations. Robotics Research: The First International Symposium, MIT Press, Cambridge, Mass. pp. 5-37.
- Chien, Y. P., Koivo, A. J. and Lee, B. H. 1988. On-line generation of collision free trajectories for multiple robots. Proc. IEEE Conference on Robotics and Automation, Philadelphia, PA, pp. 209-214.
- Choi, Y. J. 1990. Articulation of spatial robots, Ph.D. Dissertation, University of Florida.
- Conte, S. D. and de Boor, C. 1980. Elementary numerical analysis an algorithmic approach. McGraw-Hill, Inc. New York.
- Duffy, J. 1980. Analysis of Mechanisms and Robot Manipulators, John Wiley and Sons. New York.
- Freund, E. and Hoyer, H. 1986. On the on-line solution of the findpath problem in multi-robot systems. Robotics Research : The 3rd International Symposium, MIT Press, Cambridge Mass. pp. 253-262.
- Fu, K. S., Gonzalez, R. C. and Lee, C. S. G. 1987. Robotics: control, sensing, vision, and intelligence. McGraw-Hill, Inc. New York.
- Hunt, K. H. 1978. Kinematic geometry of mechanisms. Clarendon Press, Oxford.

- Kalhor, R. 1989. Obstacle avoidance for a planar RRP robotic manipulator, Master's thesis, University of Florida.
- Khatib, O. 1986. Real-time obstacle avoidance for manipulators and mobile robots. International Journal of Robotics Research, Vol. 5, No. 1, pp. 90-98.
- Krishnamurthy, V. 1985. Algorithms to provide information for a prespecified rectilinear motion of robot end effector, Master's thesis, University of Florida.
- Lee, B. H. and Lee, C. S. G. 1987. Collision-free motion planning of two robots. IEEE Trans. on System, Man, and Cybernetics, Vol. SMC-17, No. 1, pp. 21-32.
- Lehmann, C. H. 1964. Analytic geometry, John Wiley & Sons, New York, 203. pp.
- Lin, M. -J. and Duffy, J. 1989. Interference avoidance of two robot manipulators using articulation, Proc. 1st National Applied Mechanisms and Robotics Conference, Vol. II, Paper No. AMR89-8A-1, Cincinnati, Ohio, Nov. 5-8.
- Lipkin, H., Torfason, L. E., and Duffy, J. 1985. Efficient motion planning for a planar manipulator based on dexterity and workspace geometry, Conference on Mechanisms and Machinery, Cranfield Institute of Technology, Cranfield, United Kingdom, September.
- Lovell, G. H. 1983. Quantification of dexterity for some planar and spatial robots. Master's thesis, University of Florida.
- Lozano-Pérez, T. 1981. Automatic planning of manipulator transfer movements. IEEE Trans. on System, Man, and Cybernetics, Vol. SMC-11, pp. 681-698.
- Lozano-Pérez, T. 1986. Motion planning for simple robot manipulators. Robotics Research : The 3rd International Symposium, MIT Press, Cambridge, Mass. pp. 133-140.
- Lozano-Pérez, T. and Wesley, M. A. 1979. An algorithm for planning collision-free paths among polyhedral obstacles. Commun. ACM, Vol. 22, No. 10, pp. 560-570.
- Luh, J. Y. S. and Campbell, C. E. 1984. Minimum distance collision-free path planning for industrial robots with a prismatic joint. IEEE Trans. on Automatic Control, Vol. AC-29, pp. 675-680.
- Meyer, W. and Benedict, P. 1988. Path planning and the geometry of joint space obstacles. Proc. IEEE Conference on Robotics and Automation, Philadelphia, PA, pp. 215-219.



- O'Dunlaing, C. and Yap, C. 1985. A 'retraction' method for planning the motion of a disc. Journal of Algorithms, Vol. 6, pp. 104-111.
- Oommen, B. J. and Reichstein, I. 1986. On translating ellipses amidst elliptic obstacles. Int. Conf. on Robotics and Automation. pp. 1755-1759.
- Oommen, B. J. and Reichstein, I. 1987. On the problem of translating an elliptic object through a workspace of elliptic obstacles. Robotica, Vol. 5, pp. 187-196.
- Palmquist, R. D. 1985. Workspace, dexterity, and motion capabilities of tandem planar robots with interactive computer graphics simulation, Master's thesis, University of Florida.
- Reif, J. 1979. Complexity of the mover's problem and generalizations. Proc. 20th Symp. on Foundation of Computer Science, pp. 421-427.
- Roach, J. W. and Boaz, M. N. 1987. Coordinating the motions of robot arms in a common workspace. IEEE Journal of Robotics and Automation, Vol. RA-3, No. 5, pp 437-444.
- Schwartz, J. T. and Sharir, M. 1983. On the piano movers' problem I : The special case of a rigid polygonal body moving amidst polygonal barriers. Commun. Pure Appl. Math., Vol. 36, pp. 345-398.
- Shieh, M. -D. and Duffy, J. 1989a. Autonomous rectilinear motion planning. Part I : The geometry of the wrist workspace with a single circular obstacle, Proc. 1st National Applied Mechanisms and Robotics Conference, Vol. I, Paper No. AMR89-3A-3, Cincinnati, Ohio, Nov. 5-8.
- Shieh, M. -D. and Duffy, J. 1989b. Autonomous rectilinear motion planning. Part II : The geometry of the end-effector workspace and determination of a free path, Proc. 1st National Applied Mechanisms and Robotics Conference, Vol. I, Paper No. AMR89-3A-4, Cincinnati, Ohio, Nov. 5-8.
- Tseng, C. -S. 1987. Rapid generation of collision-free paths for robot manipulators with computer graphics animation, Ph.D. dissertation, University of Florida.
- Udupa, S. M. 1977. Collision detection and avoidance in computer controlled manipulators. Proc. 5th International Joint Conference on Artificial Intelligence. MIT, Cambridge, Mass. pp. 737-748.
- Wong, E. K. and Fu, K. S. 1986. A hierarchical orthogonal space approach to three-dimensional path planning. IEEE Journal of Robotics and Automation, Vol. RA-2, No. 1, pp. 42-53.

- Young, L. and Duffy, J. 1987a. A theory for the articulation of planar robots: Part I - Kinematic analysis for the flexure and the parallel operation of robots. ASME Journal of Mechanisms, Transmissions, and Automation in Design, Vol. 109, No. 1, pp. 29-36.
- Young, L. and Duffy, J. 1987b. A theory for the articulation of planar robots: Part II - Motion planning procedure for interference avoidance. ASME Journal of Mechanisms, Transmissions, and Automation in Design, Vol. 109, No. 1, pp. 37-41.

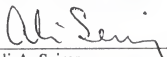
## BIOGRAPHICAL SKETCH

Ming-Jer Lin was born on February 22, 1960, in Tainan, Taiwan, R. O. C.. After graduating in 1977 from Tainan First High School in Tainan, he entered the National Tsing-Hua University in Hsin-Chu, Taiwan, and graduated with a Bachelor of Science degree in June, 1981, with a major in power mechanical engineering. In August, 1984, he began graduate study in the Mechanical Engineering Department of the University of Florida and began working with Dr. Duffy in January 1985. He received the Master of Science degree in December, 1986.


I certify that I have read this study and that in my opinion it conforms to acceptable standards of scholarly presentation and is fully adequate, in scope and quality, as a dissertation for the degree of Doctor of Philosophy.

  
Joseph Duffy, Chairman  
Graduate Research Professor of Mechanical  
Engineering


I certify that I have read this study and that in my opinion it conforms to acceptable standards of scholarly presentation and is fully adequate, in scope and quality, as a dissertation for the degree of Doctor of Philosophy.

  
Ali A. Seireg  
Ebaugh Professor of Mechanical  
Engineering

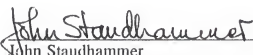
I certify that I have read this study and that in my opinion it conforms to acceptable standards of scholarly presentation and is fully adequate, in scope and quality, as a dissertation for the degree of Doctor of Philosophy.

  
Carl D. Crane III  
Assistant Professor of Mechanical  
Engineering

I certify that I have read this study and that in my opinion it conforms to acceptable standards of scholarly presentation and is fully adequate, in scope and quality, as a dissertation for the degree of Doctor of Philosophy.

  
Ralph G. Selfridge  
Professor of Computer and Information  
Sciences

I certify that I have read this study and that in my opinion it conforms to acceptable standards of scholarly presentation and is fully adequate, in scope and quality, as a dissertation for the degree of Doctor of Philosophy.

  
John Staudhammer  
Professor of Electrical Engineering

This dissertation was submitted to the Graduate Faculty of the College of Engineering and to the Graduate School and was accepted as partial fulfillment of the requirements for the degree of Doctor of Philosophy.

May 1991

for Hubert A. Bess  
Winfred M. Phillips  
Dean, College of Engineering

---

Madelyn M. Lockhart  
Dean, Graduate School